University of Genoa

School of Medical and Pharmaceutical Sciences

Department of Experimental Medicine

PhD Course in Experimental Medicine

Curriculum of Biochemistry

XXXIII cycle

Glial cells of the developing amphioxus: a molecular study

Candidate: Matteo Bozzo

Tutor: Prof. Simona Candiani

Like the entomologist in search of brightly colored butterflies, my attention hunted, in the garden of the gray matter, cells with delicate and elegant forms, the mysterious butterflies of the soul, whose beating of wings may one day reveal to us the secrets of the mind.

Santiago Ramon y Cajal

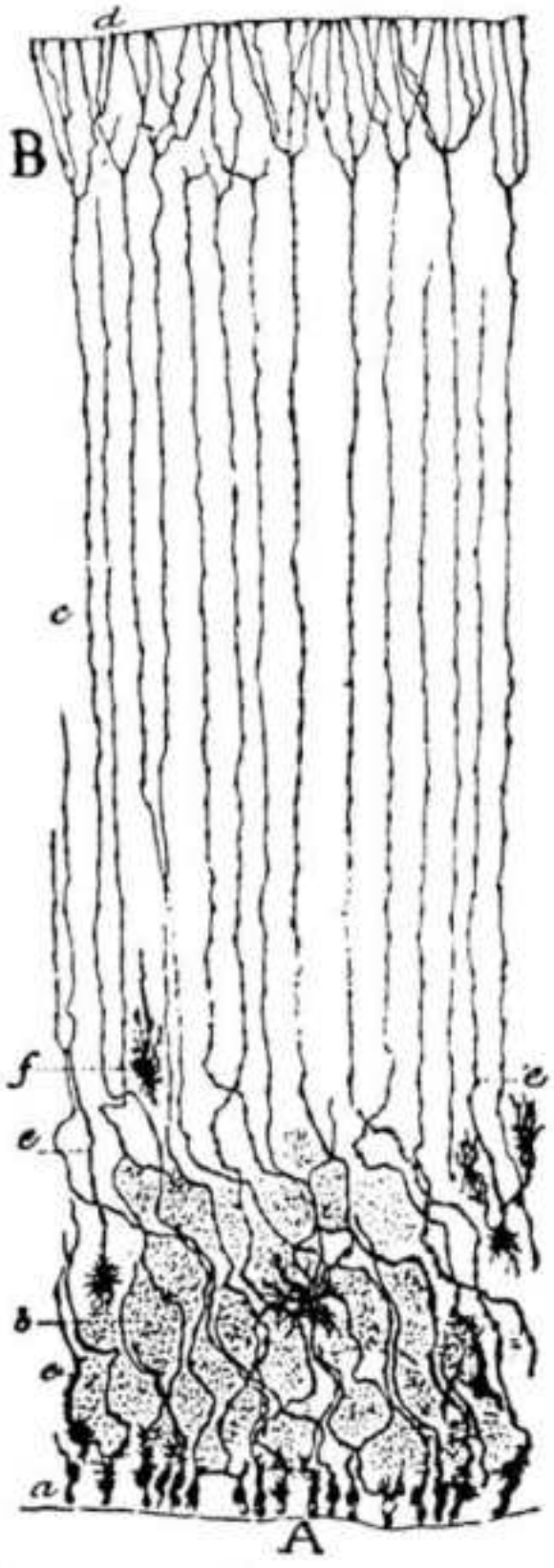

Table of contents

Figure index

Acknowledgements

First, I wish to thank my advisor, Simona Candiani, as well as Michael Schubert and Mario Pestarino, who have accompanied and supported me throughout my PhD studies. They taught me a lot.

I would also like to thank François Lahaye, Guy Lhomond, Jenifer Croce and Alessandra Contento for methodological advice and for making me feel home during my stays at the Laboratoire de Biologie du Développement de Villefranche-sur-Mer. The work presented in this dissertation was greatly implemented by TEM data produced by Federico Caicci and Lucia Manni as well as Thurston Lacalli, who also provided deep insights and helpful suggestions.

I am also very grateful to past and present members of Laboratory of Developmental Neurobiology of the University of Genoa, Valentina Obino, Tiziana Bachetti, Silvia Carestiato and Francesca Rosamilia, for creating a great working environment.

Finally, my deepest gratitude goes to my family. You were always there for me.

The research leading to these results received partial funding from the European Union's Horizon 2020 research and innovation program under grant agreement No 730984, ASSEMBLE Plus project to Matteo Bozzo and Simona Candiani.

Abstract

Glial cells play important roles in the development and homeostasis of metazoan nervous systems. However, while their involvement in the development and function in the central nervous system (CNS) of vertebrates is increasingly well understood, much less is known about invertebrate glia and the evolutionary history of glial cells more generally. An investigation into amphioxus glia is therefore timely, as this organism is the best living proxy for the last common ancestor of all chordates, and hence provides a window on the role of glial cells development and function at the transition between invertebrates and vertebrates. We report here our findings on amphioxus glia as characterized by molecular probes correlated with anatomical data at the TEM level. The results show amphioxus glial lineages express genes typical of vertebrate astroglia and radial glia and segregate early in development, forming what appears to be a spatially separated cell proliferation zone positioned laterally, between the dorsal and ventral zones of neural cell proliferation. Our study provides strong evidence for the presence of vertebrate-type glial cells in amphioxus while highlighting the role played by segregated progenitor cell pools in CNS development. There are implications also for our understanding of glial cells in a broader evolutionary context and insights into patterns of precursor cell deployment in the chordate nerve cord.

Introduction to the animal kingdom

Animal phylogeny

The first fundamental division in the animal tree is between non-bilaterians and bilaterians, that is bilaterally symmetric animals. Non-bilaterians animals are classified in the phyla Porifera (sponges), Placozoa, Ctenophora (comb jellies) and Cnidaria (hydras, corals and jellyfish). The bilaterians comprise all other animals. Non-bilaterians phyla are placed closer to the root of the animal tree and hence usually referred to as "basal" or early-branching". Bilaterians are commonly divided into two major groups: protostomes and deuterostomes. As the names suggest, these groups were originally distinguished according to the mode of mouth (*stóma*, in Greek) formation. In protostomes, indeed, the mouth derives from the blastopore (*protos* means "first" in Greek), while the blastopore of the deuterostomes produces the anus, and the mouth is secondarily formed (*deúteros* means "second" in Greek). Alternative phylogenies place the phylum Xenacoelomorpha, comprising the genus *Xenoturbella* and acoel worms, either in the deuterostomes (Cannon et al., 2016; Philippe et al., 2011) or at the base of bilaterians, prior to the split between protostomes and deuterostomes (Rouse et al., 2016). One of the most widely accepted animal phylogenies is presented in Fig. 1. The major animal groups will be briefly introduced in the following paragraphs.

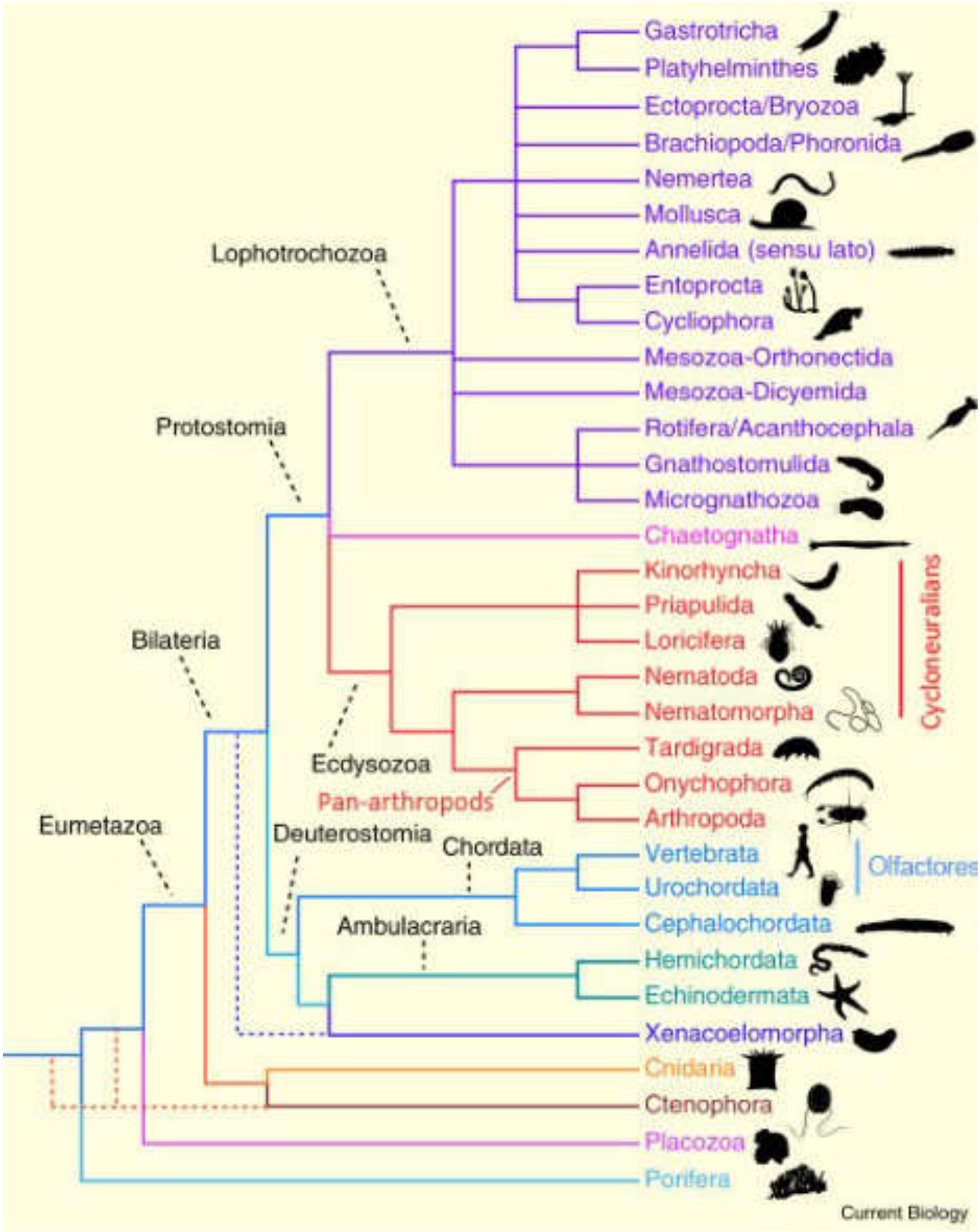

Figure 1. Current consensus tree of the major animal phyla. Alternative possible positions are indicated by dashed lines. Modified from Telford et al. (2015).

The protostomes

The protostomes consist of three branches: ecdysozoans, lophotrochozoans (or spiralians) and the phylum Chaetognatha, previously classified in the deuterostomes. The ecdysozoans are a clade of animals that grow by ecdysis, that is molting their cuticle. With 4.5 million estimated living species (Telford et al., 2008), the ecdysozoans are by far the most diverse and conspicuous animal clade, including the Arthropoda (e.g., insects, spiders, crustaceans), the Nematoda (roundworms) and six smaller phyla. The principal invertebrate model organisms, *Caenorhabditis elegans* and *Drosophila melanogaster* are ecdysozoans. Two superphyla are recognized: the pan-arthropods, which includes arthropods, onychophorans and tardigrades, and the cycloneuralians, which include nematodes, nematophorms, kinorhynchs, loriciferans and priapulids (Telford et al., 2008). The lophotrochozoans are characterized by spiral cleavage and trochophore-like larvae. They comprise well-known animals such as mollusks (Mollusca), segmented worms (Annelida) and flatworms (Platyhelminthes). The chaetognaths, commonly called arrow worms, are a phylum of planktonic or benthic predatory marine worms.

The deuterostomes

The deuterostomes represent a well-established branch of the bilaterians traditionally defined by three developmental peculiarities: deuterostomy, radial cleavage and formation of coelomic cavities by enterocoely, that is from evaginations of the archenteron. However, both deuterostomy and radial cleavage are not restricted to deuterostomes and enterocoely is not present in all deuterostomes. In particular, deuterostomy may represent the primitive bilaterian condition (Peterson & Eernisse, 2001). Despite this, the terms protostomes and deuterostomes are still in use to indicate the two main branches of bilaterians. More recently, pharyngeal slits (sometimes called gill slits) were established as a more reliable defining feature of deuterostomes (Gillis et al., 2012).

Most molecular phylogenies support the deuterostomes as a monophyletic group, that is a natural group comprising all descendants from a common ancestor (Bourlat et al., 2006). However, Telford and collaborators (2015) stressed the fact that the deuterostomes branch is short compared to that of the protostomes, suggesting that the evolutionary distance between the last common ancestor of bilaterians (urbilaterian) and the last common ancestor of deuterostomes is very short. More recently, they claimed that the deuterostomes lack support as a monophyletic group (Kapli et al., 2020). These considerations would imply that the urbilaterian was more alike deuterostomes than protostomes or, in the extreme scenario, that the urbilaterian coincides with the last common ancestor of deuterostomes.

Deuterostomes have been traditionally classified into three phyla: hemichordates, echinoderms and chordates. Recently, Satoh and colleagues (2014) proposed chordates as a superphylum consisting of three phyla: cephalochordates, tunicates and vertebrates. Molecular phylogenies support the grouping of

hemichordates and echinoderms in a clade, called Ambulacraria, and place cephalochordates at the base of tunicates and vertebrates, which together form the Olfactores clade (Delsuc et al., 2006; Jefferies, 1991).

The ambulacrarians

Although they present different adult body plans, hemichordates and echinoderms develop from similar dipleura-like larvae. On this ground, they were originally grouped as ambulacrarians (Metschnikoff, 1881), which was subsequently corroborated by molecular data (Halanych, 1995).

The hemichordates are generally divided into two classes: the colonial pterobranchs and the solitary enteropneusts, commonly called acorn worms. The position of the pterobranchs is either unresolved or basal to the enteropneusts (Winchell et al., 2002) (Fig. 2). However, some molecular phylogenies place the pterobranchs as a sister group of the harrimaniid enteropneusts, making enteropneusts paraphyletic (Cannon et al., 2009). Enteropneusts vary in size from a few centimeters to a meter and exhibit a tripartite body organization with an anterior prosome (or proboscis), an intermediate mesosome (or collar) and a posterior metasome (or trunk). Most acorn worms burrow in the sand and feed on particulate organic matter. The anterior part of the gut forms an axial supportive rod in the proboscis called stomochord, which has been proposed as a homolog of the chordate notochord (reviewed in Annona et al., 2015). The pharynx is perforated by cartilaginous gill slits, which resemble amphioxus pharyngeal slits also from the molecular point of view (Gillis et al., 2012). Pterobranchs are small (up to a few centimeters) animals that live in secreted tubes, generally in colonies. They filter-feed using a specialization of the collar, called lophophore. Compared to echinoderms, hemichordates, particularly enteropneusts, appear to have retained many tracts shared with the last common ancestor of the deuterostomes (Cameron, 2005). Enteropneusts are thus a good model to study the earliest body plan modification in the chordate lineage (reviewed in Röttinger & Lowe, 2012).

Adult echinoderms are characterized by a unique pentaradial symmetry, although some echinoids and holothurians externally appear bilateral. This is indeed a secondary character, as demonstrated by the bilaterality of their larvae. Echinoderms are further characterized by a calcareous endoskeleton, and a water vascular system used for locomotion. The echinoderms represent the sister group of the hemichordates and are divided into five classes: crinoids (feather stars and sea lilies), echinoids (sea urchins, heart urchins and sand dollars), holothuroids (sea cucumbers), asteroids (sea stars), and ophiuroids (brittle stars and basket stars).

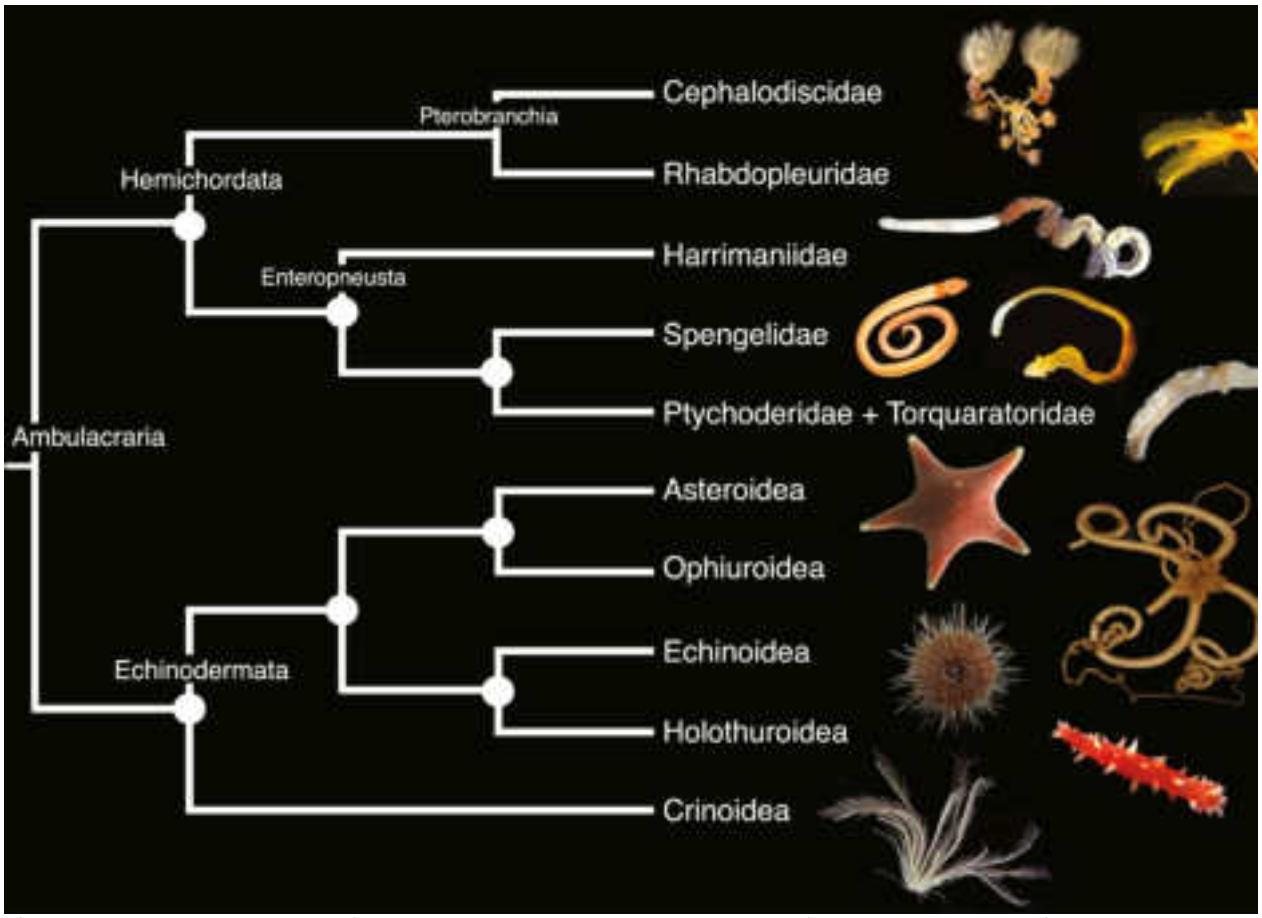

Figure 2. Tree of ambulacrarians reconstructed from phylogenomic datasets supporting pterobranchs as sister group of enteropneusts. From Cannon et al. (2014).

The chordates

The chordates have been traditionally considered a monophyletic group since the description of the notochord in the larva of the ascidian *Ciona intestinalis* (Kowalevski, 1866). On the morphological ground, tunicates were originally considered basal to cephalochordates and vertebrates. The latter two are indeed united by the presence of metameric somites, which are absent in tunicates. However, most modern molecular phylogenies agree that tunicates are the sister group of vertebrates, suggesting that they lost muscle segmentation (Delsuc et al., 2006; Holland et al., 2008; Putnam et al., 2008). The chordates present some synapomorphies, i.e., exclusive characters inherited from a common ancestor: (1) the notochord, present at least during development, (2) the dorsal hollow neural tube formed by neurulation, (3) the pharyngeal slits, (4) the endostyle, which is modified into the vertebrate thyroid and (5) the post-anal tail.

Cephalochordates are a small phylum comprising only about 35 species (Poss & Boschung, 1996) divided into three genera: *Branchiostoma*, *Epigonichtys* and *Asymmetron*. *Asymmetron* seems to be basal within cephalochordates (Igawa et al., 2017). Despite an estimated divergence time of about 42 million years (Igawa et al., 2017), all species are morphologically very similar to one another and occupy the same ecological niche of marine filter feeders. Interestingly, hybrid larvae between *Asymmetron* and

Branchiostoma can be obtained in the laboratory (Holland et al., 2015). These considerations explain the use of the same vernacular name to indicate all cephalochordate species: amphioxus or lancelets.

Tunicates, as the name suggests, are characterized by the production of an extracellular tunic made of cellulose that surrounds the organism. There are around 3000 species of tunicates, traditionally divided into three classes: ascidians (sea squirts), thaliaceans (salps, pyrosomes and doliolids) and appendicularians (larvaceans) (Holland, 2016). Phylogenomic analyses place the appendicularians sister to all other tunicates and nest thaliaceans inside ascidians, which appear to be paraphyletic (Delsuc et al., 2018; Kocot et al., 2018). The current consensus tree is reported in Fig. 3A.

The shape of adult tunicates is highly variable (Fig. 3B-J). Like cephalochordates, all tunicates are filter feeders and establish a water flow entering from the oral siphon and exiting from the atrial siphon of the tunic. Ascidians, the most abundant group of tunicates (ca. 3000 species) are benthic animals that adhere to solid substrates, such as rocks and man-made objects. Ascidians can be solitary or form colonies of several zooids. This group includes several developmental models such as *Ciona intestinalis*, *Phallusia mammillata*, *Halocynthia roretzi* and *Botryllus schlosseri*. In contrast to sessile ascidians, thaliaceans are pelagic organisms capable of swimming by water propulsion. Appendicularians are also pelagic and retain the larval body plan throughout their short life. The thaliaceans *Oikopleura dioica* is now a well-established model organism for evolutionary genomic studies.

Morphology is more conserved during development when their chordate nature is also more obvious. The tunicate larva is generally called “tadpole” since it is composed of a globular anterior part (head/trunk) containing the brain (sensory vesicle) and undifferentiated endo-mesoderm from which most adult organs will develop and a posterior rod-like part (tail) containing the dorsal hollow nerve cord, paraxial mesoderm (muscles) and the notochord. The notochord, which will be lost at metamorphosis in ascidians and thaliaceans, is thus present only in the tail. For this reason, tunicates used to be called also urochordates (*ourá* means “tail” in Greek), in contrast to cephalochordates, in which the notochord extends to the anterior-most tip of the head (*kephale* in Greek).

With over seventy thousand living species (IUCN, 2020), the vertebrate lineage had the greatest radiation among the deuterostomes and colonized a wide range of niches in marine, freshwater and land environments. Vertebrates have been traditionally classified in eight classes: *myxines* (hagfish), *petromyzontids* (lampreys), *chondrichthyans* or cartilaginous fish (sharks, rays, skates and chimaeras), *osteichthyans* or bony fish, *amphibians*, *reptiles*, *birds* and *mammals*. From a cladistic perspective, however, the bony fish are split into *actinopterygians* or ray-finned fish (comprising most species of bony fish) and *sarcopterygians* or lobe-finned fish (lungfish, coelacanth), the latter including also the *tetrapods* (i.e., amphibians, reptiles, birds and mammals). Depending on the context, additional classifications can be made such as between jawless (or agnathans or cyclostomes: lampreys and hagfish) and jawed vertebrates

(or gnathostomes: fish, amphibians, reptiles, birds and mammals) or between anamniotes (fish and amphibians) and amniotes (reptiles, birds and mammals).

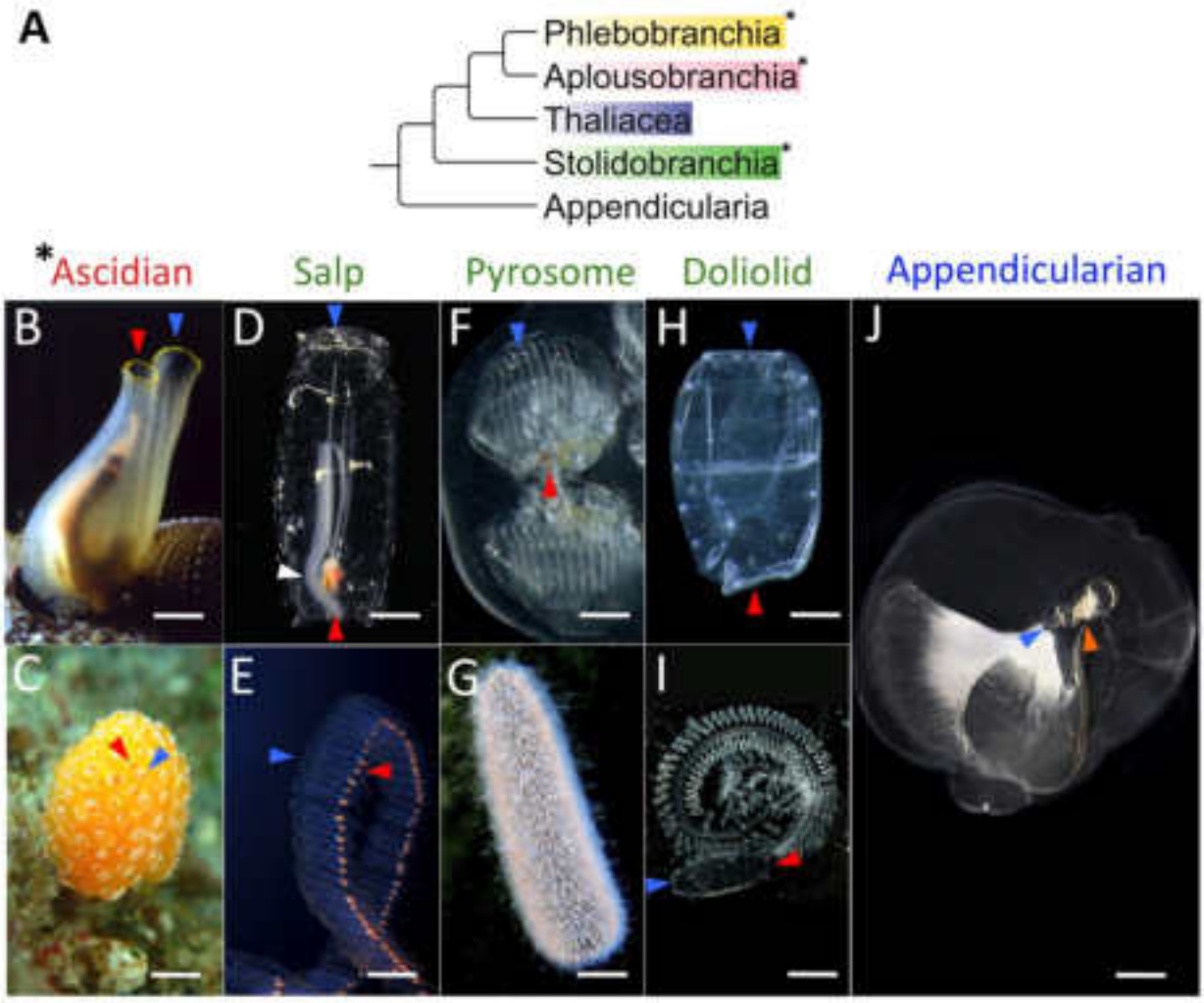

Figure 3 Phylogeny and morphology of tunicates. **A**: Tree of the main tunicate groups according to Kocot et al. (2018). **B-J:** Adult morphologies in the classic tunicate classes. Blue and red arrowheads indicate oral and atrial siphons, respectively. The species represented are: *Ciona intestinalis* (B), *Pseudodistoma kanoko* colony (C), *Salpa fusiformis* (D), *Pegea confederata* (E), *Pyrosomella verticilliata* (F), *Pyrosoma atlanticum* (G), *Doliolum denticulatum* (H), *Dolioletta gegenbauri* (I), *Oikopleura dioica* (J). Scale bars are 10 mm in B,D; 15 mm in C; 1 mm in F,H; 40 mm in E,G; 5 mm in I; 0.5 mm in J. From Lemaire (2011).

Diversification of metazoans nervous systems: a focus on glial cells

A nervous system can be defined as an organized collection of neurons interconnected through synapses that collaborate to acquire information from the periphery, process it and initiate adequate responses. Neurons are cells specialized in the generation and transmission of electrical signals in form of changes of membrane potential. Once the changes in voltage reach a certain threshold, an electrical signal, called an action potential, is generated that travel along the neurite to the synapse. Here, the action potential determines the release of neurotransmitter molecules in the synaptic cleft, which act on specific receptors located on the postsynaptic plasma membrane (belonging to another neuron or an effector cell). At the synaptic level, thus, the electrical signal is translated into a chemical stimulus. In some instances, electrical signals can pass directly from one nerve cell to another. In addition to synaptic transmission, sometimes called “wired transmission”, neurons can also communicate through volume transmission, that is the paracrine release of neurotransmitters.

The cellular components of nervous systems: neurons and glia

The cellular components of bilaterian nervous systems are neurons and glial cells. Neurons are classified into sensory neurons, which encode various stimuli (e.g., touch, light, flavors) into electrical signals, interneurons, which interconnect different neurons, and motor neurons, which control muscles and other effector organs. In the simplest nervous systems, however, the same neuron can perform sensory, motor and inter-neuronal functions and glial cells can be absent.

After over 160 years of research (Kettenmann & Verkhratsky, 2008), a proper definition of glia taking into account the diversity of glial cells found in animals is still elusive. The most widely accepted definition of glia derives from Bullock and Horridge (1965) and includes any cell residing in the nervous system that is neither a neuron nor a vascular cell. Accordingly, glial cells are a heterogenous class that differ in origin, morphology, and function. A first classification of glial cells is between microglia and macroglia. Microglia are resident macrophages that differentiate from myeloid precursors located in the yolk sac and bone marrow that infiltrate the developing nervous system (Ginhoux et al., 2013). Conversely, all macroglial cells have a neuroectodermal origin, like neurons.

Criteria to define glial cells

Glial cells can be recognized based on morphological, cytological, and molecular characters or markers that they exhibit. Two fundamental glial morphologies are recognized: cuboidal cells that line the border of the CNS (like vertebrate ependymal cells) and cells with fine processes closely associated with neuron cell bodies or neurites (Bullock & Horridge,1965). An alternative morphology can be observed: cells flattened around single neurites or axon bundles that, in some taxa, produce myelin sheaths. The identification of glial cells using morphological markers is often not straightforward. Besides, these characters are typically observed only in groups with well-developed glia (Hartline, 2011).

At the ultrastructural level, cytological markers such as cytoplasmic inclusions and cytoskeletal elements can be used to distinguish glia from neurons. For example, glial cells typically perform energetic functions and thus contain glycogen granules. Axons are characterized by microtubules while glia typically contain intermediate filaments. However, this is not always true. For instance, arthropod glia contain microtubules instead of intermediate filaments. Deuterostome glia possess both: intermediate filaments are found in ependymoglia and astroglia while oligodendroglia contain microtubules.

Molecular markers are probably the safest tool to identify and characterize glial cells, especially if coupled to morphological and cytological characters. Some genes are specifically transcribed in glial cells and can be used for determining which cells in a developing neural tube are destined to become glia. A list of molecular glial markers has been drafted for both vertebrates and drosophila but only a few have been investigated in other invertebrates (Hartline, 2011). Among these, GFAP-like intermediate filaments, EAAT transporters and glutamine synthetase have been more or less broadly analyzed in invertebrates. Using a combination of these markers, the presence of glia has been successfully assessed in most bilaterian groups (Fig. 4).

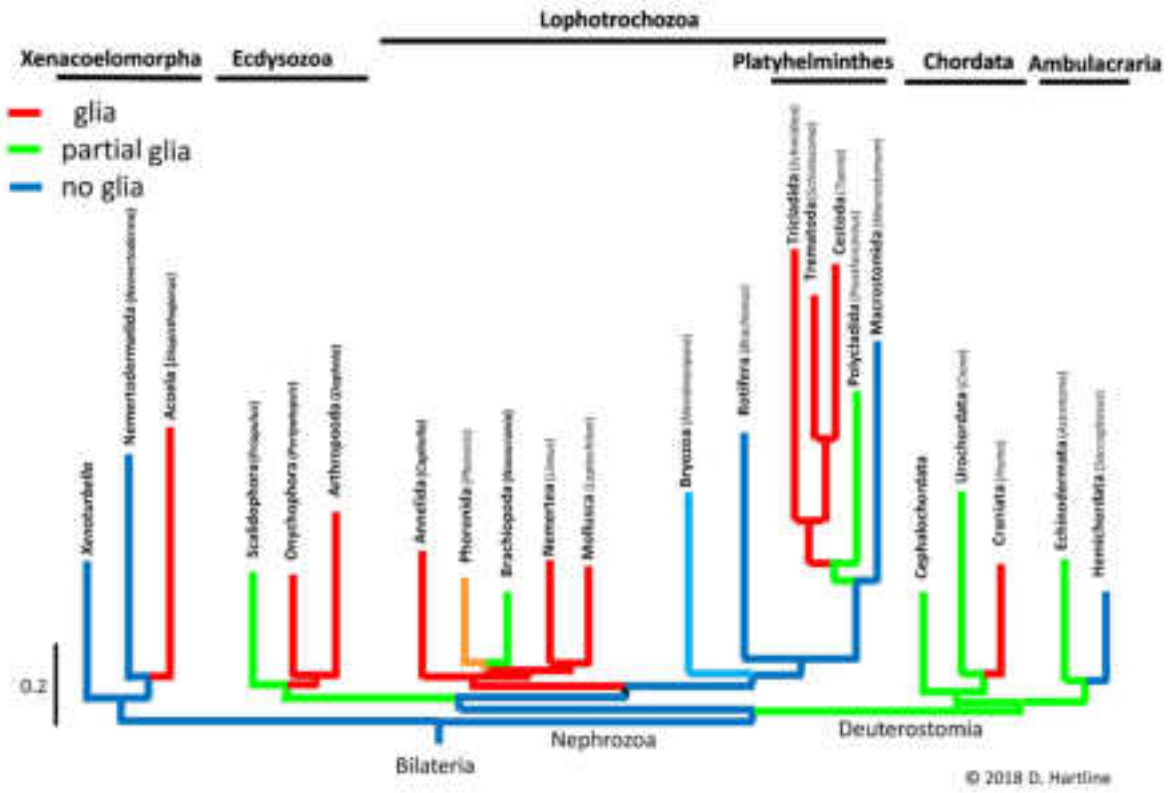

Figure 4. Glia phylogeny in bilaterians based solely on morphological data. One interpretation of the tree is that glia-like cells independently evolved five times in xenacoelomorphs, pan-arthropods, twice in lophotrochozoans and in deuterostomes. Modified from www.pbrc.hawaii.edu/~danh/GliaEvolution/ (last accessed December 20th, 2020).

Quantifying glial cells

For decades it has been erroneously thought that the number of glial cells with respect to neurons (i.e., the glia-to-neuron ratio) had increased with the evolution of complex nervous systems and reached the peak in the human brain, where glia was thought to outnumber neurons by a factor of ten (Verkhratsky & Butt, 2018). More reliable figures came with the perfecting of the isotropic fractionator (Herculano-Houzel & Lent, 2005). The technique consists of extracting nuclei from fixed neural tissue, staining them with DAPI and for the neuronal marker NeuN and, using a counting chamber, determining the ratio between non-neuronal ($DAPI^+/NeuN^-$) and neuronal ($DAPI^+/NeuN^+$) nuclei. The currently estimated glia-to-neuron ratio in the mammalian cerebral cortex is about 0.3-0.4 in rodents, 1.1 in the cat, 1.5-1.7 in humans, and between 4 and 8 in whales (Verkhratsky & Butt, 2018). Invertebrates tend to have fewer glial cells compared to vertebrates (Fig. 5). There are exceptions, though. The buccal ganglia of the great ramshorn snail (*Planorbis corneus*), for instance, has a glial-to-neuron of about 1.5, comparable to that of the human cortex (Pentreath et al., 1985).

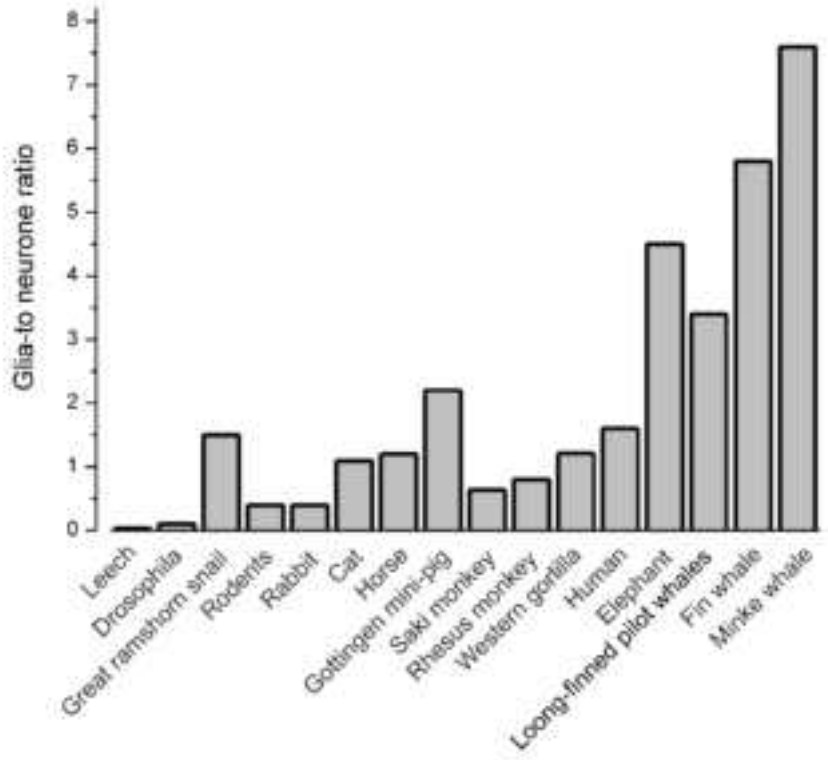

Figure 5. Glia-to-neuron ratio in invertebrates and vertebrates. From Verkhratsky & Butt (2018).

Different organizations of animal nervous systems

Placozoans and poriferans lack neurons and proper nervous systems and yet show behavior. Most sponges, for example, can regulate the diameter of their pores (called oscula) by cellular contraction, but this is a local event (Prosser et al., 1962). In addition, hexactinellid sponges can propagate electrical signals through syncytial structures to coordinate the flagellar beating of the choanocytes (Leys et al., 1999).

The other metazoans possess nervous systems that can be either diffuse or centralized or a combination of both. The entire nervous system of cnidarians and ctenophores is organized as a *plexus*, which is a coplanar net of neurons interconnected by neurites (Richter et al., 2010). The type of plexus found in these phyla is also called a nerve net because it is functionally autonomous and can transmit signals in all directions (Hejnol & Rentzsch, 2015; Richter et al., 2010). The nervous systems of ctenophores and cnidarians are devoid of glia with the possible exception of Scyphomedusae, in which some glia-like cells were reported (Bullock & Horridge, 1965). However, their identity has not been analyzed in detail and hence remains uncertain (Hartline, 2011).

A plexus is often associated with an epithelium and hence called either epidermal plexus, if associated with the epidermis, or gastrodermal, if associated with the digestive epithelium. Further distinctions can be made based on the position of the neurons with respect to the epidermal cells. An *intraepidermal plexus* has neurites between the epidermal cells. A *basiepidermal plexus* is an

intraepidermal plexus where the neurites are localized in the basal region of the epithelium, in contact with the basal lamina. A *subepidermal plexus* is located below the basal lamina (Richter et al., 2010).

In the nervous systems of bilaterians, a consistent number of neurons tend to aggregate into variously specialized structures that constitute the central nervous system (CNS). CNSs can assume various organizations in different animal groups. In the simplest form, neurons form a mass, called *ganglion*, where the cell bodies are concentrated in the cortical area project neurites to the center, forming a neuropil (Richter et al., 2010). If the cluster of neurons and their neurite bundles extend along the anteroposterior axis of the body, it is called a *nerve cord* (Fig. 6). The position of the nerve cord divides the bilaterians into gastroneuralians, which have ventral nerve cords and are protostomes, and notoneuralians, which possess dorsal nerve cords and are deuterostomes. In gastroneuralians, nerve cords may or may not contain ganglia. For instance, arthropods and annelids typically possess *rope-ladder-like* nervous systems where two longitudinal lines of ganglia are joined by neurites antero-posteriorly (connectives) or transversally (commissures). Other protostomes, such as onychophorans (Mayer & Harzsch, 2007), have *medullary nerve cords*, where cell bodies are positioned in the cortical layer and surround the central neuropil (Richter et al., 2010). The nerve cord of chordates contains a central canal filled with fluid and is thus called *neural tube*. The CNS is often associated with one or more plexuses that represent the peripheral nervous system (PNS).

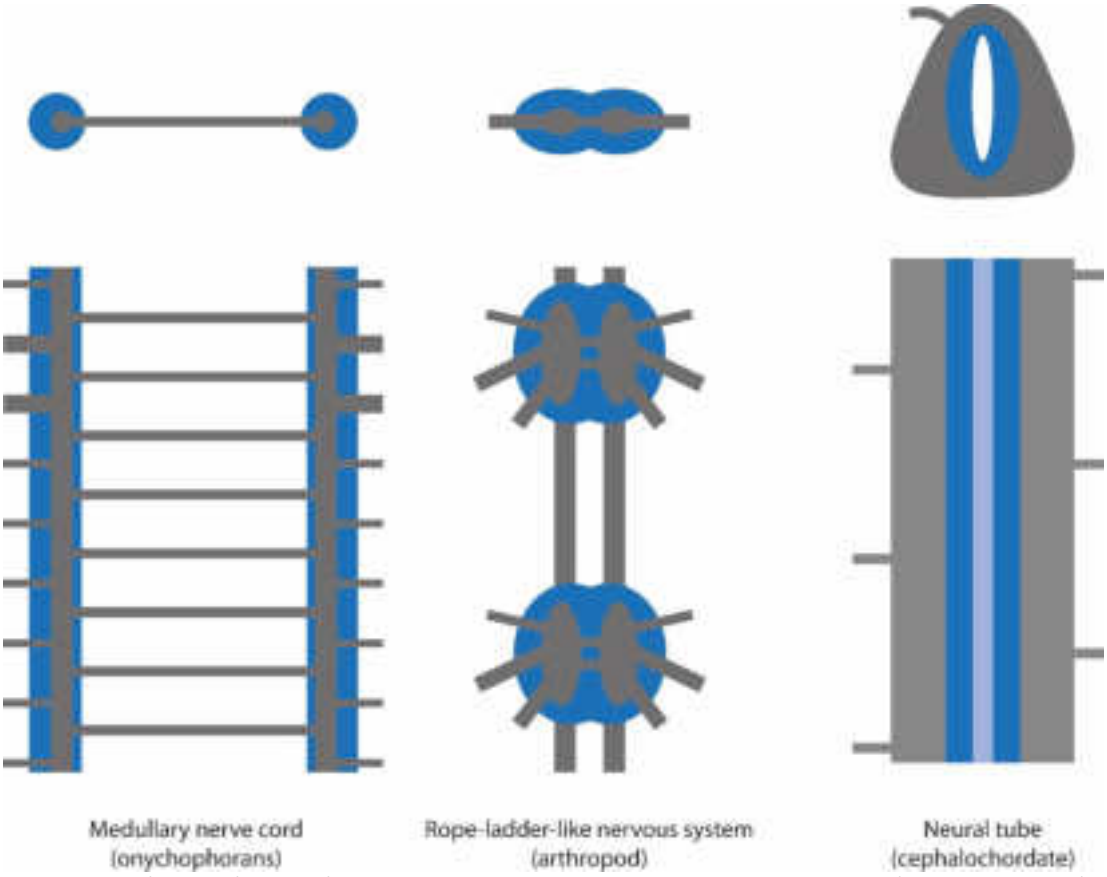

Figure 6. Schematic drawing of different types of nerve cords that can be found in metazoans viewed in transverse section (top) and dorsally (bottom). Blue: neuronal cell bodies; grey: neurite bundles (neuropil). Elaborated from Mayer & Harzsch (2007) and Richter et al. (2010).

The nervous systems of different animals, thus, may vary greatly in their organization. Morphological diversity has been extensively studied in the past (and, to a lesser extent, still is). However, molecular investigations have been limited to vertebrates and a few invertebrate models, such as *Drosophila melanogaster* and *Caenorhabditis elegans*. Detailed descriptions of glial cells in invertebrates are particularly rare. Limited mainly to anatomical descriptions (Hartline, 2011), it has proven difficult to make useful comparisons between taxa. The variety of neural organizations observed in invertebrates makes comparisons of glial cell types very difficult, not only with vertebrates but also with other invertebrate taxa (Coles, 2009; Ortega & Olivares-Bañuelos, 2020). The following sections will describe the neural organization of the main animal branches for which reliable information about glial cells is available.

The nervous systems of vertebrates

The CNS of vertebrates is a hollow nerve cord dorsal to the digestive tract and is associated with a PNS responsible for collecting sensory inputs from and distributing orders to effector organs. The CNS consists of the brain, located inside the skull, and the spinal cord, protected by the backbone. The brain originates from the neural tube, which becomes segmented into three primary vesicles: *forebrain* (prosencephalon), *midbrain* (mesencephalon) and *hindbrain* (rhombencephalon). As development proceeds, five secondary vesicles are generated as the forebrain divides into telencephalon and diencephalon and the hindbrain divides into metencephalon and myelencephalon. During vertebrate evolution, the various components of the brain changed in size and importance, according to the class and lifestyle of the organism. The PNS consists of the nerves emanating from the brain and spinal cord and the ganglia and plexuses located outside the brain and spinal cord.

A new cell type emerged in ancestral vertebrates that is responsible for many of the novelties of this group of animals: the *neural crest*. The neural crest is a transient population of stem cells that differentiate from the borders of the neural plate, migrate all over the body following specific routes and differentiate in many cell types as diverse as the facial skeleton, adrenal gland and pigment cells of the skin. In particular, the whole PNS (neurons and glia) originates from the neural crest. The emergence of the neural crest was pivotal in the evolution of a “new head” in ancestral vertebrates, which allowed the transition from filter feeders to agile predators (Gans & Northcutt, 1983).

Different glial cell types are present in the vertebrate nervous system, each contributing in specific ways to the maintenance of homeostasis. As will be discussed later in this chapter, some of these functions are also performed by invertebrate glia while others – as far as we know – are exclusive of vertebrates. Glial functions include:

- Morphogenesis: during development, glial cells guide neuronal migration and neurite extension and control synaptogenesis and synaptic pruning.
- Tissue turnover: some glial cells are stem elements.

- Metabolism: glial cells uptake glucose from the blood, store energy in form of glycogen and provide metabolic substrates to neurons in form of lactate (glia-neuron lactate shuttle).
- Ion regulation in the extracellular space.
- Neurotransmitter homeostasis: glial cells (especially astroglia) uptake neurotransmitter from the synaptic cleft, modulating neurotransmission, and recycle it to the presynaptic neuron.
- Defense: microglia are professional phagocytes, glial cells participate in the blood-brain barrier, astroglia can respond to neural damage either by astrogliosis (i.e., glial scarring) or regeneration – depending mainly on the vertebrate group.
- Axon conduction: oligodendrocytes and Schwann cells ensheathe neurites with myelin sheaths which are thought to facilitate and speed up the conduction of electrical signals.
- Signaling.

Typically, vertebrate glia are divided into PNS and CNS glia. The glial cells found in the PNS are *Schwann cells*, which either enwrap multiple non-myelinated neurites or myelinate single neurites; *satellite cells*, which surround neuronal cell bodies in peripheral ganglia; *olfactory ensheathing glia*, which are found in olfactory organs; *enteric glia*, which resides in the enteric nervous system. PNS glia derive from the neural crest. CNS glial cells of ectodermal origin are generally divided into radial glia, astroglia (comprising astrocytes) and oligodendroglia (oligodendrocytes and oligodendrocyte precursor cells – also called NG2-glia).

Astroglia, ependymal glia and radial glia

The term "astroglia" is used with different nuances. Sometimes it is used as a synonym of astrocytes (Verkhratsky & Nedergaard, 2018); other times ependymal glia and radial glia are also included (Verkhratsky, Ho, Zorec, et al., 2019). Moreover, most classifications of astroglial cells are based on mammalian cell types and thus poorly suited for comparative studies.

Astrocytes are heterogeneous cells characterized by numerous processes and a star-shaped morphology residing in the brain and spinal cord. Traditionally, two types of astrocytes have been distinguished on morphological ground: *protoplasmic astrocytes*, characterized by shorter and highly branching processes and residing in the gray matter, and *fibrous astrocytes*, characterized by longer processes and residing in the white matter. Additional specialized subpopulations of astrocytes are found in higher primates, including humans (Verkhratsky, Ho, & Parpura, 2019). Some authors classify the radial glia-like cells without an ependymal process found in adult anamniotes as *radial astrocytes* (e.g., Reichenbach & Wolburg, 2013). Despite their different morphologies, their main physiological properties are mostly conserved. Astrocytes are greatly involved in maintaining homeostasis in the CNS, with roles ranging from ion balance, trophic support, neurotransmitter uptake and recycling, neurogenesis and network establishment, development of the blood-brain barrier and glymphatic system. At least in

mammals, they tend to establish multicellular networks interconnected by gap junctions known as syncytia (Giaume et al., 2010), although the term is used *sensu lato* since the single astrocyte maintain their identity, nucleus, and plasma membrane.

Astrocytes are actively involved in intercellular communication in the CNS. Astrocytic processes typically enwrap the synapse which, together with the presynaptic and postsynaptic terminal, assume a tripartite organization (Araque et al., 1999). At glutamatergic synapses, the astrocyte uptake glutamate, thus regulating the neurotransmission event, and shuttle them back to the presynaptic terminal in the so-called *glutamate-glutamine cycle*. To do so, astrocytes use excitatory amino acid transporters (EAAT) 1 and 2 to take up glutamate from the synaptic cleft, which is subsequently converted to glutamine by the enzyme glutamine synthetase (GS). Glutamine is then released in the synaptic space and captured by the presynaptic neuron using sodium-coupled neutral amino acid transporters (SNATs). Once in the neuron, glutamine is hydrolyzed to glutamate, quickly replenishing the neurotransmitter pool. Since neurons do not express pyruvate decarboxylase (PD), they are incapable of performing *de novo* synthesis of glutamate from glucose and so are totally dependent on glutamate-glutamine cycle. The situation is similar at GABAergic synapses. To synthesize GABA using the enzyme GABA decarboxylase (GAD), the presynaptic neuron requires glutamate, which comes in form of glutamine from astrocytes. The expression of GS, thus, is a hallmark of vertebrate astroglia. In addition to these functions, astrocytes respond to extracellular neurotransmitters by releasing their own signaling molecules such as glutamate, GABA, D-serine and ATP, globally called gliotransmitters (Perea et al., 2009).

Ependymal glia include all glial cells that establish contact with the ventricular surface (Wolburg et al., 2009). According to this definition, radial glia are a subset of ependymal glia characterized by a bipolar morphology and long radial processes that span the wall of the CNS. Conversely, *ependymal cells* are epithelioid cells that form the lining of the ventricles and central canal of the CNS. Ependymal cells contact the remnants of embryonic vessels at their basal pole and present both microvilli and cilia that abut the lumen of the CNS and facilitate the movement of the cerebrospinal fluid (CSF). The CSF is produced by another type of ependymal glia, the choroid plexus cells, modified ependymal cells restricted to specific regions of the brain.

In vertebrates, *radial glia* are key elements of neural development. They differentiate early in neurogenesis and serve as neural stem cells (Alexandre et al., 2010; Malatesta et al., 2000). Their processes span the ventricular zone, which allows them to act as a scaffolding along which newborn neurons are guided to their final positions (Hatten & Mason, 1990). In mammals, most radial glia disappear at the end of neurogenesis, differentiating into neurons, ependyma, or parenchymal glia such as astrocytes or oligodendroglia (Fogarty et al., 2005; Kriegstein & Alvarez-Buylla, 2009). However, radial glia do persist in a few regions of the adult brain, as in the wall of the lateral ventricle, where they have a continuing role

as neural stem cells (Kriegstein & Alvarez-Buylla, 2009). Sometimes, these adult radial glia-like cells are called *tanycytes* (Götz, 2013; Wolburg et al., 2009).

In contrast to mammals, radial glia is found in most regions of the adult CNS in fish, amphibians and reptiles, in particular in species characterized by so-called laminar brains (as defined by Butler & Hodos 2005), including, for example, chimaeras, gars, coelacanths and amphibians. Laminar brains are virtually devoid of ependymal cells and parenchymal astrocytes (Jurisch-Yaksi, Yaksi, & Kizil, 2020; Kálmán & Gould, 2001), and radial glia thus appear to replace these in establishing the ependymal barrier and for some astrocytic functions (reviewed in Jurisch-Yaksi et al., 2020). In the adult, this population should be referred to as *ependymo-radial glia* (Becker & Becker, 2015).

The distinction between radial glia, ependymal cells and astrocytes across vertebrates is therefore not straightforward (Götz, 2013), but one key feature that does appear to distinguish radial glia from ependymal cells and astrocytes is the role played by the former as a neural progenitor, both during embryogenesis and in the adult. The brains of vertebrates with conspicuous radial glia are thus characterized by a high regenerative capacity, while those of adult mammals, which lack radial glia, respond to brain injury with glial scarring (Kroehne et al., 2011). Similar observations have been made in adults of the sea cucumber, an echinoderm, where radial glia proliferation in response to traumatic injury produces both glial cells and neurons (Mashanov et al., 2013).

Oligodendroglia

Oligodendroglia groups oligodendrocytes, non-myelinating (satellite) oligodendrocytes and adult oligodendrocyte precursor cells (OLPs), formerly known as NG2-glia. *Oligodendrocytes*, like the peripheral Schwann cells, produce myelin sheaths that insulate axons in the CNS. A single oligodendrocyte can myelinate up to 30 axon segments by sending processes that roll up around the target axon (Ransom et al., 1991). Myelin allows saltatory conduction of electrical signals, which enables faster propagation in myelinated axons compared to unmyelinated axons of the same caliber. Myelinating oligodendrocyte also provide energetic substrates such as lactate and pyruvate to the axons they envelope (Stadelmann et al., 2019).

Glia in lophotrochozoans

Knowledge of lophotrochozoans neurobiology is very patchy, with molecular and functional data available only for a few animal models. In this group, the best-studied animals are flatworms, annelids and mollusks (particularly cephalopods). It is worth to mention that the bristle worm *Platynereis durmelii*, being easily reproduced and grown in the laboratory and amenable to genetic manipulation, has been established as a genetic model organism.

Annelids

The annelid *Hirudo officinalis* (medicinal leech) was one of the first model organisms employed to study the physiology of glial cells. Leeches have a rope-ladder-like nervous system with 34 ganglia of which the anterior-most six ganglia are fused to form the ring-like anterior brain and the posterior-most seven ganglia are fused into the caudal ganglion. Between these two masses, 21 ganglia lie, each one innervating a body segment. Each ganglion contains 400-700 monopolar neurons, whose cell bodies are grouped in six packets (Fig. 7), and ten glial cells (Coggeshall & Fawcett, 1964; Deitmer et al., 1999). The glial cells consist of six packet glial cells, each one enclosing the neuron cell bodies in one packet, two giant neuropil glial cells and two connective glial cells, ensheathing neurites.

Due to their size, with a cell body of about 100 µm and processes extending across the whole neuropil, the giant neuropil cells, have been extensively studied in pioneering glia physiology studies in the 1960s (Kuffler & Potter, 1964). These cells display a vast assortment of receptors, ion channels, and transporters and likely maintain ionic and neurotransmitter homeostasis in the neuropil (Deitmer et al., 1999). The connective glial cells are probably involved in providing mechanical and metabolic support to the neurites they ensheathe (Verkhratsky & Butt, 2013). Similarly to vertebrate astrocytes, all glial cells are interconnected through gap junctions, forming a glial functional syncytium that surrounds the whole nervous system of the leech (Verkhratsky & Butt, 2013). However, due to the lack of molecular data, it is impossible to propose a homology between the giant neuropil glial cells, as well as any other glial cells of the leech, and the glia of other animals.

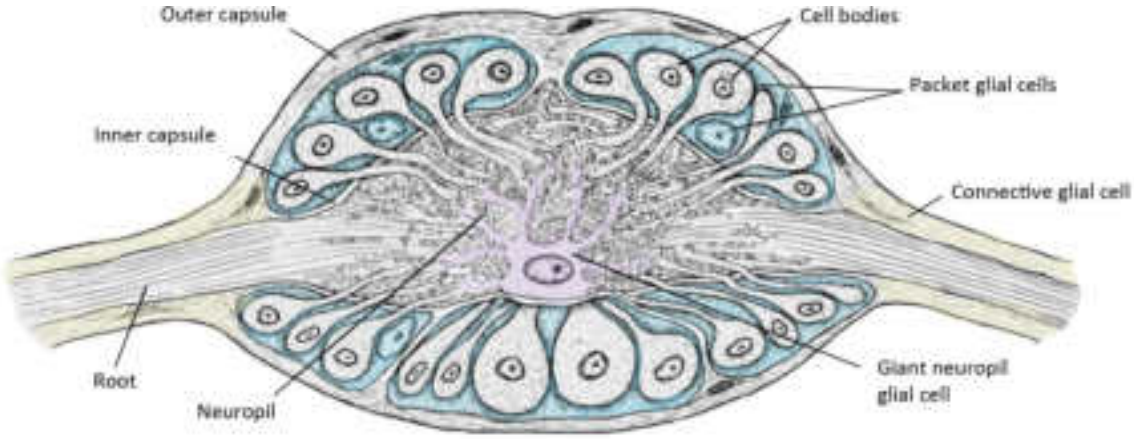

Figure 7. Schematic representation of a transverse section through a ganglion of the leech *H. officinalis*. Modified from Coggeshall & Fawcett (1964) and Coles (2009).

More recently, glial cells morphologically similar to deuterostome radial glia were found in various annelid species: the polychaetes *Platynereis durmelii* (Verasztó et al., 2020) and *Owenia fusiformis* (Beckers, Helm, Purschke, et al., 2019; Helm et al., 2017) and the magelonid *Magelona mirabilis* (Beckers, Helm, & Bartolomaeus, 2019).

Flatworms

Due to its high regenerative potential, the planarian nervous system has been well characterized over the years from both a morphological and molecular point of view (reviewed in Ross et al., 2017). Planarian CNS consists of a pair of cephalic ganglia (brain) joined by a commissure, dorsal photoreceptors and a medullary nerve cord (Fig. 8). The PNS is organized in subepidermal, submuscular and gastrodermal plexuses. The gastrodermal plexus is organized into an inner and an outer ring inserted in the wall of the pharynx. Diverse populations of planarian neurons use a variety of neurotransmitters, such as dopamine, serotonin, GABA, acetylcholine and various neuropeptides. Glial cells expressing the typical astroglial markers *eaat2*, *glutamine synthetase* and *gat* have been found in both the nerve cords and submuscular plexus of the freshwater planaria *Schmidtea mediterranea* (Roberts-Galbraith et al., 2016; Wang et al., 2016). These cells are most numerous in the neuropil of the nerve cord, where synapses are most abundant, and present electron-dense branches that extend throughout the neuropil (Roberts-Galbraith et al., 2016). Moreover, intramedullary glial cells express *ifl*, a planarian ortholog of vertebrate GFAP and neurofilaments. Overall, these cells are involved in neurotransmitter uptake and recycle and are comparable to vertebrate astroglia.

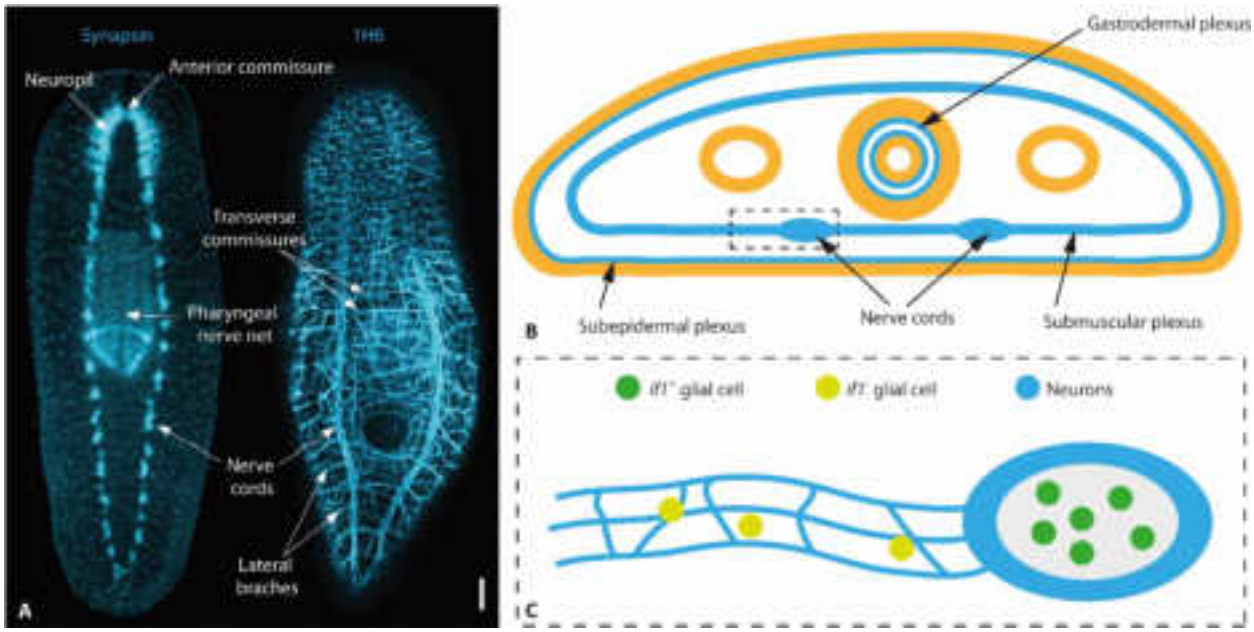

Figure 8. The nervous system of freshwater planarians. **A**: Nervous system labelled by immunohistochemistry for synapsin (staining neurons) and 1H6 (staining the PNS). Scale bar = 20 µm. **B**: Schematic representation of a planarian cross section showing the nervous system in blue. **C**: Enlargement of the nerve cord region boxed in **B**, showing distribution of glial cells. Image in A is taken from Ross et al. (2017), drawings were based on Ross et al. (2017) and Wang et al. (2016).

Glia in ecdysozoans

The ecdysozoans contain two of the most important genetic model organisms, the fruit fly *Drosophila melanogaster* and the nematode *Caenorhabditis elegans*. The nervous system of these organisms is extremely well-characterized, and so is its glial component. However, much less information is available for other groups.

Nematodes: *C. elegans*

In *C. elegans*, the number of neural cells is invariant between individuals and the whole nervous system has been reconstructed from serial TEM sections (White et al., 1986), on which the entire connectome was mapped. The nervous system of the hermaphrodite *C. elegans* adult contains 302 neurons, 50 glial cells of ectodermal origin, and 6 glial cells of mesodermal origin. Males have additional 89 neurons and 36 glial cells (Singhvi & Shaham, 2019). Like other cycloneuralians, *C. elegans* has a basiepidermal nervous system consisting of a ring-shaped brain encircling the pharynx and several ganglia located in the ventral and dorsal nerve cords (Hartenstein, 2019) (Fig. 9).

Most of the ectodermal glial cells (46 out of 50) are associated with the endings of sensory neurons in the sensilla. Each sensillum contains up to 12 sensory neurons and two glial cells: a sheath cell and a socket cell (Singhvi & Shaham, 2019). The remaining four ectoderm-derived glial cells, called CEPsh, ensheathe the brain and sense processes in the neuropil. The glial cells of mesodermal origin (GLR cells) are also located around the brain and establish gap junctions with both neurons and muscle cells.

CEPsh glia resemble vertebrate astrocytes at both molecular and morphological level. From the morphological point of view, CEPsh processes contact many synapses and ensheathe at least one of them (White et al., 1986). At the molecular-functional level, CEPsh glia express an ortholog of vertebrate *EAAT2* (*glt-1*) and likely clear glutamate from the synaptic space (Katz et al., 2019). Furthermore, like astrocytes, CEPsh glia also express an intermediate filament protein (*ifa-4*) orthologous to vertebrate GFAP (Katz et al., 2019), or more likely to type III and IV vertebrate neurofilaments. Interestingly, the development of CEPsh require orthologs of vertebrate *pax6* (*vab-3*) and *olig2* (*hlh-17*), like vertebrate spinal oligodendrocytes and, possibly, a subset of astrocytes (Tatsumi et al., 2018).

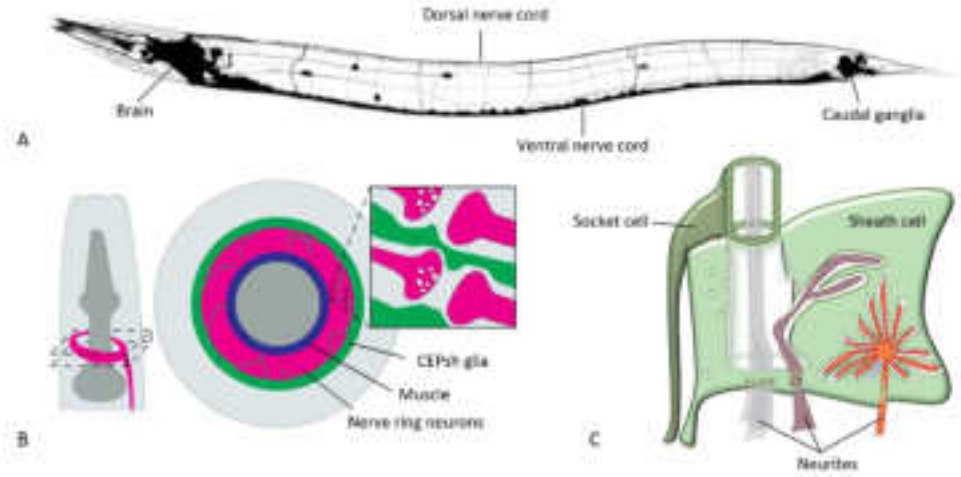

Figure 9. The nervous system of *C. elegans*. **A**: All neurons are labelled with GFP. Elaborated from www.sfu.ca/biology/faculty/hutter/hutterlab/research/Ce_nervous_system.html. **B**: Scheme of the head region (left) in dorsal view and transverse section of the region boxed (right). From Katz et al. (2019). **C**: Schematic representation of an amphid sensillum. From Singhvi & Shaham (2019).

Arthropods: the fruit fly *D. melanogaster*

Arthropods possess a subepidermal nervous system consisting of a ventral nerve cord and an anterior brain. High neural complexity is generally observed, which results into voluminous neuropil forming complex structures such as the optic lobe, the antennal lobe, and the mushroom bodies.

In insects, the nerve cord is rope-ladder-like. The brain, consisting of several fused ganglia, is divided into a supraesophageal ganglion and a subesophageal ganglion. The supraesophageal ganglion, similarly to the vertebrate brain, is further divided into three regions: the protocerebrum, receiving visual information, the deutocerebrum, receiving sensory inputs from the antennae, and the tritocerebrum, which integrates information from other systems (Edwards & Meinertzhagen, 2010).

The brain of *Drosophila* consists of around 90 thousand cells, about 10 percent of which are believed to be glial. Six glial cell types are currently recognized in adult *Drosophila* (Yildirim et al., 2019): surface glia (perineurial and subperineurial glia), cortex glia, astrocyte-like glia, ensheathing glia, and wrapping glia (Fig. 10). *Surface glia* envelop the whole nervous system and separates it from the hemolymph, establishing a two-layered blood-brain barrier. *Cortex glia* contact the subperineurial glia and form a meshwork around many neurons. Two types of glial cells delimit the neuropil. *Astrocyte-like glia* are similar to vertebrate astrocytes in many aspects. These cells extend fine processes into the neuropil, where all synapses are located, and participate in neurotransmitter homeostasis. Like their vertebrate counterpart, astrocyte-like glia uptake synaptic glutamate and GABA through ortholog of EAATs and GAT (GABA transporter). These cells further use the enzyme glutamine synthetase to convert glutamate to glutamine, which is shuttled back to the presynaptic terminal (Freeman et al., 2003a) (Fig. 10D). Astrocyte-like glia can also perform phagocytic functions like vertebrate microglia (Yildirim et al., 2019). *Ensheathing glia*

have flattened cell bodies that wrap the surface of the neuropil, providing compartmentalization. Interestingly, both larval astrocyte-like and ensheathing glia undergo programmed cell death during metamorphosis and are generated *de novo* from neuroblasts (Omoto et al., 2015). *Wrapping glia* is found exclusively in the PNS and ensheathe the axons of sensory and motor neurons, similarly to non-myelinating Schwann cells in vertebrates (Fig. 10C).

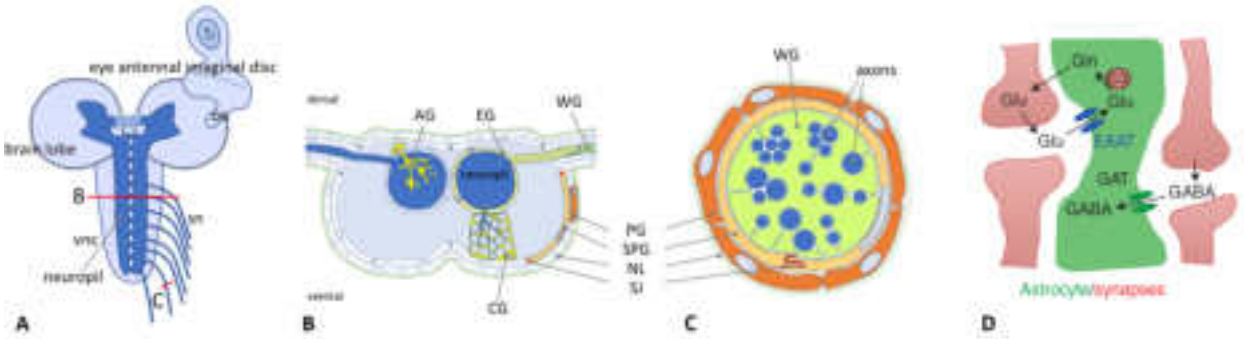

Figure 10. *Drosophila* glia. **A**: Schematic view of a larval nervous system, composed of the brain, the ventral nerve cord (vnc) and the segmental nerves (sn). **B**: The entire nervous system is separated from the rest of the body by a glial blood–brain barrier formed by the subperineurial (SPG) and perineurial (PG) glia, with the interposition of a thick extracellular matrix called neural lamella (NL). All neuronal cell bodies in the CNS reside in the cortex and are surrounded by cortex glia (CG). Axons, dendrites and synapses are found in the neuropil, which is delimited by astrocyte-like glial cells (AG) and ensheathing glia (EG). **C**: The PNS is delimited by a blood-brain barrier like that of the CNS. Wrapping glia (WG) ensheathe the axons of sensory and motor neurons and is only found in the PNS. **D**: Astrocyte-like glia recycle neurotransmitter using molecules homologous to those used by vertebrate astrocytes: GABA transporter (GAT), excitatory amino acid transporters (EAAT), and glutamine synthetase (GS). Modified from Yildrim et al. (2019) and Freeman (2015).

Glia in invertebrate deuterostomes

Compared to the rest of the invertebrates, the deuterostomes are characterized by the abundant presence of radial glial, elongated cells with long processes that span the whole thickness of the neural tissue and containing bundles of intermediate filaments. Although similar cells have been described also in protostomes (Helm et al., 2017), the presence of these cells is much more conspicuous in deuterostome nervous systems.

Hemichordates

Hemichordates are trimeric animals divided into an anterior proboscis (prosome), an intermediate collar (mesosome) and a posterior trunk (metasome). The nervous system is a basiepidermal plexus presenting various condensations (Stach et al., 2012). In the pterobranch *Cephalodiscus gracilis*, the plexus presents a prominent condensation in the collar region, which has been interpreted as a brain (Stach et al., 2012). Surprisingly, ultrastructural analyses found no glial cells in this structure (Rehkämper et al., 1987).

The enteropneust nervous systems have been more broadly characterized. Despite some minor differences, the adult neural anatomy is very similar across different genera (Nomaksteinsky et al., 2009).

The basiepidermal plexus condenses locally into two nerve cords: a dorsal nerve cord extending from the proboscis to the posterior end of the body and a ventral nerd cord restricted to the trunk (Fig. 11). Just behind the collar, a peripharyngeal nerve ring connects the dorsal and ventral cords. Interestingly the mesosomeric portion of the dorsal cord, called collar cord, is subepidermal and develops by a process similar to the neurulation of chordates (Kaul & Stach, 2010). Anterior to the collar cord, the dorsal cord is flattened and enlarged into a sort of neural plate which, at some level, fully encircle the proboscis. The cords and the neural plate, which together constitute the CNS, are associated with a nerve net of neurons interspersed in the epidermis, forming a PNS like that of invertebrate chordates. Molecular analyses of the collar cord of *Ptychodera flava* (Nomaksteinsky et al., 2009) revealed that neurons (expressing *elav* and *synaptotagmin*) are confined to a bilateral cluster in the ventral part of the cord and are separated from the lumen by non-neuronal (*elav*-negative) cells. The two stripes of neurons are dorsal to and separated by a thick neuropil (Fig. 11C-D). The part of the nerve cord dorsal to the lumen is devoid of neurons. The overall arrangement of cells and fibers of the collar cord is comparable to the vertebrate neural tube, with equivalents of a lumen, gray matter and white matter (Nomaksteinsky et al., 2009). No glial cells have been described in the collar cord of *P. flava*, despite the presence of periventricular *elav*-negative cell bodies strongly indicate their presence. Indeed, ependymal-like cells interconnected via adhesive junctions have been described in another enteropneust, *Saccoglossus kowalevskii* (Kaul & Stach, 2010). In contrast to *P. flava*, in this species the canal degenerates in the adult but some ependymal-like cells keep lining the resulting lacunae while the rest form a sheath around the neurons (Kaul & Stach, 2010). In addition, glial cells similar to vertebrate radial glia have been found in the collar cord of the enteropneusts *Balanoglossus misakiensis* (Helm et al., 2017). Interestingly, radial glia-like cells have not been described during development, at least in *S. kowalevskii* (Kaul & Stach, 2010), ruling out the possibility that they perform a neurogenetic role comparable to that of vertebrate radial glia.

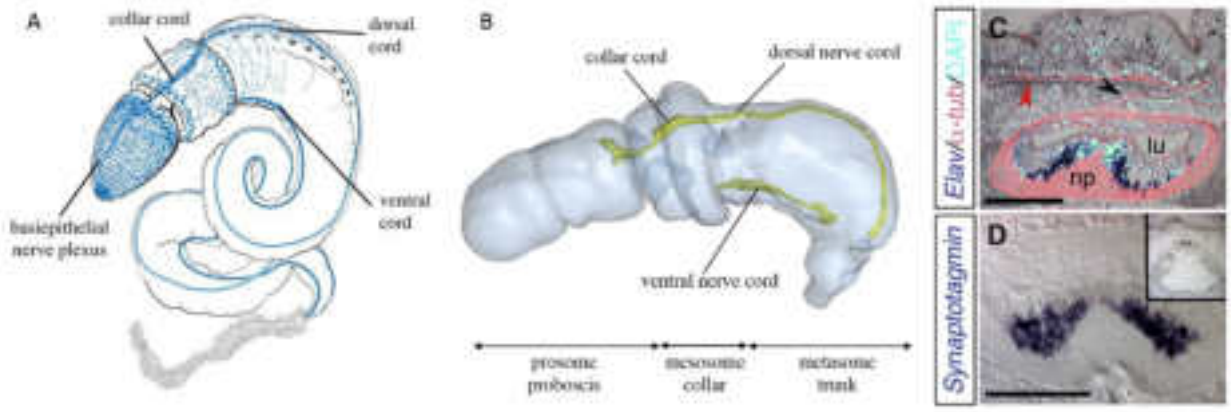

Figure 11. The nervous system of enteropneust hemichordates. **A**: The nervous system of the adult *S. kowalevskii*, from Lowe et al. (2015). **B**: The CNS of *S. kowalevskii* juvenile (18 days post-fertilization) reconstructed from serial histological sections, elaborated from Kaul & Stach (2010) to show only the epidermis (gray) and the underlying nerve cords (yellow). **C-D**: Sections of the collar cord of *P. flava* showing the position of the neuronal cell bodies (stained blue) with respect to the neuropil (np, stained red) and the lumen (lu). From Nomaksteinsky et al. (2009).

Echinoderms

Although some groups appear bilateral from the outside, adult echinoderms have a pentaradial body plan but develop from bilaterally symmetrical larvae. Consequently, the nervous system must undergo profound transformations at metamorphosis. The adult nervous system is indeed built *de novo* from the rudiment that develops on the left side of the larva (Dupont et al., 2009; Hirokawa et al., 2008). The adult nervous system consists of five nerve cords radially departing from the circumoral nerve ring, which joins them together. The radial cord and the circumoral nerve ring constitute the CNS. The PNS is composed of a basiepidermal nerve plexus and peripheral nerves innervating the appendages (Mashanov et al., 2016).

The echinoderm CNS is a superimposition of one to three layers of nervous tissue called ectoneural, hyponeural, and entoneural systems (Mashanov et al., 2016). The entoneural system is only found in crinoids, where it represents the most prominent layer of the nerve cords, while the ectoneural and hyponeural systems are present in all classes (Mashanov et al., 2016). The ectoneural system lies within or underneath the oral epidermis and is the most prominent component of the CNS in all echinoderms except for crinoids. The hyponeural system may or may not be present in the nerve ring and radial cords and is particularly well developed in echinoderms with a conspicuous musculature, such as asteroids, ophiuroids, and holothuroids (Mashanov et al., 2016). The ectoneural system is basiepidermal in crinoids and asteroids and subepidermal in ophiuroids, echinoids and holothuroids. When it is subepidermal, it is organized as a tube with an asymmetric lumen, called epineural canal. The epineural canal separates the neural tissue into two layers. The inner layer is a thick neuroepithelium containing neurons and radial glia-like cells, while the outer layer is a simple epithelium lacking neurons (Mashanov et al., 2006). The hyponeural system has a similar tubular organization with a canal called hyponeural canal (Fig. 12). The ectoneural and hyponeural systems are connected by neuronal and glial processes (Mashanov et al., 2006). The organization of the CNS is reasonably conserved in echinoids, ophiuroids and holothuroids (Formery et al., 2020; Mashanov et al., 2016).

Radial glia-like cells have been found in the nerve rings and radial cords of holothuroids (Mashanov et al., 2010), asteroids (Viehweg et al., 1998) and ophiuroids (Zueva et al., 2018). In the radial nerve cords of the adult holothurian *Holothuria glaberrima*, around 45-70% of cells are radial glia (Mashanov et al., 2010). Similarly to their vertebrate counterpart, these cells have elongated processes that contain extensive bundles of intermediate filaments and span the thickness of the cord, dividing the neuropil in organized bundles (Mashanov et al., 2006). Interestingly, a subset of these cell produces a material which presents an immunoreactivity similar to Reissner's fiber, which in chordates is produced by modified ependymal cells. Moreover, echinoderm radial glia-like cells are able to proliferate and differentiate into neurons both in physiological conditions and following traumatic injury (Mashanov et al., 2013). Data are missing investigating a possible role of echinoderm glia in neurotransmitter homeostasis.

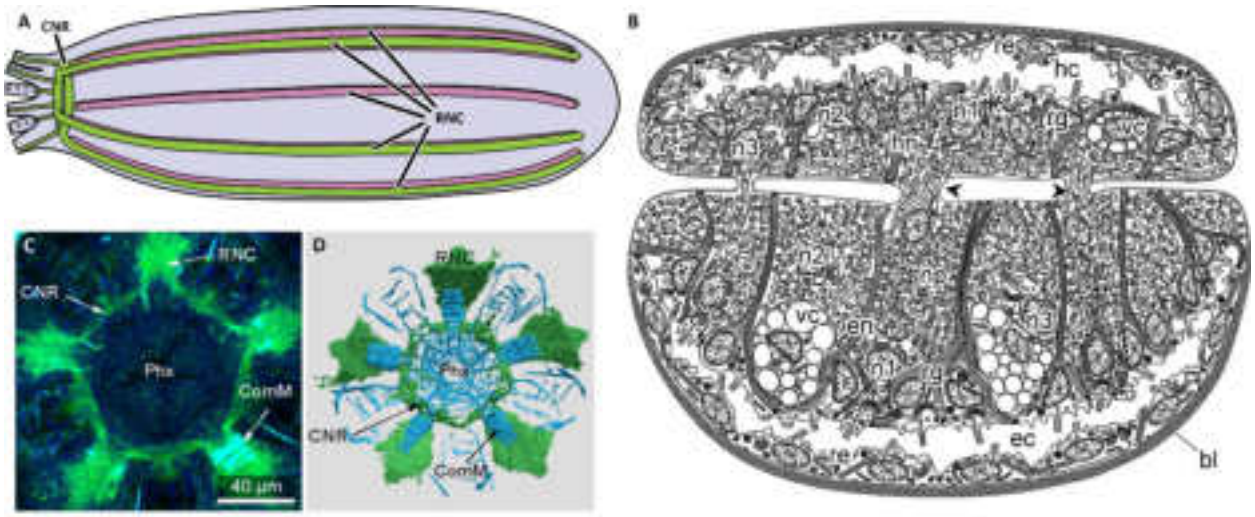

Figure 12. The central nervous system of echinoderms as represented by holothuroids (A-B) and echinoids (C-D). **A**: Schematic representation of the radial nerve cords (RNC) and circumoral nerve ring (CNR) of an adult sea cucumber. **B**: Schematic cross-section of the radial nerve cord of a sea cucumber, depicting both the hyponeural (hn) and ectoneural (en) systems. bl: basal lamina; ec: epineural canal; en: ectoneural neuroepithelium; hc: hyponeural canal; hn: hyponeural neuroepithelium; n1–n3: three morphologically distinct neuronal types; np: neuropil; nr: nerve ring; re: roof epithelium; rg: radial glia-like cell. Images from Mashanov et al. (2006). **C-D**: Neuromuscular system of the sea urchin juvenile stained for synaptotagmin-B (neurons, green) and F-actin (muscles, cyan). CNR: circumoral nerve ring; Phx: pharynx; RNC: radial nerve cords. Images from Formery et al. (2020).

Cephalochordates

Amphioxus and vertebrates share a stereotypical body plan with a dorsal CNS, a notochord, segmented body muscles, pharyngeal slits and a post-anal tail. The CNS of developing amphioxus has been extensively studied from both an ultrastructural (e.g., Lacalli et al., 1994) and a molecular point of view (e.g., Candiani, Moronti, Ramoino, Schubert, & Pestarino, 2012). Yet, while its neuronal cell types are well characterized, an unequivocal identification of glial cells has not, to date, been available.

The amphioxus neural tube is thin and un-vascularized and virtually all cell bodies line the central canal. The surface of the neural tube appears uniform, except for an anterior swelling called the cerebral vesicle. Similar to the situation in jawless vertebrates, neurites are not myelinated. In the absence of external morphological landmarks, position relative to somite boundaries is commonly used to mark anteroposterior position along the nerve cord (Wicht & Lacalli, 2005), but molecular markers have proven useful for subdividing the brain-like region of the anterior cord into a rostral hypothalamo-prethalamic (HyPTh), an intermediate diencephalo-mesencephalic (DiMes) and a caudal rhombencephalon-spinal (RhSp) region (Albuixech-Crespo et al., 2017). The HyPTh corresponds to the anterior cerebral vesicle as defined by morphological criteria and includes the frontal eye complex, homologous to vertebrate paired eyes (Vopalensky et al., 2012), and the infundibular organ, a glial-related secretory structure. The DiMes is located between the infundibular organ and the end of somite pair 1 and includes the lamellar body, a photoreceptor homologous to the vertebrate pineal organ (Bozzo et al., 2017), and the primary motor center

(Lacalli, 1996). Caudal to the first somite pair is the RhSp, which is relatively uniform in cell composition compared to more anterior regions of the amphioxus CNS.

Several types of putative glial cells have been described in amphioxus (Fig. 13). In pre-metamorphic larvae, for example, ependymoglial and ependymal cells are distinguishable by the respective presence and absence of intermediate filament bundles (Lacalli & Kelly, 2002) and morphologically resemble vertebrate radial glia (Götz, 2013). In addition, floor and roof plate cells, performing glia-like support functions, are easily identified and a category of non-neuronal glia-like cells arise at the ventral midline in close association with the floor plate, the midline glia (Lacalli & Kelly, 2002). The long axial processes formed by the latter imply a possible role in axonal guidance, but this has not been confirmed experimentally.

In the amphioxus adult CNS, putative glial cells have been reported that bridge between the neural canal and basal lamina via long radial processes. Such cells have been called ependymal glia (Bone, 1960), ependymal cells (Castro et al., 2015), radial glia (Wicht & Lacalli, 2005) or tanycytes (Obermüller-Wilén, 1979). Small parenchymal cells, called Schneider glia, have also been identified in the dorsal nerve cord (Bone, 1960). In the amphioxus peripheral nervous system, small cells, called Müller glia, are associated with dorsal nerves and motor neurons contacting the muscles (Bone, 1960). Glial cells are also said to ensheathe peripheral nerves, similar to vertebrate non-myelinating Schwann cells (Holland & Somorjai, 2020; Ruppert, 1997). Given that amphioxus lacks a definite neural crest, the peripheral glia-like cell populations are likely of intramedullary origin.

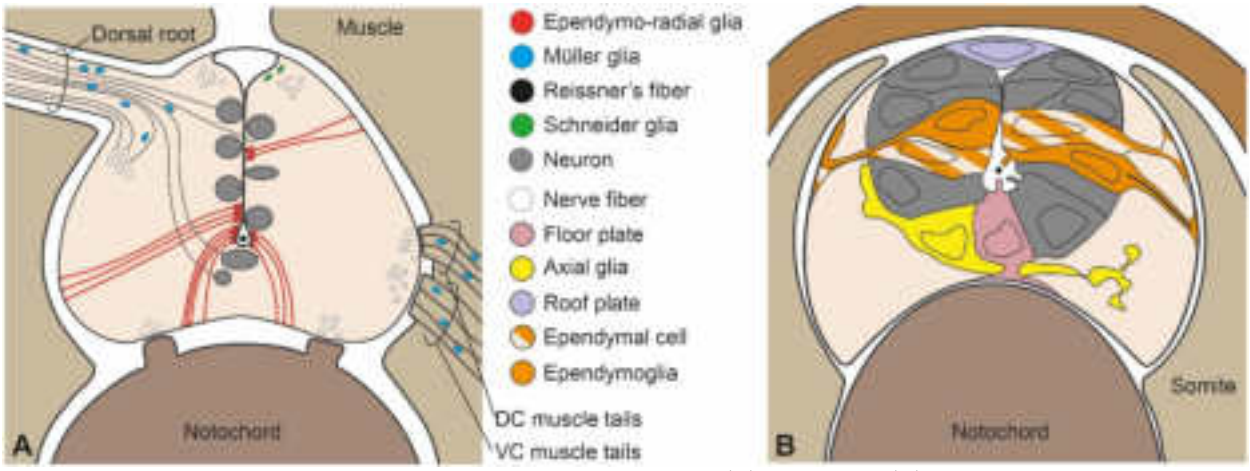

Figure 13. Diagram of representative cross-sections of adult (A) and larval (B) nerve cord. Images are not to scale, showing the position of glial cells described so far based on morphological criteria. From Bozzo et al. (2021).

In addition to the homology of specific glial cell types, the functions of amphioxus glia remain almost completely unknown. For example, there is no evidence for or against amphioxus glia-like cells acting as neural stem cells. In ascidian tunicates, ependymal cells of the larva produce neurons during metamorphosis (Horie et al., 2011), but early differentiating neurons arise directly from the neuroepithelium. But in amphioxus, proliferation sites and rates of proliferation are incompletely documented. From the work of Holland & Holland (2006), proliferation rates in the nerve cord appear to decrease at the mid-neurula stage,

but possible problems with penetration of the probe mean that actual proliferation rates may be much higher. This suggests that there is much that remains to be determined about the rates and localization of cell division within the embryonic CNS in amphioxus, making it more difficult to explain the precise distribution of glia and neurons along the axis of the developing nerve cord.

Tunicates

Among the chordates, tunicates, and particularly ascidians, have a highly derivate body plan. They possess a free-swimming tadpole-like larva that undertakes a radical metamorphosis that produces a sessile adult. The CNS of tunicate larvae is divided into three domains: the anterior sensory vesicle, the visceral ganglion and the caudal nerve cord (Nicol & Meinertzhagen, 1991). The sensory vesicle contains a large ventricle filled with fluid and lined by ependymal cells (Katz, 1983) and harbors the ocellus and the gravity-sensing otolith (Imai & Meinertzhagen, 2007). The visceral ganglion might function as the integrative center of the CNS, receiving sensory inputs from various structures and initiating swimming (Imai & Meinertzhagen, 2007). It contains cell bodies of motor neurons whose neurites project into the tail. The caudal nerve cord does not contain neurons but comprises four longitudinal files of ependymal cells limiting the neural canal (Nicol & Meinertzhagen, 1991). The larval CNS of the ascidian *Ciona intestinalis*, a widely used model organism in developmental biology, contains about 300 cells, two-thirds of which are ependymoglial cells lining the lumen of the neural tube (Nicol & Meinertzhagen, 1991). At metamorphosis, which comprises the almost complete destruction of the larval nervous system, some of these ependymoglial cells give origin to adult neurons (Horie et al., 2011; Katz, 1983), showing to possess a neurogenetic potential similar to vertebrate radial glia.

The adult CNS of ascidians, the best-studied among tunicates, originates from a portion of the neural ectoderm of about 40 cells in *C. intestinalis*, called the rudiment, which expands after metamorphosis (Mackie & Burighel, 2005). The brain consists of a ganglion with a central neuropil and cortical cell bodies and is sometimes called cerebral ganglion. Two paired nerves exit the brain and further ramify to innervate the viscera and body wall. Differently from the tadpole, the adult nervous system of ascidians does not contain clearly recognizable glial cells (Mackie & Burighel, 2005). Non-neuronal cells are present in the neuropil of the cerebral ganglion, but they have been interpreted as phagocytes (Burighel & Cloney, 1997).

Glial cells in vertebrates and invertebrates: a single origin?

As presented in the previous sections, there are similarities between vertebrate and invertebrate glial cells both on the morphological and molecular point of view. The presence in different phyla of glial cells expressing *EAAT, GS* and *GFAP*-like intermediate filament protein orthologs is particularly noteworthy, as this is considered an astroglial signature in vertebrates (Table 1). These glial cells share at least one common function: the glutamate-glutamine cycle. The question remains open whether these morphological

and functional similarities are due to the existence of a glial cell type performing a similar function in the common ancestor of bilaterians or rather to convergent evolution in different lineages. To answer this question, it will be important to analyze as many invertebrate glial cells as possible in search of this conserved toolkit as well as lineage-specific characters.

A similar approach has been recently applied by Helm and colleagues (2017), who looked for the same molecular marker – SCO-spondin – in different animals, both deuterostome and protostome. This work highlighted the presence of radial glia-like cells producing the same glycoprotein in various animal lineages, suggesting that secretory radial glia is an ancestral feature of bilaterians. Unfortunately, the function of SCO-spondin in invertebrates is unknown, while in vertebrates it has only started to being elucidated (Cantaut-Belarif et al., 2018; Driever, 2018; Troutwine et al., 2020). This fact complicates the interpretation of the evolutionary story of this cell type.

One thing that should always be kept in mind when performing comparative studies on distantly related species is that "*whatever roles glia may play in more advanced nervous systems, such as are seen in vertebrates, arthropods, and molluscs, the same roles may not be those that were instrumental in inducing the initial evolution of the character. As time went on other opportunities to contribute to organism fitness by assuming additional roles likely appeared, making glia what we see today. We might barely recognize the original form were we to encounter it*" (Hartline, 2011).

Table 1. Astroglial signature in invertebrate glia.

	GFAP-like IFs	**GS**	**EAATs**
Vertebrates	+	+	+
Tunicates	n.a.	n.a.	n.a.
Cephalochordates	[+]	n.a.	n.a.
Hemichordates	[+]	n.a.	n.a.
Echinoderms	[+]	n.a.	n.a.
Insects	-	+	+
Nematodes	+	+	+
Annelids	+	+	+
Mollusks	(+)	(+)	n.a.

[+]: Ultrastructural evidence; (-): Immunohistochemical evidence; +: molecular evidence; n.a.: data not available.

Amphioxus as a model to understand the origin of the vertebrates

Amphioxus and its kinship with vertebrates have puzzled zoologists and evolutionary biologists since its discovery in the 19th century, roughly contemporary with the publication of the first edition of Darwin's *"Origin of Species"*.

Amphioxus adult morphology

Amphioxus adults have a slender body tapering at both ends (Fig. 14). From the external examination, several structures are apparent. Since the skin, composed of a simple columnar epithelium and a thin dermis, is translucent, some features of the internal organization can also be guessed. The oral cavity, located ventromedially below the rostrum, is surrounded by a fringe of 20-30 tentacle-like cirri that guard the opening. The cirri present bilateral papillae containing putative mechanosensory cells and close around the oral opening in response to touch, preventing the ingestion of oversized food particles. The oral cavity consists of two portions, an outer vestibule and an inner mouth. The inner surface of the vestibule presents longitudinal finger-like stripes of thick ciliated epithelium that unite to form the wheel organ. The ciliary movements of the wheel organ create an inward water current that allows food particles to enter the mouth. Anteriorly, the wheel organ has a dorsal invagination known as Hatschek's pit and groove, which might be homologous to the vertebrate adenohypophysis (Candiani, Holland, et al., 2008; Holland, 2015). The proper mouth is surrounded by the velum, a diaphragm muscle with 12 sensory tentacles radiating from the margin of the mouth.

The mouth opens into the pharynx, which is perforated by numerous pharyngeal slits commonly referred to as gill slits, although they probably do not contribute to respiration. The pharynx occupied approximately one-half of the body and presents two longitudinal grooves: the dorsal epipharyngeal (or hyperpharyngeal) groove and the ventral endostyle, which is considered homologous to the vertebrate thyroid (Ogasawara, 2000). The pharynx – as well as the gonads – is enclosed in the atrium, a body cavity that runs for two-thirds of the animal length and terminates with an external opening, the atriopore. The pharynx joins posteriorly to the stomach (or midgut) via a short esophagus. At the esophagus-stomach junction originates a finger-like extroflection of the gut that extends anteriorly along the right side of the pharynx for about two-thirds of its length. This is the hepatic cecum, which is likely related to the vertebrate liver (Fan et al., 2007). Posteriorly to the stomach, the gut continues with the iliocolon and the intestine (or hindgut) and terminates with the anus, located near the posterior end of the body. Water entering from the mouth is pushed through the pharyngeal slits, where the food particles are trapped by a mucous net produced by the endostyle, passes into the atrium and leaves the body via the atriopore. The mucus containing the food forms a thread that is channeled into the ciliated epipharyngeal groove and transported to the gut by ciliary movements. In the midgut, the food-mucus thread is rotated and mixed with digestive enzymes produced by the hepatic cecum. Food particles detach from the thread and are absorbed while the rest of the mass is transported to the anus and expelled.

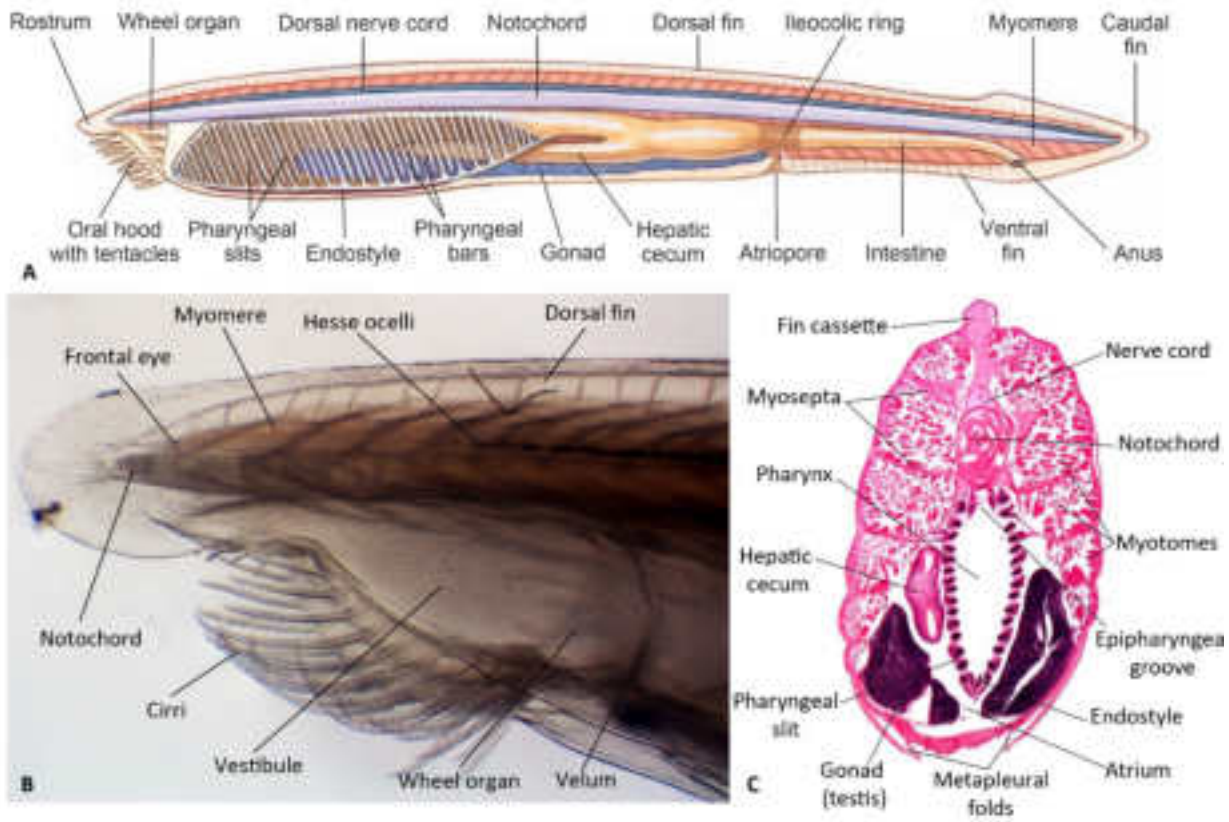

Figure 14. Adult anatomy. **A**: Diagram of an adult amphioxus il lateral view. From Hickman et al. (2017). **B**: Head region of a living *B. lanceolatum* as viewed under a stereomicroscope. **C**: Cross-section at the level of the pharynx.

The flanks of the body present bilateral V-shaped segmental muscles or myotomes that span most of the dorsoventral distance and extend from the oral region to almost the tip of the tail. Contralateral myotomes are out of register. Myomeres are separated by collagenous myosepta, which transmit to the notochord the force resulting from the contraction. The notochord, composed of stacked discoidal muscular cells, extends from the rostrum to the tip of the tail and constitutes the only skeletal element of the locomotory system. Amphioxus lacks paired fins, but there is a median dorsal fin running along the whole length of the back. At the posterior end, the dorsal fin continues with the tail fin. The fin is supported by gel-filled coeloms called fin rays.

The vascular system is well developed, including arteries, veins and capillary plexuses. Blood is colorless due to the absence of respiratory pigment and circulating cells, although hemocytes are present as an endothelial-like lining of the vessels (Ruppert, 1997). Since a true heart is missing, many vessels are contractile.

The excretory system consists of two serially homologous organs: the unpaired Hatschek's nephridium and the paired branchial nephridial (Ruppert, 1997). Differently from vertebrates, a common nephric duct is missing and each nephridium opens independently into the atrium. Hatschek's nephridium is the largest and anterior-most of the nephridia in the body and its single collecting tubule lies on the left side of the notochord. It develops from the left side of the first somite, in association with the larval mouth, and represents a homolog of the pronephros of basal vertebrates (Langeland et al., 2006).

The dorsal part of the notochord is in direct contact with the nerve cord, which in the living animal is highlighted by a stretch of darkly pigmented photoreceptors, called Hesse ocelli, that runs along the ventral part of the nerve cord for most of its length. As discussed in the previous chapter, the nerve cord is a hollow tube that shows no external signs of regionalization, except for the anterior cerebral vesicle, a caudal ampulla and serially repeated dorsal nerves that lack ganglia (Ruppert, 1997). The lumen of the cerebral vesicle opens to the exterior via a neuropore, which is located in a shallow depression (Kölliker's pit) at the base of the rostrum on the left side of the body. Ventrally in the posterior part of the anterior cerebral vesicle, the modified ependymal cells of the infundibular organ secrete Reissner's fiber, which runs in the central canal of the nerve cord to the caudal ampulla (Obermüller-Wilén & Olsson, 1974).

Segmental nerve pairs emerge dorsolaterally from the nerve cord. The first pair differs, originating ventrolaterally from the anterior end of the cerebral vesicle. Except for the first and last pairs, the nerves emerge in correspondence with the myosepta through which they pass and, consequently, are slightly out of register. The first two pairs, sometimes called "cranial nerves" project into the rostrum and present clusters of primary sensory cells on their branches enclosed in capsules called corpuscles of de Quatrefages, which are putative mechanoreceptors. The first nerve pair also innervates other sensory cells of the rostrum. The other nerve pairs, generally called "spinal nerves", contain motor and sensory fibers. Each spinal nerve crosses the corresponding myoseptum to reach the dermis and splits into a dorsal ramus, which innervates

the subepidermal nerve plexus of the dorsal part of the body, and a ventral ramus innervating the subepidermal nerve plexus of the rest of the body and the atrial nervous systems (Ruppert, 1997).

Cephalochordates are gonochoric but lack evident sexual dimorphism. Ripe males and females can be told apart only by looking at the gonads through the translucent skin under a stereomicroscope: ovaries contain small corpuscles (i.e., eggs), while the testes are filled with a creamy fluid (i.e., sperm). Gonads are bilateral segmental sacs in the wall of the atrium, extending from the middle of the pharynx up to the atriopore. At sunset during the spawning season, ripe animals leave the sediment and swim to the water surface. They release the gametes into the atrium, which are expelled from the atriopore by the water current. Fertilization is external.

Development and larval morphology

After the seminal work of Kowalevsky (1867), other scientists improved the description of the embryology of the European *B. lanceolatum* (Cerfontaine, 1906; Hatschek, 1893). More recently, the microscopic anatomy of early developmental stages was documented by TEM for the Chinese *B. belcheri* (Hirakow & Kajita, 1990, 1991, 1994) and a first morphological staging was proposed. Most of the molecular studies of amphioxus development were performed in the Florida lancelet *B. floridae*, although more recently European researchers resorted to local populations of *B. lanceolatum*, more easily exploitable. So, differently from canonical model organisms such as drosophila, zebrafish and mouse, more than one species of cephalochordates is used as a model organism. Recently, a staging system based on morphology and gene ontology data valid for all amphioxus species has been proposed (Carvalho et al., 2020, Fig. 15) and will be employed in the present dissertation. The bulk of ultrastructural information on the larval nervous system comes from the work of Thurston Lacalli on pre-metamorphic *B. floridae* (reviewed in Wicht & Lacalli, 2005).

Amphioxus egg is small (about 130 μm in diameter) and microlecithal. The spawned oocyte is arrested at the second meiotic metaphase, and the second meiotic division happens around 10 minutes after fertilization (Holland, 2015). A few minutes after sperm entry, the vitelline membrane lifts from the surface of the egg and expands, producing the fertilization envelope (also called chorion). The first developmental period, until the early neurula stage (N1), happens inside the fertilization envelope. The cleavage is holoblastic radial and specification of cell fate is conditional, except for the germ plasm, which is already determined in the unfertilized egg through asymmetrical localization of germ cell markers (Zhang et al., 2013). The cleavage proceeds mostly synchronously and at the 32-cell stage produces a blastula constituted by a monolayer of cells disposed around the central blastocoel. At the 8th cycle of division (B stage), one side of the blastula is slightly thicker and will become flat at the onset of gastrulation (G1 stage). This is the side of the embryo that will invaginate into the blastocoel, forming the mesendoderm. The invagination progressively reduces the blastocoel until a cap-shaped (G4 stage) embryo without blastocoel is produced.

As gastrulation proceeds, the archenteron – the cavity that replaced the blastocoel – becomes progressively deeper and the blastopore becomes smaller. By the end of gastrulation (G6 stage), the dorsal side of the embryo is flattened. Here, the neural plate forms by primary neurulation starting from the N0 stage. Expression patterns of *hox1*, *hox3*, *otx* and *foxq2* suggest that, except for the tissue closest to the blastopore, almost all the gastrula is destined to produce the head, including the HyPTh, the DiMes and part of the RhSp (Albuixech-Crespo et al., 2017; Holland & Onai, 2012).

At the same time, the embryo covers its surface with cilia and starts to rotate inside the fertilization envelope. From the dorsal mesendoderm, the notochord and first somites pinch off anteroposteriorly (stage N1) so that the embryo becomes truly triploblastic. The neural plate starts to separate from the ectoderm and the blastopore is internalized and forms the neurenteric canal, which joins the neural tube and the archenteron. With the addition of 4-6 somite pairs, the embryo hatches from the chorion and starts swimming around by ciliary movement. At the late neurula (N4) stage, the tissue around the neurenteric canal forms the tail bud, which differentiates into somites, gut, and nerve cord, sustaining larval elongation. From the ectoderm of the ventral midline, ectodermal sensory neurons differentiate and migrate all over the embryo to form the subepithelial PNS (Kaltenbach et al., 2009). The late embryo with 12 somite pairs (T0 stage) presents a transitional morphology between the neurula and larva. The head can be clearly distinguished from the tail as the pharyngeal region starts to grow. At the T1 stage, the first pigment spot forms in the ventral neural tube at the border between somites 4 and 5, the rostrum begins to grow and the preoral pit develops from Hatschek's left diverticulum. (Candiani, Holland, et al., 2008). Although the embryo still relies on ciliary beating for its movement, the muscles start to contract.

The larval period of development starts as the mouth opens on the left side of the body (stage L0), while the club-shaped gland and the endostyle form on the right side. The first pharyngeal slit – commonly called gill slit – starts to be visible on the ventral midline, although it will open on the right side. At the same time, the anus opens at the posterior end of the gut and the L1 larva starts feeding. More pharyngeal slits are progressively added on the right side of the body until the metamorphosis, which starts at around L8 (8-gill slit stage) in *B. floridae* (Holland, 2015) but likely not before L15 in *B. lanceolatum* (Wickstead, 1967).

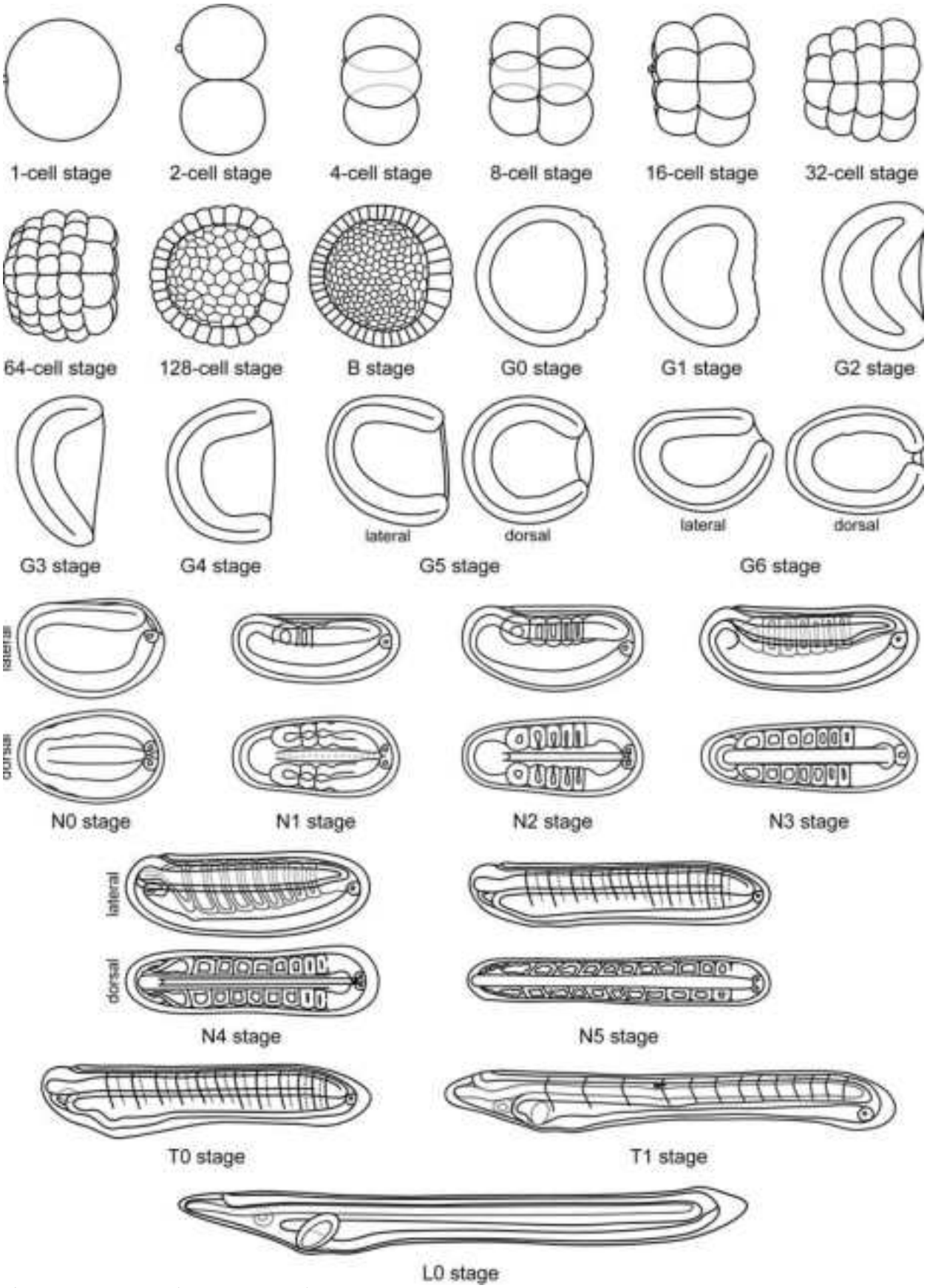

Figure 15. Schematic representation of lancelet development from the 1-cell stage to the L0 stage. Animal pole and anterior to the left. From Carvalho et al. (2020).

First descriptions and classification attempts

The first scientific description of a cephalochordate was recorded in 1774 (Pallas, 1774), when Peter Pallas, a German naturalist based in Russia described two fixed specimen of amphioxus shipped from England. The short description (Fig. 16A) can be translated as follows: "*Two-headed body, planar, linear-lanceolate, pointy at both ends. Edge enlarged on both sides by a membranous rim. The edge, however, for two-thirds of the length of the inferior part is bi-labiated and furrowed and can be very narrow, like the foot of a slug. No tentacles. The sides present V-shaped stripes, pointing anteriorly so that they look almost like the scaled fillet of a little fish.*" So, despite a fish-like external appearance, amphioxus was initially classified as a mollusk of the genus *Limax* and consequently named *L. lanceolatus*. In 1834, the Italian naturalist Oronzio Costa discovered amphioxus in the Gulf of Naples (Costa, 1834) and described it as a new species. He wrongly interpreted the oral cirri as gills and thus named the genus *Branchiostoma* (meaning "mouth slits") and classified it as a syngnathid fish, together with sea horses. A few years later, in 1836, amphioxus was independently reclassified as a basal vertebrate by William Yarrell, who was unaware of the work of Costa and renamed it *Amphyoxus lanceolatus* (Yarrell, 1859). Due to the principle of priority, the valid name is now *Branchiostoma lanceolatum*, while amphioxus became a common name.

The correct classification of amphioxus came only from the study of its development. Alexander Kowalevsky observed in amphioxus an invertebrate-like mode of gastrulation followed by a vertebrate-like later development (Kowalevski, 1865, 1867). He also observed similar development in ascidians (Kowalevski, 1866), which at the time were classified as mollusks. Building on these embryological data, Ernst Haeckel placed amphioxus in a new group, called at first Acraniata and then Cephalochordata, and placed it together with tunicates and vertebrates in the new group of the chordates (Nielsen, 2012).

Based on morphological and, more importantly, embryological characters, Haeckel further formulated the tunicate theory of vertebrate origin. In his *"Natural history of the Creation"*, Haeckel proposed that an invertebrate similar to the larval tunicate originated two branches, both degenerating into ascidians and progressing into amphioxus and vertebrates (Haeckel, 1868). According to this theory, which will be mostly accepted and incorporated into zoology textbooks from the 1870s, amphioxus gains importance as a link to understand the first events of vertebrate radiation: *"We must thus contemplate amphioxus with special reverence, […] as that venerable animal which of all still living animals is alone in a position to give us an approximate idea of our oldest Silurian ancestors with backbones"* (Haeckel, 1868, as translated in Hopwood, 2015). Alternatively, amphioxus was interpreted as a degenerate vertebrate (Dohrn, 1875). The sequencing of the first amphioxus genome swapped the position of amphioxus and tunicates in the chordate tree (Delsuc et al., 2006; Putnam et al., 2008) and strengthened the use of amphioxus as a proxy for the ancestral chordate condition.

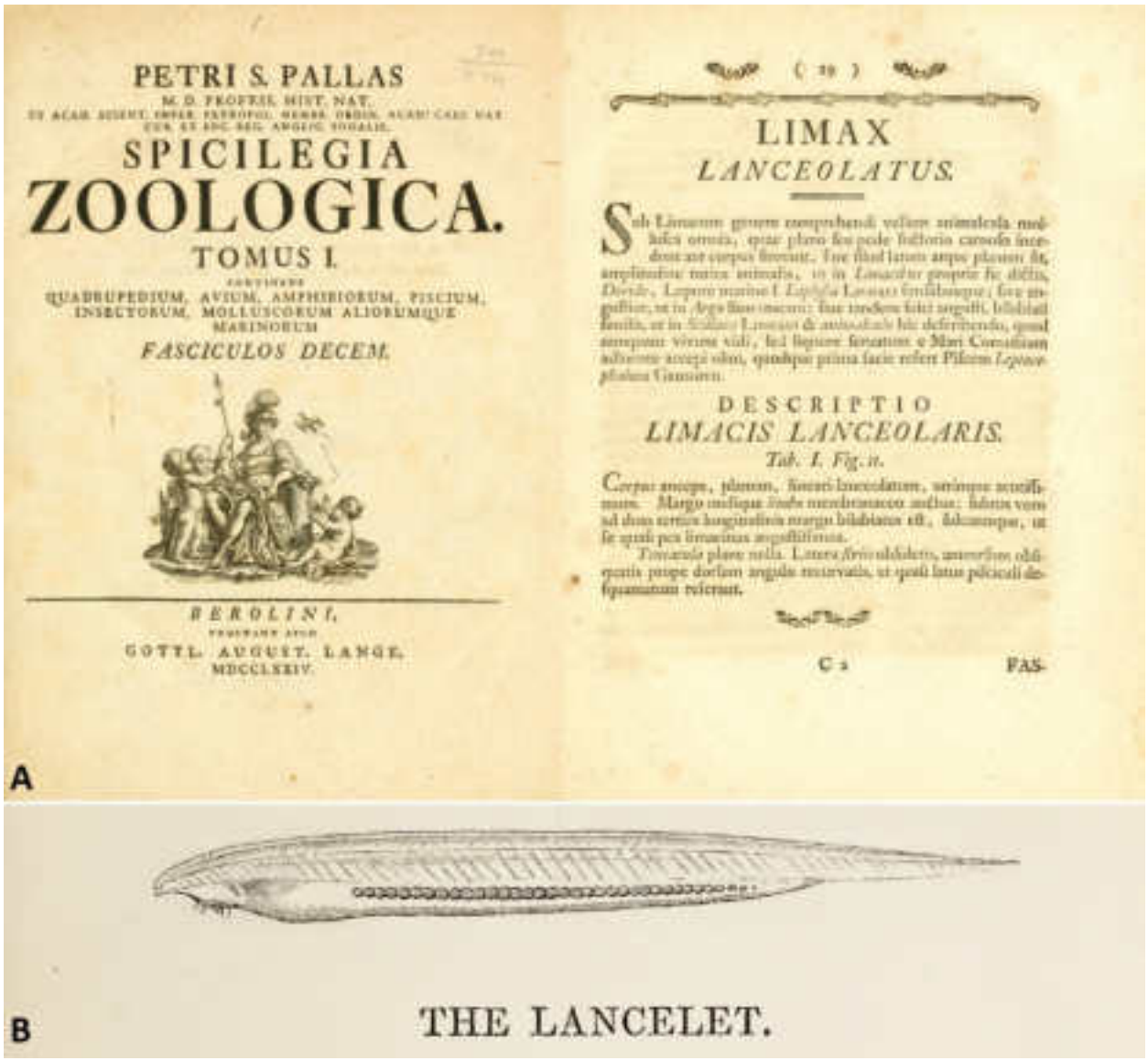

Figure 16. First description of amphioxus. **A**: The description of the European lancelet (here called *Limax lanceolatus*) contained in Pallas's "Spicilegia zoologica" (1774) is the first zoological description of a cephalochordate. **B**: Illustration of *Branchiostoma lanceolatum* (here called *Amphyoxus lanceolatus*) from Yarrell's "A history of British fishes" (1859).

Amphioxus as an evo-devo model

Although amphioxus is the earliest branch of the chordate lineage, it presents a body plan more similar vertebrate-like compared to tunicates, which represent the sister group of the vertebrates. However, amphioxus does not possess important vertebrate anatomical traits, such as a bony skeleton and paired sense organs, likely due to the lack of neural crests and placodes. This is hardly a disadvantage and cephalochordates are therefore suitable models for studying the evolutionary emergence of vertebrate novelties. On the morphological level, amphioxus is also similar to Cambrian invertebrate chordates and stem vertebrates, such as *Pikaia* and *Hikouella* (Chen, 2008; Cong et al., 2015; Lacalli, 2012; Morris & Caron, 2012). Amphioxus evolves slowly also at the genomic level, having retained a large degree of

synteny with vertebrate genomes and showing comparatively little loss or independent duplication of developmental genes (Holland et al., 2008; Putnam et al., 2008). Amphioxus genomes did not undergo the two rounds of whole-genome duplication that characterize jawed vertebrates, facilitating the functional characterization of developmental genes and providing a simple model for investigating complex developmental processes (Holland, 2015). Taken together, morphological, paleontological, genomic and developmental genetic data strongly support the use of amphioxus as a proxy for the ancestral chordate and stem vertebrate.

At the experimental level, laboratory culture and spawning protocols have been established for three species of amphioxus, *B. lanceolatum*, *B. floridae* and *B. belcheri* (Bertrand & Escriva, 2011; Carvalho et al., 2017). The genomes of these three species are also available (Holland et al., 2008; Huang et al., 2014; Marlétaz et al., 2018; Putnam et al., 2008). All cephalochordate species develop in a similar way (Carvalho et al., 2020) and embryos and larvae are very small and transparent, allowing easy microscopical analyses, especially in fluorescence (Bozzo et al., 2020). Pharmacological disruption of developmental signaling pathways is easy to perform and routinely used in amphioxus (Bertrand et al., 2017; Bozzo et al., 2020). Although technically challenging, several gene-editing techniques have been successfully employed in amphioxus, including mRNA overexpression, TALEN, Tol2 and, more recently, CRISPR-Cas9 (Hirsinger et al., 2015; Kozmikova & Kozmik, 2020; Ren et al., 2020; Su et al., 2020).

Results

To date, no molecular markers are available for glial cells in amphioxus. To compile a molecular toolkit, we searched the genomic and transcriptomic resources available for the European amphioxus, *B. lanceolatum* for orthologs of the main marker genes of vertebrate glial cells (Table 2). Astroglial cells (i.e., astrocytes), the most abundant glia in vertebrates, are characterized by active glutamate recycling and thus by the presence of glutamine synthetase (GS) and sodium-dependent glutamate/aspartate transporters, EAAT1/GLAST and EAAT2/GLT-1 (Anlauf & Derouiche, 2013; Chaudhry et al., 1995). Intermediate filament proteins, such as vimentin and GFAP, are commonly used to discriminate between undifferentiated and mature astroglia (Bramanti et al., 2010): immature astrocytes use vimentin as the major intermediate filament which is replaced by GFAP upon astrocyte differentiation. vimentin is also expressed by early radial glia, but not by neuroepithelial cells, and is thus one of the earliest markers of the glial cell lineage (Götz, 2013). In addition, we analyzed the amphioxus homolog of *scospondin* (*sspo*), which encodes the secreted glycoprotein sspo, the main component of Reissner's fiber. sspo has been proposed to be a conserved marker of radial glia in all bilaterians (Helm et al., 2017).

For oligodendroglia, we searched orthologs of vertebrate myelin regulatory factor (*myrf*) and *olig* transcription factors. However, we could not detect *myrf* transcripts by *in situ* hybridization at any of the developmental stages analyzed. In vertebrates, the *olig* gene family members *olig1*, *olig2*, *olig3* and *olig4* have important roles in the specification of oligodendrocytes, motor neurons and dorsal interneurons. *olig1* and *olig2* are thus expressed by progenitors and mature oligodendrocytes, and, in zebrafish, *olig2* is further expressed by a subset of radial glial cells that persist into adulthood and maintain the ability to produce oligodendrocytes (Kim et al., 2008). *olig3* marks progenitor cells of the dorsal spinal cord that will produce interneurons (Müller et al., 2005).

Table 2. List of commonly used glial markers and their expression in vertebrates.

	Neuroepithelial cells	Radial glia	Ependymal cells	Astrocytes	Oligodendrocytes
EAAT1	-	+	+	++	-
EAAT2	-	+	++	++	-
GS	-	+	+	++	(+)
GFAP	-	++	+	++	-
vimentin	-	++	++	-	-
sspo	-	(+)*	(+)*	-	-
olig2	-	(+)	-	-	++

(*) In vertebrates, sspo is only found in specialized ependymo-radial glial cells of the sub-commissural organ.

To distinguish between glial and neuronal lineages, we examined the expression of the neural markers *hu-elav* and *synapsin* relative to that of the glia markers (Candiani et al., 2010; G. Satoh et al., 2001). To provide a morphological context for interpreting the molecular results, ultrastructural surveys were carried out on comparable developmental stages and combined with information from TEM sections of an older, 12-day larva.

Phylogeny and expression of *scospondin* in developing amphioxus

We first focused on the *sspo* gene, for which we retrieved a single amphioxus sequence from our database queries. Phylogenetic analysis (Fig. 17) shows that a single *sspo* gene is found in the genomes of all chordates so far investigated, and the tree further revealed the presence of a single *sspo* gene in cnidarians. As in vertebrates, the amphioxus *sspo* gene encodes a very large glycoprotein of the thrombospondin family. Expression of *sspo* during amphioxus development was already detectable at the N3 stage in the anterior neural tube (Fig. 18A). By the T1 stage, *sspo* transcripts were still limited to the anterior neural tube, to an unpaired median structure in the posterior cerebral vesicle. This wedge-shaped domain (Fig. 18B) consisted of at least five cells, occupying a medioventral position in the cerebral vesicle (Fig. 18C), and persisted to the L1 larvae stage (Fig. 18D). By then, the labeled cells were elongated and inclined anteriorly towards the neuropore (Fig. 8E,F), as is characteristic of the infundibular cells at this stage. Taken together, the position of the signal and the morphology of the cells strongly suggest that *sspo* marks the infundibular organ (Lacalli et al., 1994; Olsson et al., 1994), which would appear then to be the only source of Reissner's fiber in embryos and young larvae.

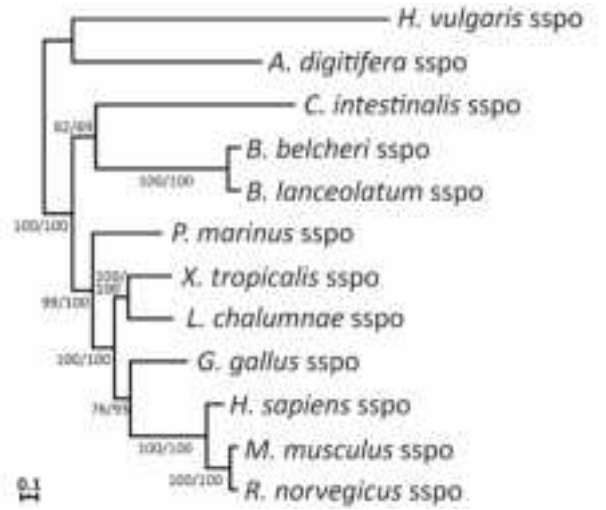

Figure 17. Phylogenetic tree of SCO-spondin (sspo) proteins. The phylogeny was calculated using both Maximum Likelihood (ML) and Neighbor Joining (NJ) methods and a JTT matrix-based model with 5 gamma categories (+*G*, parameter 1.3575). The ML tree is shown with bootstrap percentages for both ML and NJ analyses (first and second values, respectively), obtained in 1000 replicates. Cnidarian sequences were used as outgroup. List of animal taxa featured in the tree: *Acropora digitifera* (acroporid coral, cnidarian), *Branchiostoma belcheri* (Chinese amphioxus, cephalochordate), *Branchiostoma lanceolatum* (European amphioxus, cephalochordate), *Ciona intestinalis* (sea squirt, ascidian), *Gallus gallus* (chicken, bird), *Homo sapiens* (human, mammal), *Hydra vulgaris* (hydra, cnidarian), *Latimeria chalumnae* (coelacanth, crossopterygian fish), *Mus musculus* (house mouse, mammal), *Petromyzon marinus* (sea lamprey, jawless fish), *Rattus norvegicus* (common rat, mammal), *Xenopus tropicalis* (western clawed frog, amphibian). From Bozzo et al. (2021).

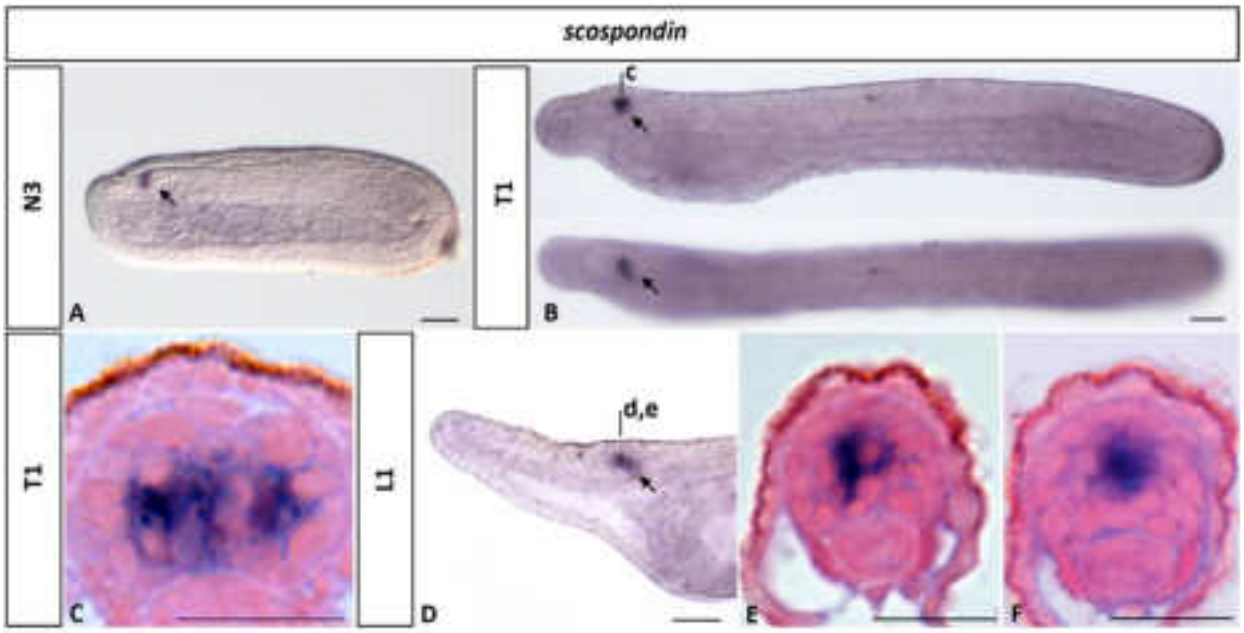

Figure 18. Expression of *scospondin* (*sspo*) during amphioxus development. **A**: Whole mount N3 neurula in lateral view. **B**: Whole mount T1 embryo in lateral (top) and dorsal (bottom) views. **C**: Transverse section of the cerebral vesicle at level indicated in B. **D:** Anterior part of a whole mount L1 larva in lateral view. **E,F**: Transverse sections at level of the infundibular organ of a L1 larva. At all stages, *sspo* is in the infundibular organ of the cerebral vesicle (arrows). Scale bars are 25 μm for whole mounts and 10 μm for sections. Whole mount embryos are oriented with anterior to the left and, if not shown in dorsal view, with dorsal to the top. From Bozzo et al. (2021).

Phylogeny and expression of *EAAT* genes in developing amphioxus

Excitatory amino acid transporters (EAATs) are required for the regulation of synaptic activity in the vertebrate CNS. In mammals, there are five *EAAT* genes (*EAAT1-5*), with *EAAT1* (or *GLAST*) and *EAAT2* (or *GLT-1*) predominantly expressed in glial cells, while *EAAT3*, *EAAT4* and *EAAT5* are exclusively expressed in neurons. Our *in silico* analyses identified three amphioxus *EAAT* genes: a clear *EAAT2* ortholog plus two additional *EAAT*s (*EAATa* and *EAATb*), which were more closely related to the vertebrate *EAAT1*, *EAAT3*, *EAAT4* and *EAAT5* subfamilies (Fig. 19).

In situ hybridization analyses suggested that only two of the three amphioxus *EAAT* genes were expressed during early development. We thus obtained expression patterns only for *EAAT2* and *EAATa*, but not for *EAATb*. *EAATa* expression was detectable in the forming somites at the N3 stage (Fig. 20A-C). At the T0 stage, *EAATa* was expressed in a subset of somite cells dorsolaterally, in proximity of the overlying ectoderm (Fig. 20D-F). In T1 embryos, *EAATa* was further expressed in a group of floor plate cells at the level of somite pairs 3 and 4 and just anterior to the first pigment spot (Fig. 20G,H). Double *in situ* hybridization of *EAATa* and *hu-elav* revealed that the *EAATa*-positive cells in the somites were located close to, but not in contact with, ectodermal sensory neurons (ESNs) (Fig. 20I). These experiments further showed that *EAATa* and *hu-elav* expression did not co-localize in the CNS (Fig. 20J,K).

Amphioxus *EAAT2* was first expressed at the T0 stage, in the CNS. In T1 embryos, *EAAT2* expression was further detectable in a population of ESNs in the mid-trunk region (Fig. 21A,H) that are known to be *soxb1c*-positive and glutamatergic (Zieger et al., 2018). In the CNS, *EAAT2* expression extended roughly from somite pair 1 through somite pair 6 (Fig. 21A). Stretching from the posterior cerebral vesicle to the first pigment spot (at the junction somite pairs 4 and 5), *EAAT2* was continuously expressed in the floor plate (Fig. 21C-F). *EAAT2* was also expressed in mediolateral cells of the neural tube (Fig. 21B-E), in a position where ultrastructural analyses of older larvae had previously identified ependymoglial and ependymal cells that resembled vertebrate radial glial cells (Lacalli & Kelly, 2002). Double staining of *EAAT2* and *hu-elav* demonstrated that the *EAAT2*-positive ESNs in the periphery also expressed *hu-elav*, while the *EAAT2*-positive floor plate and mediolateral cells in the CNS did not (Fig. 21H-J), strongly supporting their glial nature. Since, in vertebrates, *EAAT2* is expressed by radial glia and astroglia, the mediolateral *EAAT2*-positive cells of amphioxus CNS might thus be homologous to radial glia and/or astroglia. Further posteriorly, at the level of somite pair 6, *EAAT2* transcripts were present in a few ventrolateral cells of the neural tube (Fig. 21G).

In the L1 larva, *EAAT2* expression in the CNS still extended from the posterior cerebral vesicle to roughly the end of somite pair 6 (Fig. 21K). ESNs were also conspicuously stained, particularly in rostrum, oral plexus and mid-trunk region (Fig. 21K,O). In addition, a weak signal was detectable in the preoral pit (Fig. 21K). In the neural tube, *EAAT2* was expressed by floor plate and mediolateral cells, both of which

were characterized by slender and elongated cell bodies compared to those of ventrolateral cells (Fig. 21L-N). We further found that *EAAT2* was detectable in more ventrolateral cells than at earlier developmental stages (Fig. 21L-O). Of note, an antibody raised against the rat EAAT1 protein labeled a subset of ESNs in amphioxus L1 larvae (Fig. 21P). Given that only amphioxus *EAAT2* was expressed in ESNs, it seems likely that the antibody recognized the amphioxus EAAT2 protein.

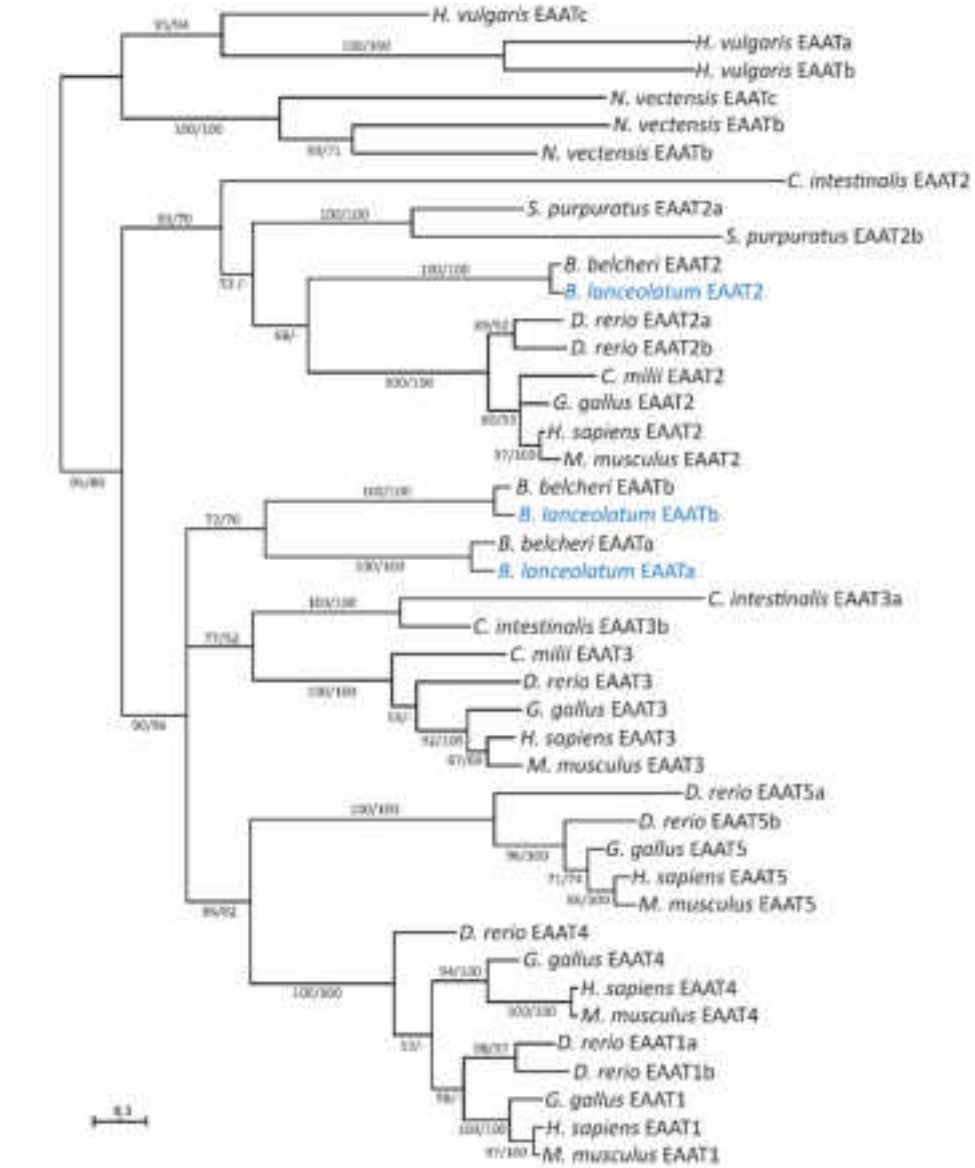

Figure 19. Phylogenetic tree of EAAT proteins. The phylogeny was calculated using both Maximum Likelihood (ML) and Neighbor Joining (NJ) methods and a JTT matrix-based model with 5 gamma categories (+*G*, parameter 0.6956). The ML tree is shown with bootstrap percentages for both ML and NJ analyses (first and second values, respectively), obtained in 1000 replicates. Cnidarian sequences were used as outgroup. List of animal taxa featured in the tree: *Branchiostoma belcheri* (Chinese amphioxus, cephalochordate), *Branchiostoma lanceolatum* (European amphioxus, cephalochordate), *Callorhinchus milii* (plough-nosed chimaera, cartilaginous fish), *Ciona intestinalis* (sea squirt, ascidian), *Danio rerio* (zebrafish, teleost fish), *Gallus gallus* (chicken, bird), *Homo sapiens* (human, mammal), *Hydra vulgaris* (hydra, cnidarian), *Latimeria chalumnae* (coelacanth, crossopterygian fish), *Mus musculus* (house mouse, mammal), *Nematostella vectensis* (starlet sea anemone, cnidarian), *Petromyzon marinus* (sea lamprey, jawless fish), *Rattus norvegicus* (common rat, mammal), *Strongylocentrotus purpuratus* (purple sea urchin, echinoderm), *Xenopus tropicalis* (western clawed frog, amphibian). From Bozzo et al. (2021).

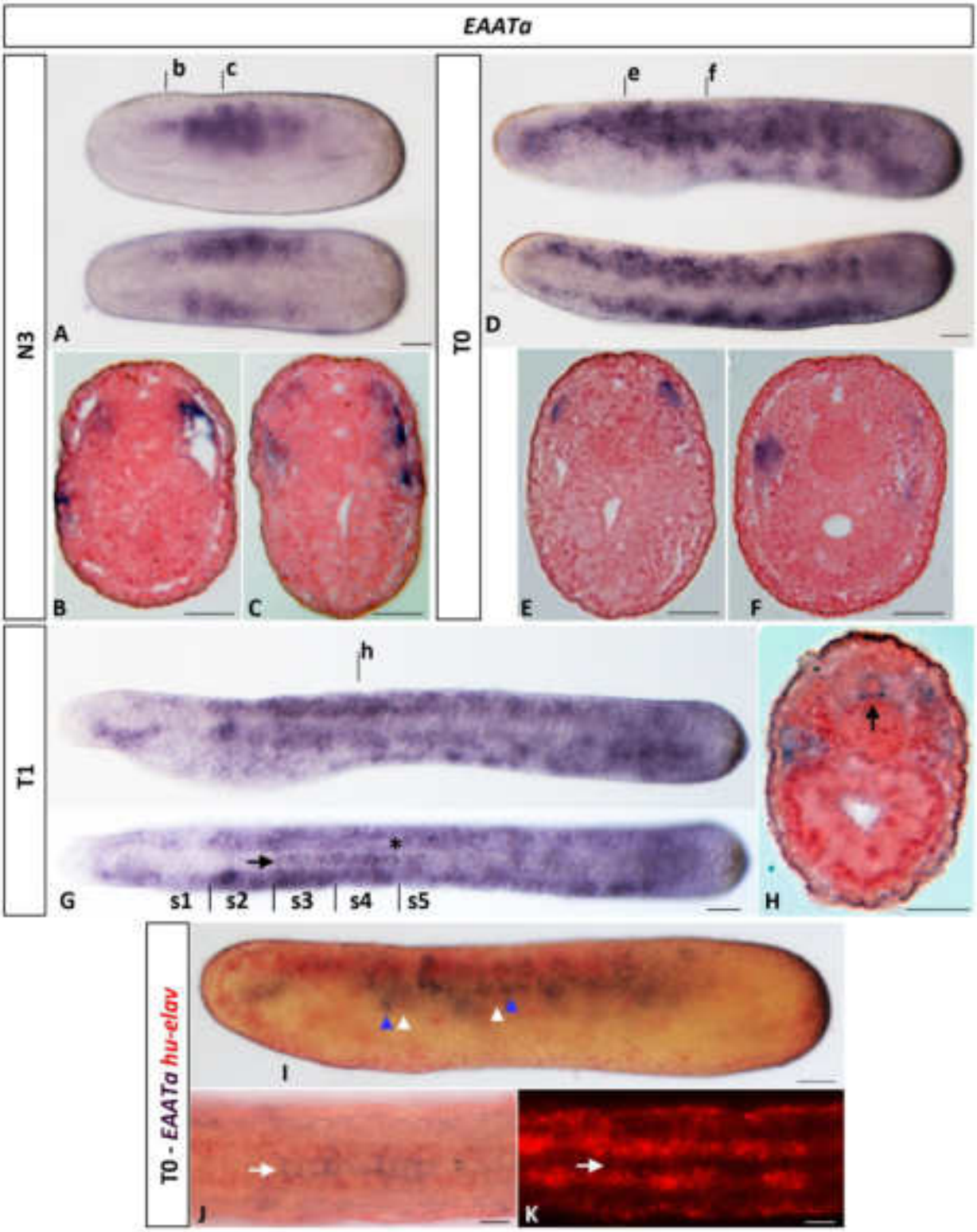

Figure 20. Expression of *EAATa* during amphioxus development. **A**: Whole mount N3 embryo in lateral (top) and dorsal (bottom) views showing *EAATa* expression in the somites. **B,C**: Transverse sections at levels indicated in A. **D**: Whole mount T0 embryo in lateral (top) and dorsal (bottom) views. *EAATa* is expressed in the somites. **E,F**: Transverse sections at levels indicated in D. **G**: Whole mount T1 embryo in lateral (top) and dorsal (bottom) views with the borders of the first five somite pairs indicated (s1-5). *EAATa* is expressed in the somites, in the head coelom and in a line of floor plate cells (arrow) at level of somite pairs 3 and 4, just anterior to the first pigment spot (asterisk). **H**: Transverse section at the level indicated in G, showing *EAATa* expression in somites and in floor plate. **I-K**: Double *in situ* hybridization for *EAATa* (purple) and *hu-elav* (red). *EAATa* is expressed in individual mesodermal cells

(blue arrowheads) that are close to, but not in contact with, *hu-elav*-positive ectodermal sensory neurons (white arrowheads). **J,K**: Magnification of the region of somite pairs 4 and 5 of the embryo in I in dorsal view in brightfield (J) and epifluorescence (K). The *EAATa* signal is only in the floor plate (arrow) and does not co-localize with *hu-elav*. Scale bars are 25 μm for whole mounts and 10 μm for sections. Whole mount embryos are oriented with anterior to the left and, if not shown in dorsal view, with dorsal to the top. From Bozzo et al. (2021).

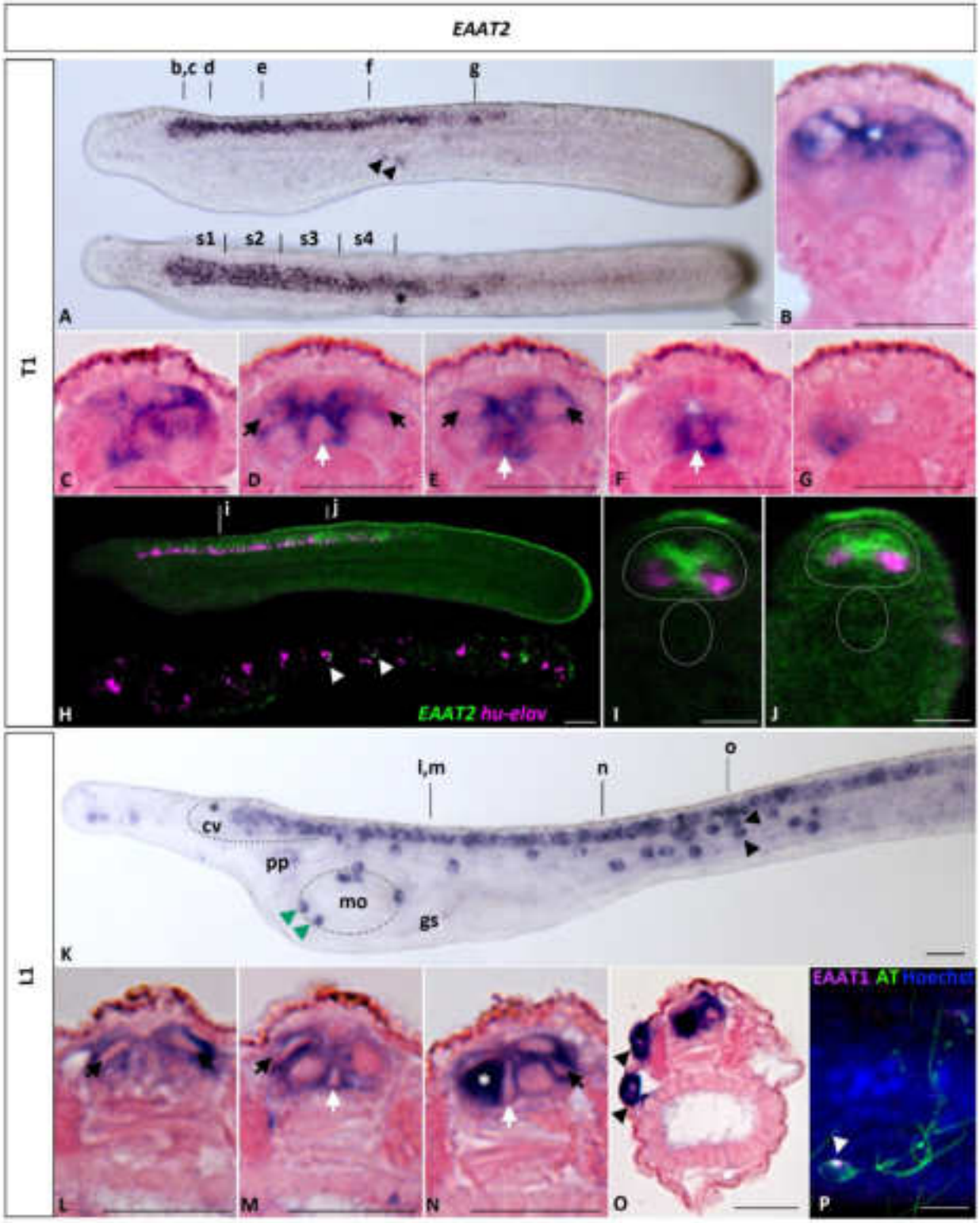

(Caption on following page)

Figure 21. Expression of *EAAT2* during amphioxus development. **A**: Whole mount T1 embryo in lateral (top) and dorsal (bottom) views with the borders of the first four somite pairs indicated (s1-4). *EAAT2* is expressed in the posterior cerebral vesicle and in the neural tube to the end of somite pair 6. Weak expression is also detectable in a few ectodermal sensory neurons (arrowheads) located in the mid-trunk region of the embryo. The asterisk indicates the first pigment spot. **B-G**: Transverse sections of the neural tube at levels indicated in A. Posterior to the cerebral vesicle, *EAAT2* is detected in the floor plate (white arrows), in glia-like cells (black arrows) and in ventrolateral cells, which are likely neurons (G). **H**: Median (top) and superficial (bottom) focal planes of a whole mount T1 embryo stained for *EAAT2* (green) and *hu-elav* (magenta), showing co-expression in ectodermal sensory neurons (arrowheads). **I,J**: Optical sections at levels indicated in H showing absence of co-localization of *EAAT2* and *hu-elav* in the neural tube. Dotted lines indicate limits of neural tube (top) and notochord (bottom). **K**: Anterior half of a whole mount L1 larva in lateral view. Dotted lines delimitate the cerebral vesicle and the oral plexus. *EAAT2* is expressed in ectodermal sensory neurons (black arrowheads), some of which are part of the oral plexus (green arrowheads). **L-O**: Transverse sections of the neural tube at levels indicated in K. *EAAT2* signal is detected in glia-like cells (black arrows), floor plate cells (white arrows), ventrolateral neurons (asterisk) and ectodermal sensory neurons (arrowheads). **P**: The anti-EAAT1 antibody Ab416 (Abcam) co-localizes with anti-β-tubulin (AT) in cell bodies of trunk ectodermal sensory neurons (white). Scale bars are 25 μm for whole mounts and 10 μm for sections. Whole mount embryos are oriented with anterior to the left and, if not shown in dorsal view, with dorsal to the top. Abbreviations: cv, cerebral vesicle; gs, gill slit; mo, mouth; pp, preoral pit. From Bozzo et al. (2021).

Phylogeny and expression of *glutamine synthetase* in developing amphioxus

Our database searches retrieved single *GS* gene candidates in all assayed taxa, including amphioxus, and the phylogenetic analysis yielded a tree with an expected branching pattern, placing the amphioxus GS sequence at the base of a clade with the ascidian plus vertebrate sequences (Fig. 22).

In developing amphioxus, the *GS* gene was first expressed by *in situ* hybridization at the N3 stage, in the anterior CNS and weakly in mesoderm and endoderm (Fig. 23A,B). In T1 embryos, *GS* transcripts were found in the cerebral vesicle and in scattered floor plate, ventrolateral and mediolateral cells of the RhSp (Fig. 23C-H), in the same region where *EAAT2* was expressed (Fig. 23D-F). This suggests that at least some of the amphioxus glial cells share similarities with vertebrate astroglia. Expression was particularly conspicuous in lateral cells of the anterior cerebral vesicle, closely associated with the glutamatergic neurons of the frontal eye complex (Candiani et al., 2012). *GS* was also expressed in the first pigment spot as well as the tail bud region (Fig. 23C,G). At the L1 stage, neural expression was detected in the frontal eye complex, in the floor plate and in ventrolateral and mediolateral cells of the RhSp (Fig. 23I-M).

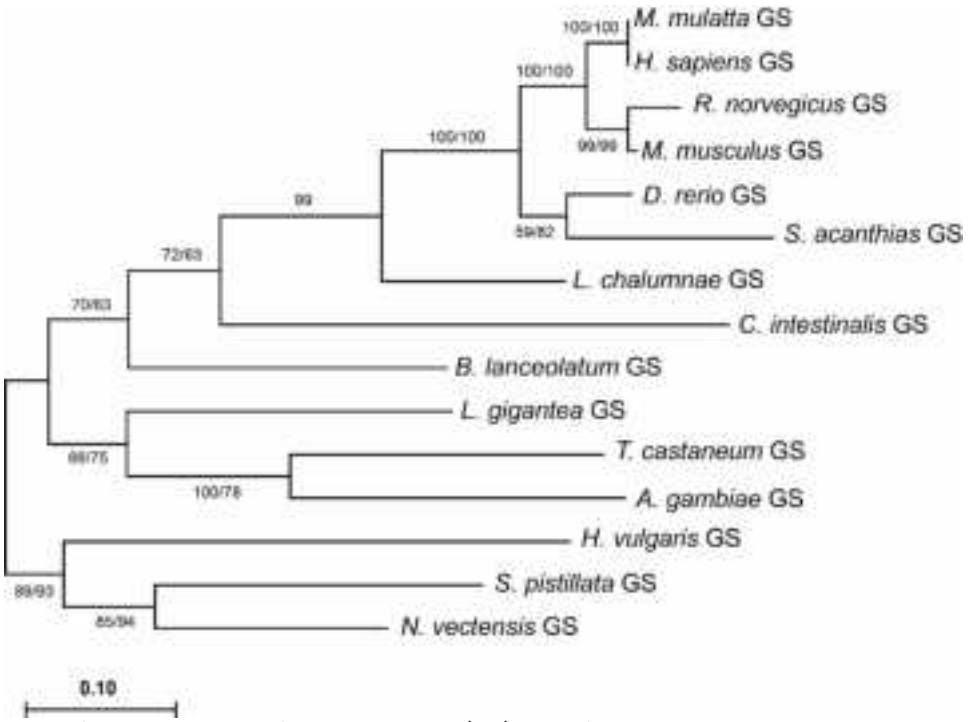

Figure 22. Phylogenetic tree of glutamine synthetase (GS) proteins. The phylogeny was calculated using both Maximum Likelihood (ML) and Neighbor Joining (NJ) methods and a Le Gascuel 2008 model with 5 gamma categories (*+G*, parameter 0.5101). The ML tree is shown with bootstrap percentages for both ML and NJ analyses (first and second values, respectively), obtained in 1000 replicates. Cnidarian sequences were used as outgroup. List of animal taxa featured in the tree: *Anopheles gambiae* (mosquito, insect), *Branchiostoma lanceolatum* (European amphioxus, cephalochordate), *Danio rerio* (zebrafish, teleost fish), *Homo sapiens* (human, mammal), *Hydra vulgaris* (hydra, cnidarian), *Latimeria chalumnae* (coelacanth, crossopterygian fish), *Lottia gigantea* (owl limpet, gastropod mollusc), *Macaca mulatta* (rhesus macaque, mammal), *Mus musculus* (house mouse, mammal), *Nematostella vectensis* (starlet sea anemone, cnidarian), *Rattus norvegicus* (common rat, mammal), *Squalus acanthias* (spiny dogfish, cartilaginous fish), *Stylophora pistillata* (hood coral, cidarian), *Tribolium castaneum* (red flour beetle, insect). From Bozzo et al. (2021).

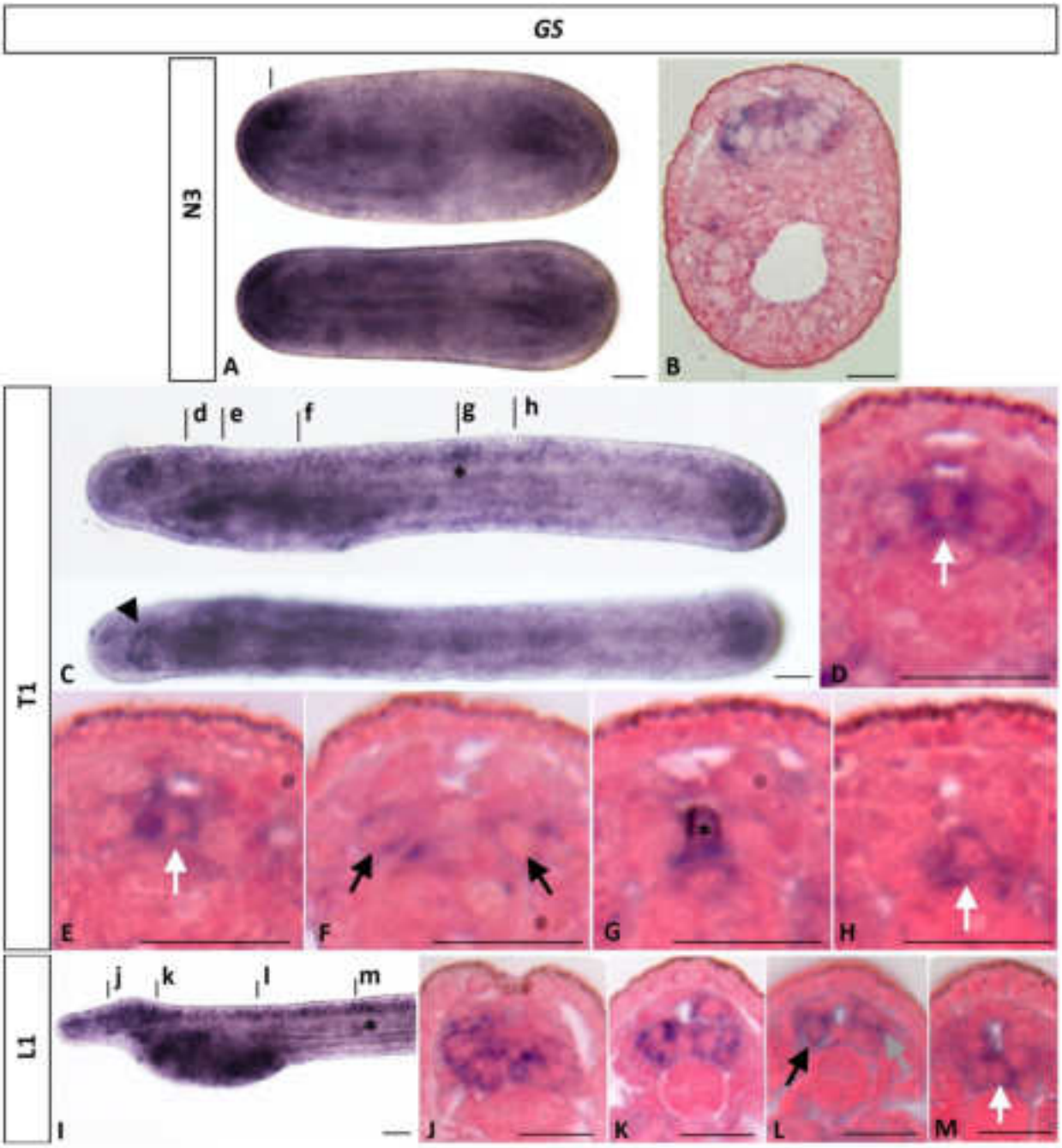

Figure 23. Expression of *glutamine synthetase* (*GS*) during amphioxus development. **A**: Whole mount N3 embryo in lateral (top) and dorsal (bottom) views. **B**: Transverse section at level indicated in A showing *GS* expression in the anterior central nervous system, in a region corresponding to the prospective cerebral vesicle. **C**: Whole mount T1 embryo in lateral (top) and dorsal (bottom) views. **D-H**: Transverse sections at levels indicated in C showing *GS* transcripts in floor plate (white arrow) and ventrolateral cells (black arrows) of the neural tube and in the first pigment spot (asterisk). **I**: Magnification of the anterior part of a whole mount L1 larva in lateral view. *GS* transcripts are detectable in the neural tube as well as in the endoderm. The asterisk indicates the first pigment spot. **J-M**: Transverse section of the larva in I showing signal in floor plate (white arrow), ventrolateral (black arrow) and mediolateral (grey arrow) cells of the neural tube. Scale bars are 25 μm for whole mounts and 10 μm for sections. Whole mount embryos are oriented with anterior to the left and, if not shown in dorsal view, with dorsal to the top. From Bozzo et al. (2021).

Phylogeny and expression of *GFAP*/*vimentin*-like genes in developing amphioxus

Animal intermediate filaments are subdivided into six types (I through VI), and GFAP and vimentin are type III intermediate filaments. It has previously been shown that the amphioxus genome contains 26 genes encoding intermediate filaments (Karabinos, 2013). Our phylogenetic analyses revealed that six of them were closely related to a clade including both vertebrate type III and IV intermediate filaments: *IF B1*, *IF B2*, *IF A1*, *IF A2*, *IF A3* and *IF N2*, according to the nomenclature proposed by Karabinos (2013). Of these, *IF N2* branched at the base of the vertebrate type III and IV intermediate filaments, while the other five amphioxus sequences formed an independent clade, indicating that these genes might have originated by lineage-specific duplication (Fig. 24). We were able to retrieve sequence information for five of the six genes from the *B. lanceolatum* genome. Based on the available transcriptome data (Marlétaz et al., 2018), three of these genes (*IF N2*, *IF B1* and *IF B2*) were expressed during development.

While the *IF B2* gene was exclusively expressed in the notochord of the larva (Fig. 25), *IF B1* was widely expressed in different territories of both embryo and larva (Fig. 26). *IF B1* transcripts were first detectable at the N4 stage in the somites and in a few cells of the anterior CNS, at level of the DiMes (Fig. 26A-C). In T0 and T1 embryos, *IF B1* was strongly expressed in somites (Fig. 26D-G), ventral mesoderm (Fig. 26F) and scattered cells of the nerve cord (Fig. 26D-F). Expression was detected at contact points of neural tube and somites, as shown by co-localization of *IF B1* and *synapsin* (Fig. 26H,L). In the CNS, *IF B1* was further co-expressed with *synapsin* in ventral cells of the posterior cerebral vesicle (Fig. 26H,I,K) as well as in ventrolateral cells at more posterior levels (Fig. 26H,L,M). At T0 and T1 stages, *IF B1* and *synapsin* were also detectable in most ESNs (Fig. 26D,G,H,J-M). In the L1 larva, *IF B1* was still expressed in the posterior cerebral vesicle and in ventrolateral cells of the neural tube, but not in ESNs (Fig. 26N-T). Outside the CNS, expression of the gene was detectable in the endoderm, in particular around the mouth and in the dorsal roof of the pharynx, as well as in the mesoderm lining the body cavities (Fig. 26N-T). However, we found virtually no expression in the somites. *IF N2* was first expressed at the T0 stage. At the T1 stage, the gene was expressed dorsally in cerebral vesicle and neural tube, in ESNs of the mid-trunk region as well as in the tail bud (Fig. 27A-F). Double *in situ* hybridization experiments revealed that *IF N2*-positive cells in the CNS did not co-express *hu-elav* (Fig. 27G-H). Expression of *IF N2* was subsequently downregulated along the neural tube and persisted only in the dorsal cerebral vesicle (Fig. 27I,J). However, transcription of *IF N2* in ESNs and tail bud was maintained (Fig. 27I,K). Expression of *IF N2*, the best candidate for an amphioxus *GFAP*/*vimentin* homolog, in cells not expressing markers of neuronal commitment suggests that the dorsal neural tube of developing amphioxus contains a pool of undifferentiated neural precursors.

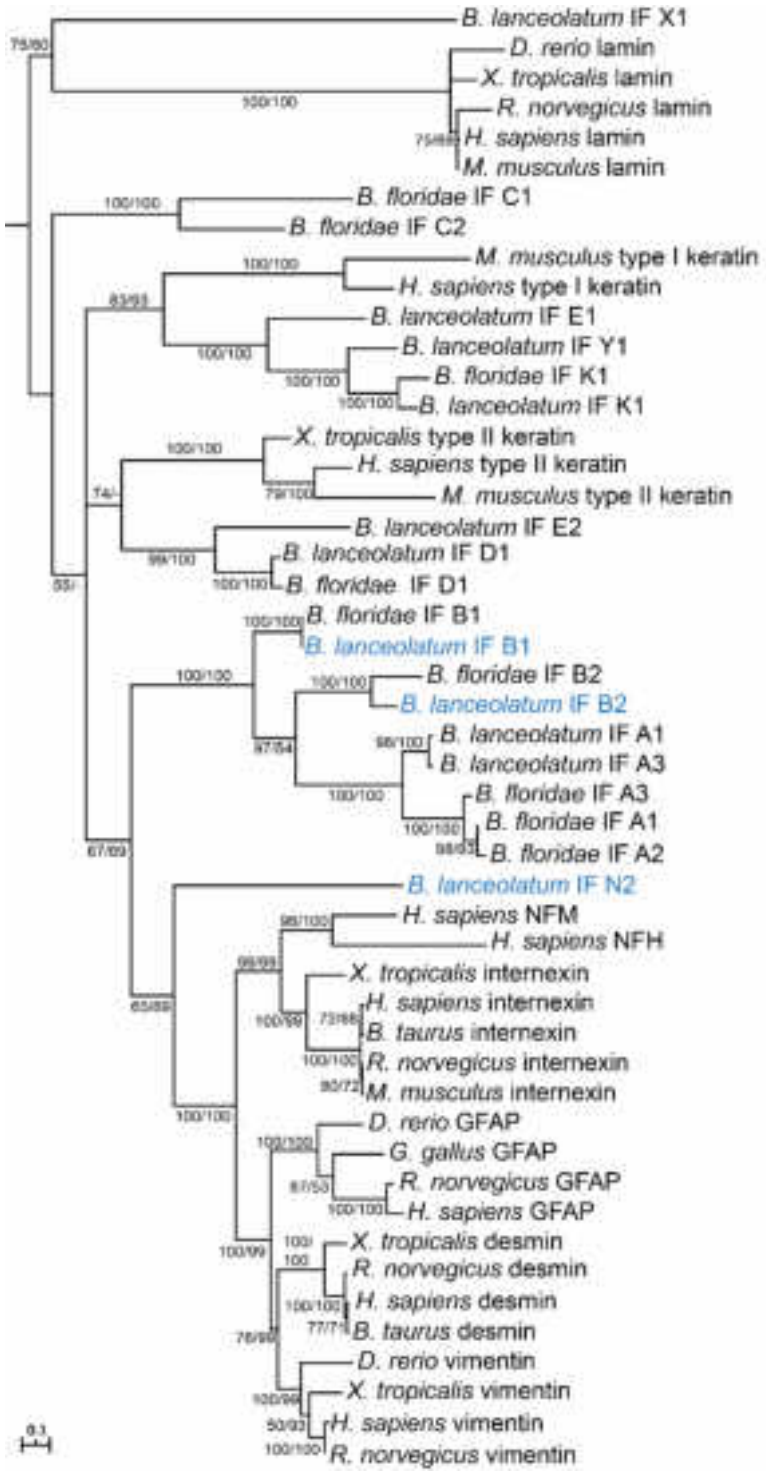

Figure 24. Phylogenetic tree of intermediate filament (IF) proteins. The phylogeny was calculated using both Maximum Likelihood (ML) and Neighbor Joining (NJ) methods and a JTT matrix-based model with 5 gamma categories (+*G*, parameter 4.3353). The ML tree is shown with bootstrap percentages for both ML and NJ analyses (first and second values, respectively), obtained in 1000 replicates. Lamin (type V intermediate filament proteins) and related amphioxus sequences were used to root the tree. List of animal taxa featured in the tree: *Bos taurus* (cattle, mammal), *Branchiostoma floridae* (Florida amphioxus, cephalochordate), *Branchiostoma lanceolatum* (European amphioxus, cephalochordate), *Danio rerio* (zebrafish, teleost fish), *Gallus gallus* (chicken, bird), *Homo sapiens* (human, mammal), *Mus musculus* (house mouse, mammal), *Rattus norvegicus* (common rat, mammal), *Xenopus tropicalis* (western clawed frog, amphibian). From Bozzo et al. (2021).

Figure 25. Expression of *IF B2* in the notochord of an amphioxus L3 larva. Scale bar is 50 µm. From Bozzo et al. (2021).

Figure 26. Expression of *IF B1* during amphioxus development. **A**: Whole mount N4 embryo in lateral (top) and dorsal (bottom) views. *IF B1* is expressed in the somites and in a group of cells located in the anterior central nervous system. **B,C**: Transverse sections at levels indicated in A showing *IF B1* in the neural plate (B) and somites (C). **D**: Whole mount T1 embryo in lateral (top) and dorsal (bottom) views with the borders of the first four somite pairs indicated (s1-4). *IF B1* transcripts are present in the posterior cerebral vesicle, along the neural tube, in somites, the notochord and ectodermal sensory neurons (arrowhead). **E-G**: Transverse sections at levels indicated in D. **E**: At the level of the posterior cerebral vesicle, *IF B1* is expressed in nerve cord and adjacent mesoderm. **F**: Posterior to the cerebral vesicle, *IFB1* is expressed in ventrolateral cells of the nerve cord and in ventral mesoderm surrounding the gut endoderm (white arrowhead). **G**: *IF B1* is expressed in ectodermal sensory neurons (black arrowheads). **H**: Whole mount T0 embryo in lateral (top and middle, different focal planes) and dorsal (bottom) views, showing *IF B1* (red) and *synapsin* (green) expression. **I**: Magnification of the cerebral vesicle (dotted box at the top in H). *IF B1* and *synapsin* are co-expressed by ventral cells in the posterior cerebral vesicle (yellow arrow). **J**: Magnification of the ectoderm (dotted box in the middle in H) showing co-expression of *IFB1* and *synapsin* in ectodermal sensory neurons. **K-M**: Optical transverse sections at levels indicated in H with dotted lines outlining the CNS (top) and the notochord (bottom). *IFB1* and *synapsin* co-localize in the ventral posterior cerebral vesicle (yellow arrow), in somite cells contacting the neural tube to receive motor inputs (white arrow) and in ventrolateral cells (arrowhead). **N**: Whole mount L1 larva in lateral view. **O-T**: Transverse sections at levels indicated in N. Transcripts are detected in ventral and dorsal cells of the posterior cerebral vesicle (O), in ventral cells of the neural tube (P-T), in the endoderm of the pharynx (double- arrow in P) and gut (double-headed arrow in T) and in ventral mesoderm cells surrounding the gut (arrows in P,T). Scale bars are 25 µm for whole mounts and 10 µm for sections. Whole mount embryos are oriented with anterior to the left and, if not shown in dorsal view, with dorsal to the top. Abbreviations: cv, cerebral vesicle; gs, gill slit; mo, mouth; n, notochord; nt, neural tube; pp, preoral pit; s, somite. From Bozzo et al. (2021).

(Figure on the next page)

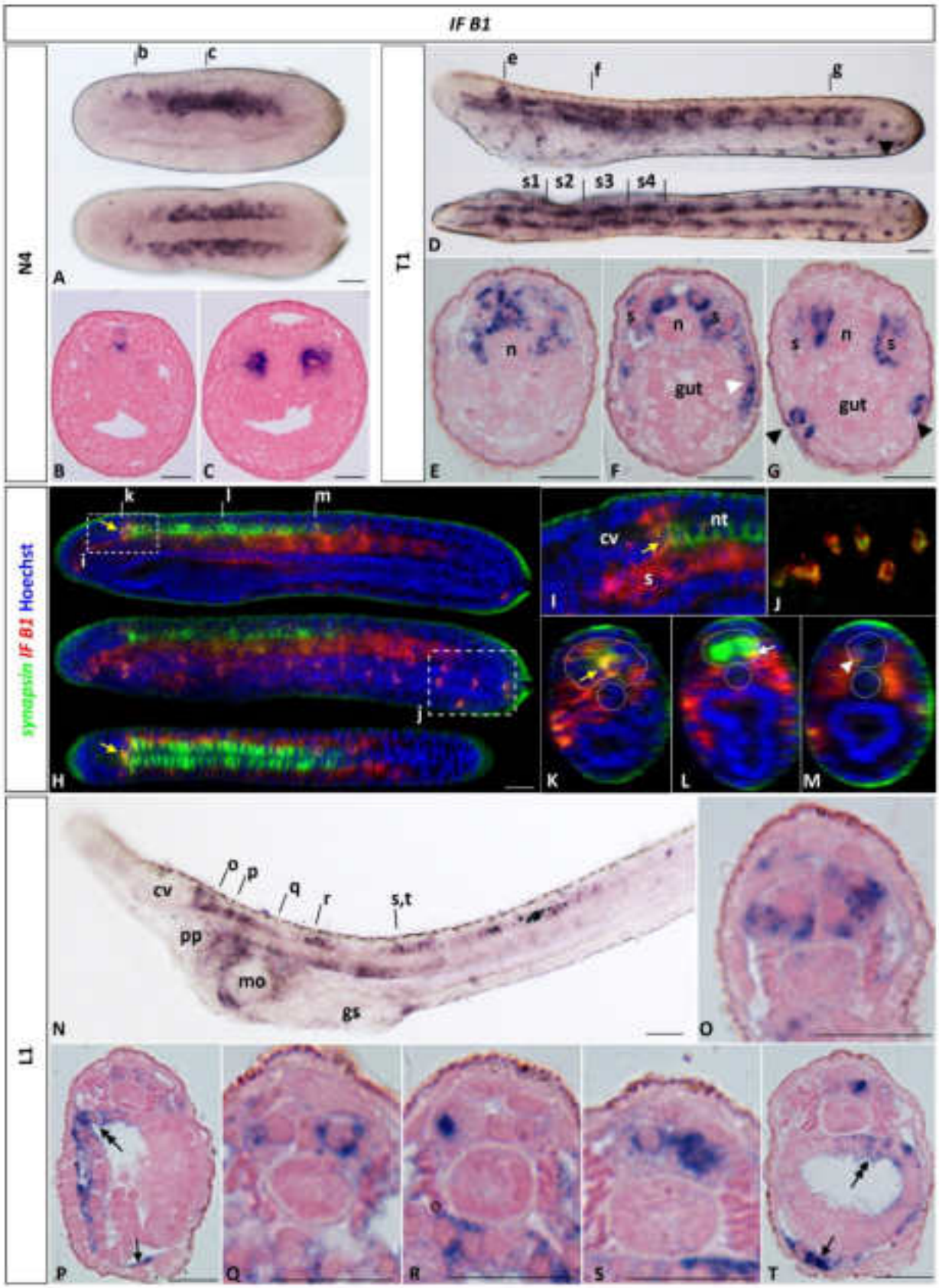

Figure 26. (Caption on the previous page)

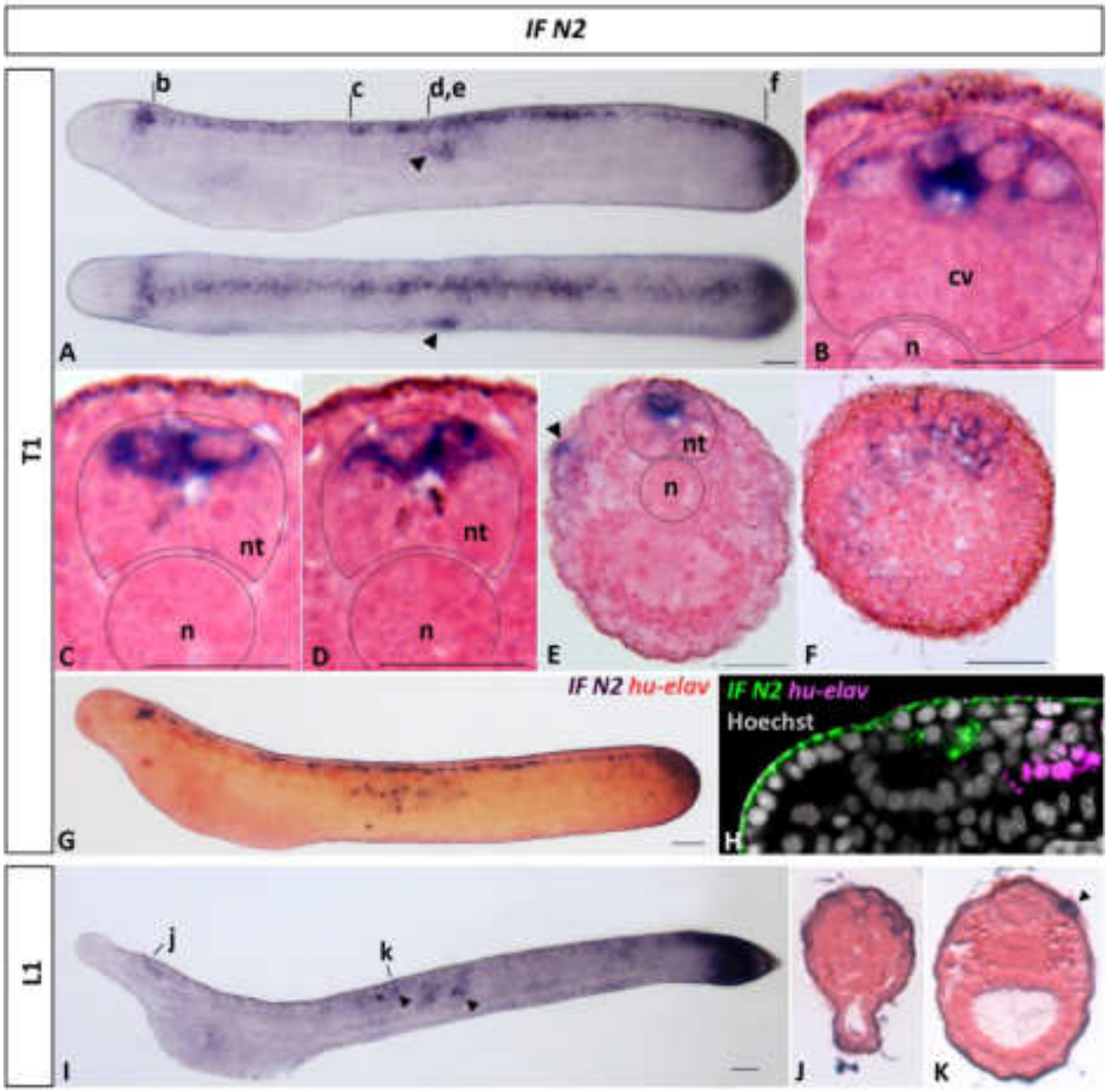

Figure 27. Expression of *IF N2* during amphioxus development. **A**: Whole mount T1 embryo in lateral (top) and dorsal (bottom) views. *IF N2* is expressed in the central nervous system from the posterior cerebral vesicle to the tail bud as well as in ectodermal sensory neurons in the mid-trunk region (arrowheads). **B-F**: Transverse sections at levels indicated in A showing expression of *IF N2* in the cerebral vesicle, along the neural tube and in ectodermal sensory neurons (arrowheads). **G,H**: Double *in situ* hybridization for *IF N2* and *hu-elav* in brightfield (G) and epifluorescence (H) showing lack of co-expression in the central nervous system. **I**: Whole mount L1 larva in lateral view. *IF N2* transcripts are located in the posterior cerebral vesicle, ectodermal sensory neurons in the mid trunk region (arrowheads) and in the tail bud. **J,K**: Transverse sections at levels indicated in I, showing expression in the dorsal cerebral vesicle (J) and ectodermal sensory neurons (arrowhead in K). Scale bars are 25 μm for whole mounts and 10 μm for sections. Whole mount embryos are oriented with anterior to the left and, if not shown in dorsal view, with dorsal to the top. Abbreviations: cv, cerebral vesicle; n, notochord; nt, neural tube. From Bozzo et al. (2021).

Phylogeny and developmental expression of *olig* genes in amphioxus

Vertebrates generally have four *olig* genes (*olig1-4*), with *olig4* having been lost in amniotes. We also identified three *olig* genes in amphioxus that, in our phylogenetic tree, formed a single clade at the base of the vertebrate *olig* genes (Fig. 28). We named these amphioxus genes *oliga*, *oligb* and *oligc*, with the letters corresponding to the *B. floridae* orthologs (Ren et al., 2020). Our *in situ* hybridization experiments revealed that the three amphioxus *olig* paralogs have remarkably similar expression patterns during development (Fig. 29). We thus decided to use the gene with the most conspicuous signal for our detailed expression analyses, which was *oliga*, and to refer to the observed patterns as those of amphioxus *olig*.

At the N0 stage, *olig* transcripts were widely distributed in median and lateral cells of the neural plate (Fig. 30A,B). By the N2 stage, *olig* expression was downregulated along the future floor plate, but remained expressed in paired domains (Fig. 30C) that correspond to the basal and alar plates (Albuixech-Crespo et al., 2017). At the N3 stage, the *olig* pattern changed into a series of small cell clusters, and the *olig*-positive cells of the basal and alar plates adopted, respectively, ventrolateral and dorsal positions in the forming neural tube (Fig. 30D-E). In the most posterior part of neural plate, *olig* was expressed in all cells except in those of the floor plate (Fig. 30F). This differential expression pattern was even more evident at the N4 stage (Fig. 30G-J). In N4 embryos, *olig* expression in the dorsal and ventral cell clusters was out of register, with dorsal cells located at somite boundaries and ventral cells at the level of the somites (Fig. 30G). Double *in situ* hybridization experiments revealed that the ventrolateral cells co-expressed the *VAChT* gene (encoding the vesicular acetylcholine transporter), a marker of cholinergic neurons (Candiani, Lacalli, et al., 2008), while the dorsal cells did not (Fig. 30A-C). Contrary to previous reports (Beaster-Jones et al., 2008), *olig* expression was not detected in somites.

At the T0 stage, *olig* was expressed, anteriorly, in five that the *olig*-positive cells in the RhSp are motor neurons. The posterior *olig* domain became more conspicuous at the T1 stage, the signal extending from somite pair 6 to the tail bud, with *olig* expressed by most cells of the neural tube, excepting the floor plate (Fig. 30L,Q). In L1 larvae, *olig* was expressed in the anterior cerebral vesicle, posterior and dorsal to the frontal eye complex (Fig. 30R,S) and by mediolateral clusters of cells in the RhSp (Fig. 30T-W). The posterior expression domain extending to the tail bud was also maintained (Fig. 30R). In sum, *olig* expression in the developing amphioxus nervous system is complex and dynamic, marking both differentiated and undifferentiated cell populations.

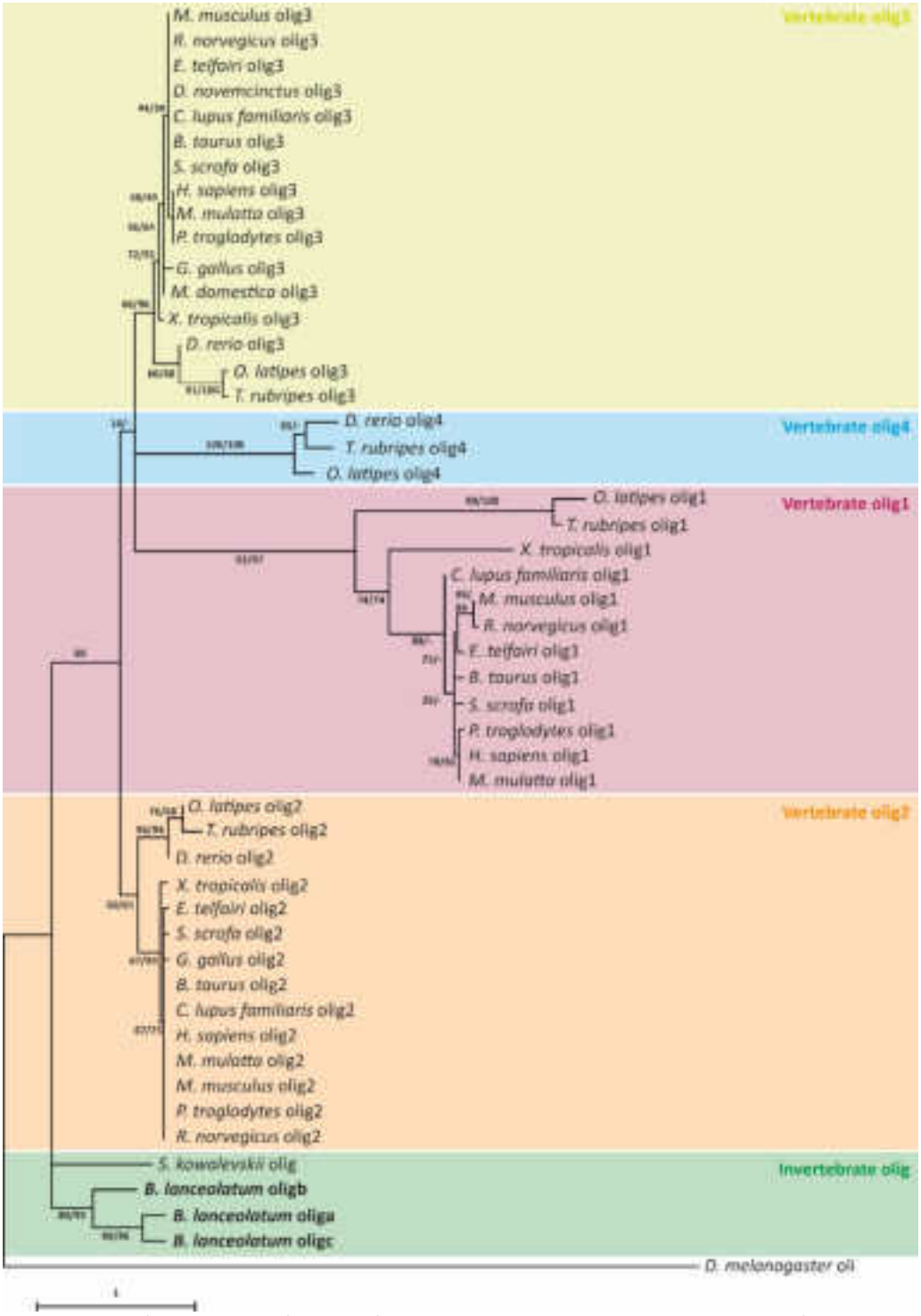

Figure 28. Phylogenetic tree of olig proteins. The phylogeny was calculated using both Maximum Likelihood (ML) and Neighbor Joining (NJ) methods and a JTT matrix-based model with 5 gamma categories (+*G*, parameter 2.0677). The ML tree is shown with bootstrap percentages for both ML and NJ analyses (first and second values, respectively), obtained in 1000 replicates. Neurogenin-1 (NGN-1) from the cnidarian *Nematostella vectensis* was used as outgroup. List of animal taxa featured in the tree: *Branchiostoma belcheri* (Chinese amphioxus, cephalochordate), *Branchiostoma lanceolatum* (European amphioxus, cephalochordate), *Danio rerio* (zebrafish, teleost fish), *Gallus gallus* (chicken, bird), *Homo sapiens* (human, mammal), *Mus musculus* (house mouse, mammal), *Nematostella vectensis* (starlet sea anemone, cnidarian), *Rattus norvegicus* (common rat, mammal), *Saccoglossus kowalevskii* (acorn worm, hemichordate), *Xenopus tropicalis* (western clawed frog, amphibian). From Bozzo et al. (2021).

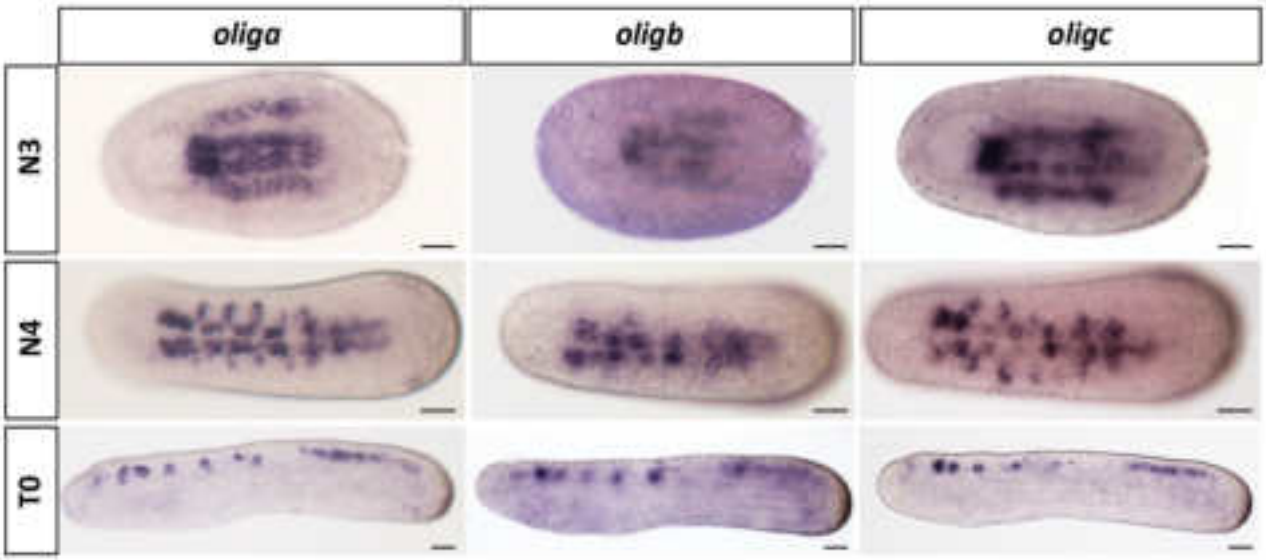

Figure 29. Comparison of the expression patterns of the three amphioxus *olig* genes. Scale bar is 25 µm. From Bozzo et al. (2021).

Figure 30. Expression of *olig* during amphioxus development. **A**: Whole mount N0 embryo in dorsal view showing expression in the neural plate. **B**: Transverse section at level indicated in A. **C**: Whole mount N2 embryo in lateral (top) and dorsal (bottom) views. **D**: Whole mount N3 embryo in lateral (top) and dorsal (bottom) views. **E,F**: Transverse sections at levels indicated in D showing expression in ventrolateral and dorsal cells of the neural plate. **G**: Whole mount N4 embryo in lateral (top) and dorsal (bottom) views with the borders of the first four somite pairs indicated (s1-4). **H-J**: Transverse sections at levels indicated in G, showing *olig* expression laterally in the cerebral vesicle, ventrolaterally and dorsally along the neural tube and in most cells of the posterior neural tube. **K,L**: Whole mount T0 (K) and T1 (L) embryos in lateral (top) and dorsal (bottom) views with the borders of the first four somite pairs indicated (s1-4), showing segmented expression in cell pairs stretching from the posterior cerebral vesicle to the first pigment spot (asterisks) and continuous expression in the posterior neural tube. Labeled cell pairs are in register with somite boundaries, marked by a double-pointed arrow in the cerebral vesicle and by arrows more posteriorly. **M-Q**: Transverse sections of the neural tube at levels indicated in L. *olig* is expressed in the posterior cerebral vesicle, in ventrolateral cells located at the borders between the first four somite pairs as well as in most cells of the posterior neural tube. **R**: Whole mount L1 larva in lateral view. **S-W**: Transverse sections at levels indicated in R, showing *olig* expression dorsally in the cerebral vesicle, laterally posterior to the cerebral vesicle and in most cells of the posterior neural tube. Scale bars are 25 µm for whole mounts and 10 µm for sections. Whole mount embryos are oriented with anterior to the left and, if not shown in dorsal view, with dorsal to the top. Abbreviations: gs, gill slit; pp, preoral pit. From Bozzo et al. (2021).

(Figure on the next page)

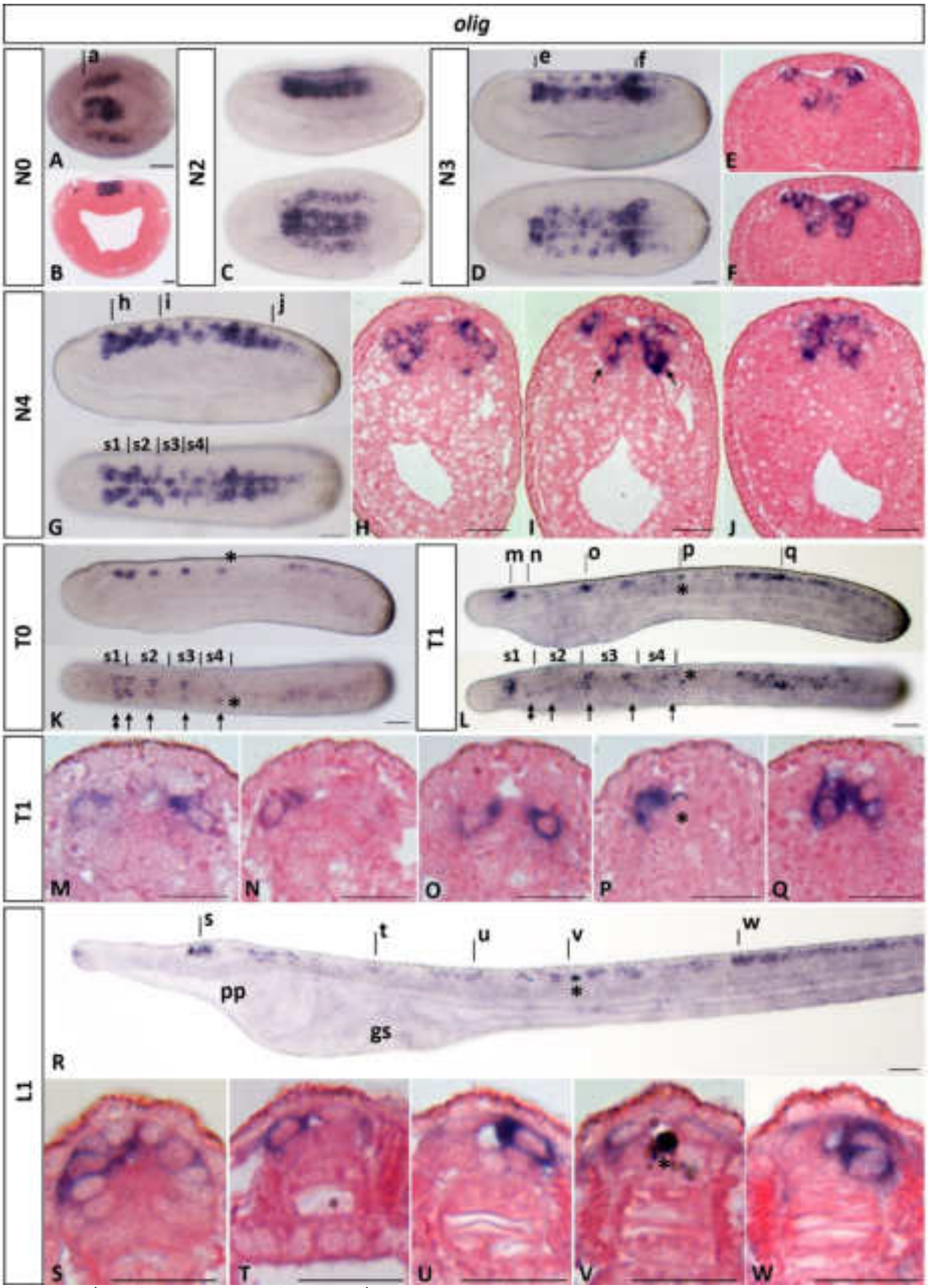

Figure 30. (Caption on the previous page)

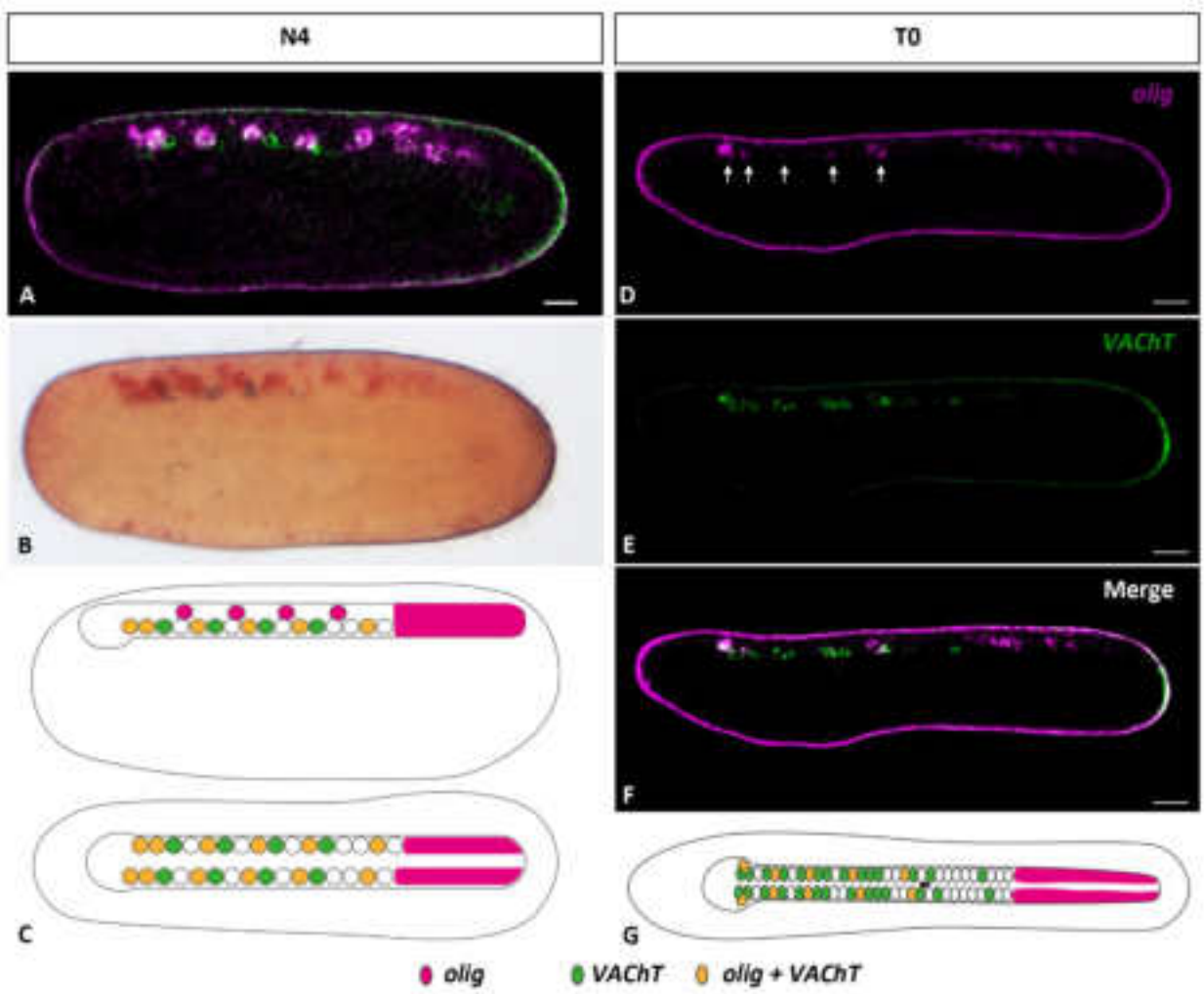

Figure 31. Co-expression of *olig* and the cholinergic marker *VAChT* (*vesicular acetylcholine transporter*) during amphioxus development. **A,B**: Lateral view of a N4 embryo in epifluorescence (A) and brightfield (B). For epifluorescence, *olig* is in magenta, *VAChT* is in green and white indicates co-localization. For brightfield, *olig* is in red and *VAChT* is in purple. **C**: Schematic drawing of N4 embryo in lateral (top) and dorsal (bottom) views. **D-F**: Lateral view of a T0 embryo in epifluorescence, showing *olig* (D), *VAChT* (E) and *olig* plus *VAChT* (F) expression. **G**: Schematic drawing of a T0 embryo in dorsal view. Scale bars are 25 μm. Whole mount embryos are oriented with anterior to the left and, if not shown in dorsal view, with dorsal to the top. From Bozzo et al. (2021).

Ultrastructure of the developing amphioxus nerve cord

Serial TEM sections through the nerve cord of a 12-day larva, available from previous studies of *B. floridae* (Lacalli et al., 1994; Lacalli & Kelly, 2002), were re-examined in order to provide a more meaningful anatomical context for assessing the molecular results described above (Fig. 32). Most of the glia-like cells identified at this stage appear to be involved in maintaining the shape and structure of the cord itself. This included the roof plate and floor plate, each of which consists of a single file of cells. The floor plate cells were distinctive and easily identified based on location and their pyramidal shape, evident even at the T1 stage (Fig. 33). Glia-like cells with irregular branching processes developed subsequently in association with the floor plate. These are referred to as axial glia by Lacalli & Kelly (2002), who found six such cells in the nerve cord to the end of somite pair 2 in a 12-day specimen, all attached to the central

canal adjacent to floor plate, and two to three cells per somite pair more caudally in younger larvae. The latter cells were typically found embedded in the neuropile, but their proximity to the ventral midline suggested the latter as their most likely place of origin, ruling out lateral or more dorsally positioned glial precursors as a source.

The other structural feature of interest in the 12-day nerve cord is the presence of a lateral zone of lozenge-shaped cells with basal end feet that attached to the basal lamina on each side at or just below the mid-point of the cord as measured along its dorsoventral axis (Fig. 33). These are categorized here as belonging to a class broadly characterized as "support cells", which typically occur in compact groups of three to four cells of radial glial-type morphology, including ependymoglial cells, whose basal process contained a densely stained fiber bundle, or ependymal cells, with no visible fiber bundle. The fiber-containing cells usually occur in pairs (Fig. 32A), though three were found together in some cases. Counting the number of individual fiber-containing cells to the end of somite pair 2, and excluding the most dorsal examples, we found 18 on the right side and 20 on the left. Compared to about 10 *EAAT2*-positive cells (n = 5) on each side of the floor plate over the same distance at the T1 stage (Fig. 21A), this implies that one further round of cell division is required subsequent to T1 before enough precursors are in place to account for the clusters observed at 12 days. It was not obvious whether the cells without fibers, i.e., the lateral ependymal cells as we define them here, were in fact differentiated cells or undifferentiated precursors for something else. Their position and morphology at this stage are consistent with their performing an accessory support function, while the same cannot be said of the assortment of other non-neural cells we found in the ependymal layer, including the rather dense, compact cells that occupied the spaces between the much larger ventral neurons (Fig. 33). For the floor plate itself, the *EAAT2* staining showed an average of 13 cells at T1 (n = 5), compared with 34 floor plate cells and 6 axial glia in the 12-day specimen, which implies between one and two further divisions is needed to account for the observed number of floor plate cells at 12 days, despite the fact that the T1 floor plate cells look fully differentiated (Fig. 33). If the latter do continue to divide after the T1 stage, it seems unlikely they would retract their extensive basal end-feet to do so. This could explain why the divisions, as judged from apex morphology, are mainly transverse or oblique, which may be the only way to reliably divide the basal compartment of the cell so that each daughter cell still bridges the midline.

The basal projections from lateral ependyma and ependymoglial cells form, in effect, a barrier between the ventrolateral neuropile on each side and the dorsal fiber tracts, which contain peripheral sensory fibers and the cell bodies of intramedullary dorsal bipolar neurons. The barrier is breached at numerous points (vertical bars in Fig. 32B), so the neuropile and dorsal tracts communicate, especially in the regions with significant sensory input to interneurons involved in the locomotory response. Groups of support-type cells also occur more dorsally. Their end feet and fibers attach to the lamina more dorsally than the lateral clusters, in a few cases passing above rather than below the dorsal tracts. It has proven difficult to document these fully, as the fiber bundles were often quite small, which makes it difficult to

decide, for example, if the cell with the broad apex on the right between sections 1000 and 1070 is an ependymoglial type comparable to more ventral examples, or something else (Fig. 32C). In fact, cells facing the central canal lumen in this more dorsal region often have expanded apices that comprise a large fraction of the region of contact between the apposed sides of the nerve cord epithelium, suggesting a structural role whether the cells contain fiber bundles or not.

Because most of the cells in the nerve cord retain their apical cilium and connection to the central canal, the pattern formed by their apices is potentially a better guide to division patterns and lineage relationships than the locations of the cell body. Apex length can, in fortuitous circumstances, be used to identify when, in relation to nerve cord elongation, a differentiated neuron completes its final division. This requires that the plane of division be close to transverse, which was unfortunately not the case with most support cells, which can be seen in the preponderance of narrow apices oriented with the long axis of the cord (Fig. 32C). Among these are cells that almost certainly arose from the same precursors, e.g., the paired ependymoglial cells on either side between sections 1050 and 1120. Their apices are parallel and of similar length, implying that they are sister cells of a division that divided the cell apex lengthwise in equal halves. We also noted a tendency for dorsal support cells to have quite small apices in some instances, consistent with at least some of these arising later in development. There were exceptions, however, including the cell mentioned above (apex between 1000 and 1070), and because of these and other apparent anomalies, we have not yet found a way of consistently identifying clusters of lineage-related cells from data of this type.

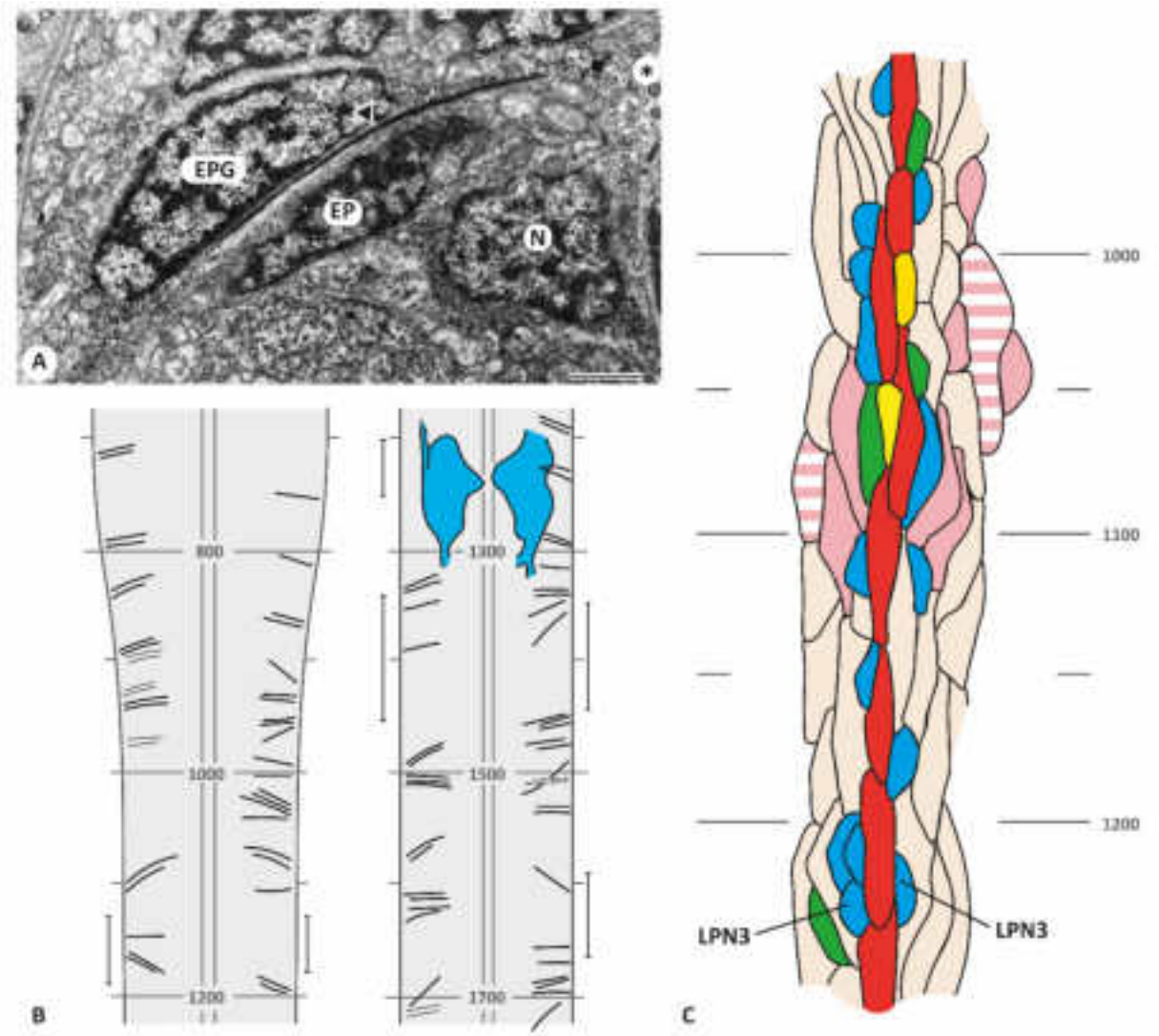

Figure 32. Transmission electron microscopy (TEM) data from serial sections of a 12-day amphioxus (*Branchiostoma floridae*) larva. **A**: A typical pair of lateral support cells, one ependymal (ep), the other, based on the presence of a fiber bundle, ependymoglial (epg). Asterisk indicates the central canal. Scale bar is 1 µm. **B**: Dorsal view of the nerve cord from about the middle of somite pair 1 to the middle of somite pair 2. Section numbers (100 sections = 6.8 µm) correspond to previously published maps for this section series, with the third pair of large paired neurons (LPN3, in blue) marking the approximate location of the junction of somite pairs 1 and 2. Fiber bundles are shown as line segments, slightly thinner for the dorsal-most examples, which are often much smaller. Support cell end feet typically project slightly caudally as they approach the lateral surface of the cord, but some do the reverse, usually because the cell from which they arise has itself been displaced by one or more large neurons. **C**: Map of the apices of cells projecting into the central canal, a segment of a larger map published as Fig. 3 in Lacalli (2000), showing the ventral surface of the nerve cord as it would appear from above if it were opened out flat with the midline in the center. Cilia are present, one per cell, but are not shown. Apices are color-coded by cell type: floor plate (red), ependymoglia (pink, hatched for two cells whose fiber bundle was so small as to be questionable as a marker), axial glia (yellow), motoneurons (green), interneurons (blue), all other cells, including other support cells and undifferentiated precursors (beige). Abbreviations: ep, ependymal cell; epg, ependymoglial cell; LPN3, third pair of large paired neurons; n, neuron. From Bozzo et al. (2021).

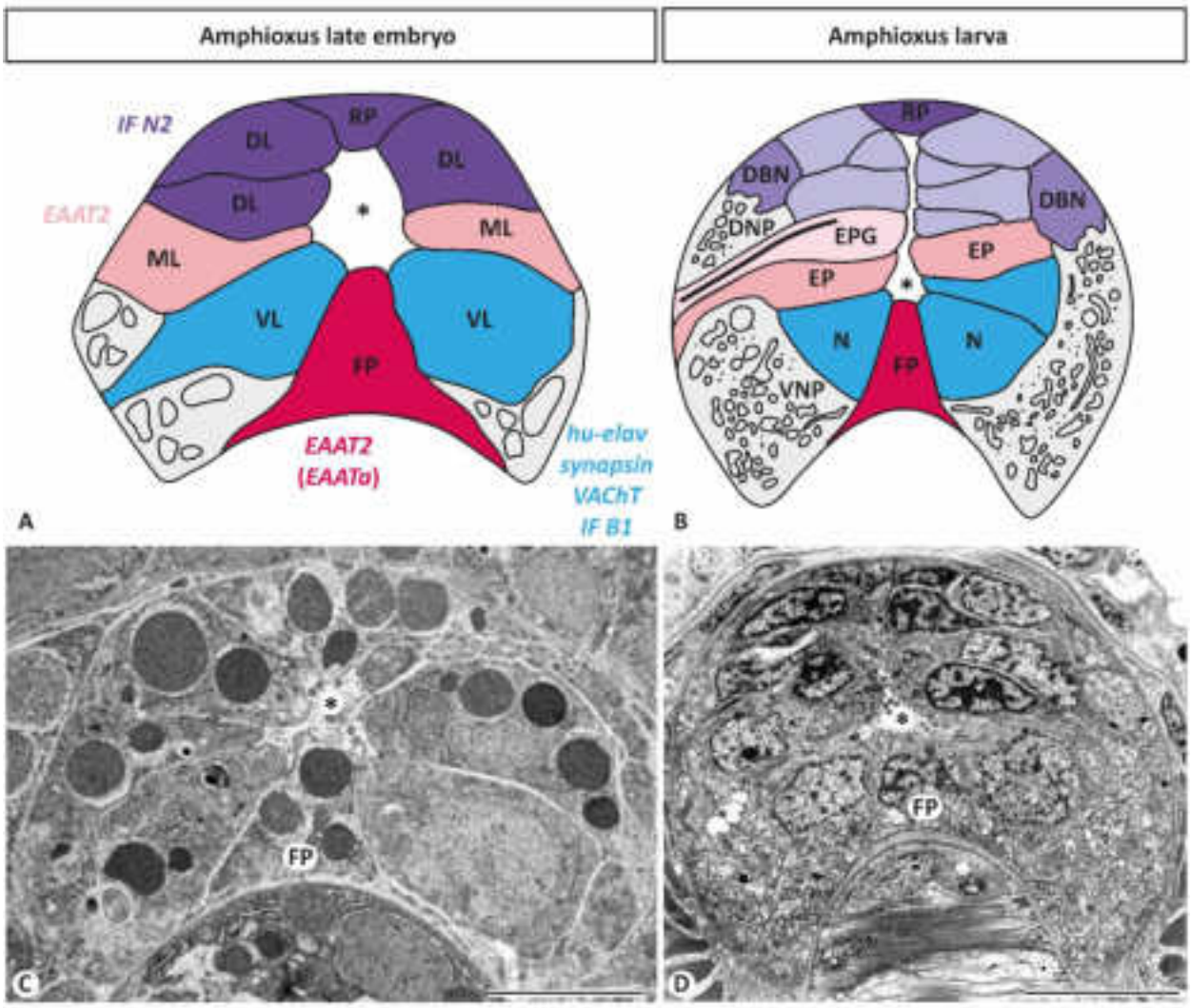

Figure 33. Cross-sections of the nerve cords of amphioxus late embryos and larvae, at the level of somite pair 2. **A,B**: Schematic representation of the different cell populations characterized in this study: dorsolateral (DL, violet), mediolateral (ML, pink), ventrolateral (VL, blue) and floor plate (fp, red). Genes marking the respective cell populations are shown in corresponding colors. Neuropile is in grey, separated, in the larva, into dorsal and ventral compartments (dnp and vnp, respectively) by ependymal (ep) and ependymoglial (epg) cells, which are derived from mediolateral precursors. Dorsal neuropile includes both dorsal sensory nerve tracts and medullary sensory cells, called dorsal bipolar neurons (dbn). **C,D**: Transmission electron microscopy (TEM) images corresponding to the two diagrams shown in A,B, respectively. Scale bars are 5 µm. Asterisks indicate the central canal. Abbreviations: dbn, dorsal bipolar neurons; DL, dorsolateral cell; dnp, dorsal neuropile; ep, ependymal cell; epg, ependymoglial cell; fp, floor plate; ML, mediolateral cell; n, neuron; rp, roof plate; VL, ventrolateral cell; vnp, ventral neuropile. From Bozzo et al. (2021).

Discussion

The glial cells of amphioxus embryos and young larvae were identified and characterized here by combining ultrastructure with gene expression analyses of orthologs of the main vertebrate glial markers: *sspo*, *EAATs*, *GS*, *GFAP/vimentin* and *olig*. Our results demonstrate the presence of glial cells and identify local domains of cell proliferation and differentiation in the nerve cord. In the sections that follow, we discuss the implications of our findings in relation to amphioxus neural development and the evolution of glia in chordates more generally.

scospondin is produced only by the infundibular organ in amphioxus

scospondin (sspo) is a phylogenetically ancient glycoprotein that, in most metazoans, is secreted by specialized cells of the nervous system (Table 3) (Gobron et al., 1999; Helm et al., 2017; Holmberg & Olsson, 1984; V. S. Mashanov et al., 2009; Olsson, 1956, 1972; Olsson et al., 1994). In vertebrates, sspo is secreted into the lumen of the central nervous system and aggregates to form a thread-like structure, called Reissner's fiber, which extends caudally to the terminal ampulla of the spinal cord where it is disassembled (Obermüller-Wilén & Olsson, 1974; Troutwine et al., 2020). During development, sspo is first produced by the floor plate, which expands laterally at the midbrain-hindbrain boundary, forming the so-called flexural organ (Meiniel et al., 2008; Olsson, 1956). Later in development, the subcommisural organ differentiates from the roof plate at the diencephalon-mesencephalon border and starts producing sspo. Eventually, the subcommisural organ becomes the only source of Reissner's fiber. In amphioxus, immunohistochemical studies of larvae and adults have identified the infundibular organ, a likely homolog of the vertebrate flexural organ (Olsson, 1956), as the source of Reissner's fiber (Gobron et al., 1999;

Olsson et al., 1994), which, as in vertebrates, extends caudally in the central canal to the terminal ampulla (Olsson, 1955).

In zebrafish, it has been demonstrated by *sspo* knockout experiments that Reissner's fiber is essential for establishing a straight anteroposterior body axis (Cantaut-Belarif et al., 2018; Rose et al., 2020; Troutwine et al., 2020). This process is likely mediated by GABAergic sensory neurons that are in direct contact with the cerebrospinal fluid (Orts-Del'Immagine et al., 2020). Reissner's fiber has further been implicated in the transport of small signaling molecules (Gobron et al., 1996; Meiniel et al., 2008) that regulate developmental patterning events along the anteroposterior axis (Driever, 2018). It is conceivable that Reissner's fiber has similar functions during axis extension in the amphioxus larva. The earliest expression of *sspo* in the infundibular organ of the cerebral vesicle would thus mark both the anterior limit and the developmental origin of Reissner's fiber in amphioxus.

Outside chordates, there is no clear evidence for structures comparable to Reissner's fiber or instances of fibrous secretory products involving sspo proteins. However, expression of *sspo* in non-chordates is frequently used as an argument for the presence of glia-like cells (Table 2). In hemichordates and echinoderms, for example, glia-like cells producing sspo are scattered in the neural parenchyma (Helm et al., 2017; Mashanov et al., 2009), and sspo is secreted from the apical surface of the neuroepithelium without forming a recognizable fiber (Mashanov et al., 2009). *sspo* expression has been suggested as an ancestral feature of glial cells, shared by both deuterostomes and protostomes (Helm et al., 2017), but to test this hypothesis, one would need to better characterize the *sspo*-expressing glia-like cells in non-chordates and to assess their function.

Table 3. scospondin (sspo) expression in metazoans.

Taxon	General localization of sspo expression	Reissner's fiber
Vertebrates	Floor plate and flexural organ (embryo) Sub-commissural organ (embryo and adult)	Yes
Tunicates	Fibrogen cells (larvacean adult)	Yes
Cephalochordates	Infundibular organ (embryo and adult)	Yes
Echinoderms	Neuroepithelium (holothurian and asteroid adult)	No
Hemichordates	Proboscis plexus (enteropneust adult)	No
Annelids	Brain and anterior ventral nerve cord (oweniid larva and adult)	No
Priapulids	Intraepidermal nerve cord and epidermis (adult)	No

Neurons, glia and precursor cells occupy different dorsoventral domains in the amphioxus neural tube

From our ultrastructure results, a typical cross-section of the anterior RhSp region of late-stage amphioxus embryos contains 6-8 cells. The dorsal and ventral midline are occupied, respectively, by a single roof plate and a single floor plate cell, and large dorsolateral, mediolateral and ventrolateral cells lie on each side of the neural tube (Fig. 33A,C). All of the cells contact the central canal at this stage, which is filled with their cilia (Fig. 33C). Virtually all ventrolateral cells are *synapsin*- and *hu-elav*-positive and thus are neurons, some of which already express specific neurochemical markers (Candiani et al., 2012) and are therefore terminally differentiated. In older amphioxus larvae, we identified two types of radial glia-like cells in the mediolateral domain (Fig. 33B,D), which are distinguishable by the presence or absence of intermediate filament bundles (Lacalli & Kelly, 2002) and named, respectively, ependymoglial and ependymal cells (Lacalli et al., 1994). At the T1 stage, these mediolateral cells express *EAAT2*, but not *hu-elav*. Given that *EAAT2* is expressed by both radial glia and astroglia in vertebrates (reviewed in Götz, 2013), these results strongly suggest that the mediolateral cells in the amphioxus nerve cord are glia and not neurons. However, although all mediolateral glia cells of amphioxus express *EAAT2*, they are probably a heterogeneous population of cells, since only a subset expresses *GS* and some of them express *olig* at the larval stage. Thus, while the glial cells expressing both *EAAT2* and *GS* are very similar to vertebrate astroglia, there appear to be other cells in the mediolateral population in amphioxus where comparison with vertebrate glia is less straightforward.

Type III intermediate filaments have been considered a landmark of radial glia in both vertebrates and non-chordate deuterostomes (Helm et al., 2017). *IF N2* encodes the amphioxus intermediate filament most closely related to vertebrate type III intermediate filaments, including the glia markers GFAP and vimentin. During amphioxus development, *IF N2* is transiently expressed by roof plate and dorsolateral cells from the anterior neuropore to the posterior tip of the neural tube. Although these cells do not express markers of neuronal commitment, they also do not co-express any of the glial markers. This observation supports the idea that the *IF N2*-positive cells represent a pool of neural precursors destined to contribute to neural tube growth in later larvae and possibly even through metamorphosis (Lacalli, 2004). Amphioxus *IF N2* might thus be a marker of undifferentiated neural cells, more similar in function to vertebrate vimentin than to vertebrate GFAP. Support for this hypothesis comes from structural analyses of IF N2 proteins that found IF N2 to be more similar to vimentin than to GFAP (Karabinos, 2013) and from *IF N2* expression in parts of the embryo characterized by the presence of undifferentiated neural cells, such as the tail bud (Henrique et al., 2015) and the neurogenic niche of ESNs located in the mid-trunk region (Zieger et al., 2018). These results also cast doubts on the reliability of intermediate filaments as markers for glial cells, at least in invertebrates, although it has previously been shown that GFAP even fails to label the majority of astroglial cells in cartilaginous fish (Anlauf & Derouiche, 2013).

Mediolateral and floor plate cells of amphioxus express astroglial markers

In vertebrates, neurotransmission mediated by glutamate (and to a lesser extent GABA and glycine) is modulated by transporters located on the surface of glial cell processes that surround the synapse. As an example, astrocytes use EAAT1 and EAAT2 transporters to take up glutamate from the synaptic cleft, which is subsequently converted to the non-excitotoxic glutamine by GS enzyme. Glutamine is then transported to the pre-synaptic terminal and hydrolyzed to glutamate, quickly replenishing the neurotransmitter pool. A comparable division of labor between neurons and glia-like cells has been described in insects (Freeman et al., 2003b; Rival et al., 2004). In amphioxus, this glutamate recycling mechanism does not seem to be active in all *EAAT2*-positive cells in the RhSp, as *GS* is co-expressed only in some, but not all, mediolateral *EAAT2*-positive cells and in some of the *EAAT2*-positive cells in the floor plate. However, GS is also expressed in ventrolateral cells of the RhSp as well as in the anterior cerebral vesicle, in close association with the glutamatergic neurons of the frontal eye complex. It is thus likely that *GS* has functions in the amphioxus CNS that are independent of the glial cell-mediated protection from glutamate excitotoxicity.

Although *EAAT2* and *GS* are not co-expressed in all cells of the amphioxus CNS, glial cells expressing both *EAAT2* and *GS* nonetheless greatly outnumber glutamatergic neurons (Candiani et al., 2012). In addition to the frontal eye complex of the cerebral vesicle, *VGlut*-expressing neurons in the CNS are only found in the primary motor center and in association with the first pigment spot (Lacalli, 1996; Lacalli & Candiani, 2017). This seeming disparity between a limited number of glutamate-releasing neurons and a large number of glial cells capable of glutamate uptake can be explained by non-synaptic volume transmission (Lacalli & Kelly, 2000; Nieuwenhuys, 2000). The glutamatergic neurons of the amphioxus primary motor center have been identified as the third set of large paired neurons, called LPN3 (Lacalli & Candiani, 2017). They have long descending axons bearing conspicuous varicosities, which could release their transmitter by paracrine means (Nieuwenhuys, 1998). The *EAAT2*- and *GS*-expressing glial cells are thus well positioned to regulate extracellular glutamate levels, in particular at larval stages, when they extend processes through the neuropile containing the axons of the LPN3 (Lacalli, 2002). Moreover, a pool of glutamatergic ESNs in the amphioxus ectoderm projects axons into in the CNS (Zieger et al., 2018), further increasing the overall number of glutamatergic synapses, whose activity needs to be regulated by *EAAT2*- and *GS*-positive glial cells. It might further be possible that amphioxus glial cells are involved in the processing of excitatory neurotransmitters other than glutamate. Aspartate, for example, has already been found in the nerve cord of amphioxus adults (Pascual-Anaya & D'Aniello, 2006).

Changing nerve cord dimensions: a stabilizing function for glia

Our results show that neural and glial lineages are segregated relatively early in amphioxus development, approximately at the time the neurula is beginning to elongate. Whatever the advantages of this as a developmental strategy, one consequence of early specification is that a scaffolding of glial cells can then be in place to resist forces that, during subsequent development, might otherwise disturb the internal organization of the nerve cord. To understand why this is important, the consequences of changing nerve cord dimensions need to be considered in some detail. Basically, nerve cord diameter decreases as the cord itself lengthens (Fig. 34), so that, for a typical section at the level of somite pair 2, the cross-sectional area of the cord decreases from about 300 μm^2 in the late embryo to 190 μm^2 in the larva, while corresponding somite length increases from 38 μm to 48 μm. This means that the volume of the cord decreases from 11,400 μm^3 to 9120 μm^3, i.e., by 20%, while the surface area, excluding the notochord sheath, is essentially unchanged, at 1965 μm^2 for the late embryo and 1985 μm^2 for the larva. The lamina thus acts in effect like a mesh that stretches in one direction while being compressed in the other, in this case by the forces generated by the elongation of the notochord and somites.

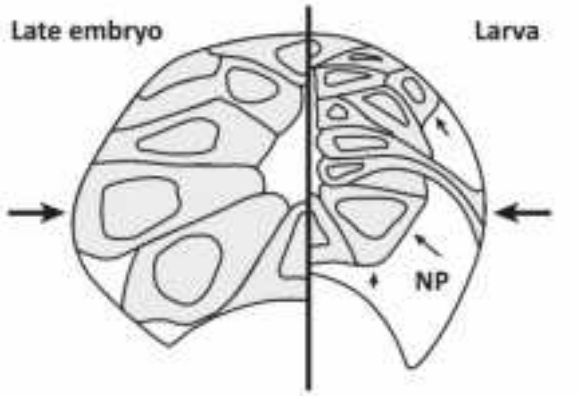

Figure 34. Comparison of the nerve cords of amphioxus late embryos and larvae, both to the same scale. The T1 stage of *B. lanceolatum* is on the right; the 12-day larva of *B. floridae* is on the left. Our observations on changing cord dimensions are consistent with the interpretation that the expanding neuropile (np) compresses the ependymal layer (small arrows), and that the lateral compartment glial cells play a role in stabilizing the nerve cord against deformation, as their attachment site (large arrows) is one that would assist in maintaining a uniformly tubular shape (see text for details).

Simultaneously, nerve tracts begin to form and the neuropile expands, eventually reducing the space available for the cell somata by up to 40% based on calculations from sections. This means there is a continuing pressure on the ependymal layer as the neuropile expands, pressing it inward and upward (Fig. 34). And, since differentiated neurons are quite large cells, there is no alternative to having them arranged in columns down the long axis of the cord because there is insufficient space to accommodate clumps of large cells of any size. Most of the undifferentiated cells found adjacent to neurons, presumably sister progeny of the same precursors, are compressed and deformed to fit what little space remains. In consequence, there are a number of forces acting on the nerve cord in the larva, both externally, because of elongation, and internally, due to the proliferation and rearrangement of cells and the formation of fiber

tracts and neuropile. These events have the potential to disturb the internal organization of the cord unless there is a framework in place to prevent this, which, in our view, is the principal reason why a system of lateral support cells is required, and why the latter are specified, differentiate and are deployed at a comparatively early stage of development.

Dynamic expression of *olig* genes in the amphioxus central nervous system

In amphioxus, *olig* shows a dynamic expression pattern in the central nervous system. At the onset of neurulation, *olig* is widely expressed in the neural plate, except for a longitudinal stripe at a position corresponding to the future mediolateral ependymal cells. As neurulation proceeds, two distinct populations of *olig*-positive progenitors are recognizable, each forming a segmented pattern. The ventrolateral population expresses *VAChT* and thus consists predominantly or entirely of cholinergic motor neurons and their precursors. The dorsolateral population consists of six to seven paired clusters of *VAChT*-negative cells, whose position corresponds to gaps in the domains occupied by the ventrolateral *olig*-positive cells. In the vertebrate spinal cord, opposing hedgehog (HH) and BMP gradients define a series of dorsoventral domains destined to produce different neuron and glial cell types. For instance, progenitors residing in the ventral pMN domain are instructed by HH signaling to first produce motor neurons and then oligodendrocytes (Orentas et al., 1999). At later developmental stages, oligodendrocytes also develop in the dorsal spinal cord, but this process is independent of HH signaling (Cai et al., 2005). However, olig transcription factors are always key components of the gene regulatory networks leading to motor neuron and oligodendrocyte differentiation. Similarly, in the developing amphioxus RhSp, *olig* genes are expressed in a subset of ventrolateral motor neurons and *olig* expression in the basal plate, but not in the alar plate, is dependent on HH signaling (Ren et al., 2020). From a topological point of view, this situation is thus comparable to what is observed in vertebrates.

When it comes to the identity of the dorsal clusters of *olig*-positive cells in the neurula, there are only two possibilities: that they are precursors of either dorsal bipolar neurons (DBNs) or translumenal neurons (TNs). The DBNs form continuous, but irregular dorsolateral files of cells that are integrated into the dorsal nerve tract to which they each contribute a rostral- and a caudal-projecting neurite. The TNs, in early larvae at least (Lacalli & Kelly, 2003) are more numerous and more evenly distributed, i.e. less clustered than DBNs, though this observation is based on limited data for somite pairs 1 and 2. For DBNs, the clustering may be a temporary feature, as overt clustering is not obvious for DBNs at later stages (Bone, 1959). This leads us to the provisional conclusion that the dorsal *olig*-positive cells are DBN precursors whose early specification and development is required because they are key contributors to the first locomotory reflexes, with additional DBNs being added to the series as development proceeds. The expectation is that DBNs should be closely associated with other early-developing neurons, and this appears to be the case, as they

participate in the earliest and most rostral circuits involving putative dopaminergic neurons (Zieger et al., 2017).

If this assignment is correct, that dorsal *olig*-positive cells are DBN precursors, then we find it interesting that there is an apparent pattern in the way the cells are arranged relative to their ventral *olig*-positive counterparts. This is not evident in all preparations, but is in some, notably in N4 neurulae where the position of the dorsal clusters corresponds closely with gaps in the ventral series. Molecular data on the early development of amphioxus neurons has so far revealed few cases where the specification events can be tied to a well-defined, repeating pattern. The repeating groupings and gaps we see with *olig* may be one such example.

At T0 and T1 stages, *olig* is expressed in five pairs of cells segmentally arranged along somite pairs 1 to 4. All these cells are cholinergic and clearly motor neurons, likely a subset of those expressing *olig* at earlier stages. The anterior-most cluster lies just anterior to the LPN3 of the primary motor center (Lacalli & Candiani, 2017) and is dorsolateral, while the other four pairs are located ventrolaterally in the RhSp. In the larval CNS, *olig* is expressed dorsally in the anterior cerebral vesicle, where no differentiated neurons have previously been reported (Lacalli et al., 1994). In the RhSp, *olig* is downregulated in motor neurons but it is expressed by groups of mediolateral cells extending from the end of the cerebral vesicle to some extent posteriorly to the first pigment spot. The identity of these cells is not clear but given their position, they could be a subset of radial glia-like cells or neural progenitors. Expression in mediolateral radial glia-like cells would indicate that a subpopulation of amphioxus glial cells shares at least some similarities with vertebrate oligodendrocytes.

It is noteworthy that from stage N4 onwards, *olig* is expressed in the posterior neural tube. This part of the CNS derives from progenitors located in the tail bud rather than the neural plate (Schubert et al., 2001). Despite the quite different origin, both rely on *olig* for their specification. A striking difference is that *olig* expression is highly dynamic in the anterior part of the central nervous system, but remarkably stable in the posterior part. In other words, the anterior neural tube quickly produces the neural types required for the survival of the planktonic larva, motor neurons and interneurons regulating locomotory reflexes (such as DBNs) above all (Lacalli & Candiani, 2017). *olig* is then redeployed in the specification of the posterior neural tube, whose differentiation is delayed to later larval stages. Thus, although *olig* has a broad proneural role in amphioxus, its activity is tightly regulated in both space and time.

Conclusions

Our results provide strong support for the presence of vertebrate-like glia in amphioxus. A subset of floor plate and mediolateral cells are shown to share the typical molecular signature of vertebrate astroglia, which implies also that these cells engage in a similar form of glutamate recycling, while cells resembling vertebrate radial glia are involved in establishing a pool of dividing progenitor cells with putative support functions.

Outside the chordates, convincing evidence for the existence of vertebrate-like glial cells is scarce. One of the best-studied examples is from the fruit fly *Drosophila melanogaster*. The fruit fly possesses cells that express *EAAT* and *GS* and that are involved in synaptogenesis, neurotransmitter uptake and recycling (reviewed in Freeman, 2015). Given the similarities with vertebrate astrocytes, it is tempting to consider the two cell populations to be homologous. However, although our data support the notion that astroglia-like cells already existed in the last common ancestor of amphioxus and vertebrates, due to the lack of information from other bilaterian animals, it is currently impossible to reliably infer the evolutionary ancestry of these cells. Another example concerns data from sea cucumbers, which are echinoderms. The nerve cords of adult sea cucumbers contain support cells that are scattered among the neurons and that are morphologically similar to vertebrate radial glia (Mashanov et al., 2010). Moreover, these support cells proliferate in response to injury and act as progenitors to regenerate the nervous system (Mashanov et al., 2013). Again, while it is certainly tempting to assume a homology between this cell population in sea cucumbers, the amphioxus radial glia-like cells we described here and vertebrate radial glia, additional work in other deuterostomes will be required to further strengthen the argument.

Even if one accepts the common ancestry of radial glia in deuterostomes, the functions of these cells in different lineages vary significantly. During early vertebrate neurogenesis, neuroepithelial cells

differentiate into radial glia, which subsequently produce both neurons and glia (Kriegstein & Alvarez-Buylla, 2009). In amphioxus, neurons and glia seem to arise from separate precursor populations. Although the radial glia-like cells in amphioxus can divide as the larva elongates, our data suggest that late neural differentiation is concentrated in the dorsal neural tube, from which differentiated glial cells are largely absent. Consequently, the radial glia in amphioxus appear to play a more limited role in the ongoing process of neurogenesis than is the case for vertebrate radial glia. The radial glia-like cells of sea cucumbers do, however, have the capacity to produce both neurons and glia, at least during regeneration (Mashanov et al., 2013), suggesting that a multipotent radial glial progenitor cell population may already have been present in the last common ancestor of all deuterostomes, though a predominant role in generating neurons and glia is restricted to the vertebrate lineage.

Material and methods

Maintaining adult amphioxus in the laboratory

Sexually mature adults of European amphioxus (*Branchiostoma lanceolatum*) are collected in Argelès-sur-Mer (France) (Fuentes et al., 2004, 2007) before the beginning of the spawning season and kept in a seawater facility in the laboratory (Carvalho et al., 2017; Theodosiou et al., 2011). 20-25 amphioxus adults are kept in 5 l tanks containing around 3 cm of autoclaved sand on a 14/10 h inverted light/dark cycle (light: 9 pm-11 am; dark: 11 am-9 pm). Each tank is continuously aerated. Open systems with seawater flowing continuously through the tanks are preferable, but closed systems with filtration devices can also be used (Carvalho et al., 2017).

Animals are fed with a mixture of live microalgae (such as *Tisochrysis lutea* and *Chaetoceros gracilis*). Algae are collected in 50 ml centrifuge tubes, pelleted by centrifugation at 4,000 x g for 10 min, washed twice with seawater and resuspended in fresh seawater. The resuspended algae are pooled to a final volume of 50 ml and half a teaspoon of powdered green algae (such as *Spirulina*) is added to the mixture. Each tank receives 1 ml of concentrated algae, corresponding to 15 ml of unspun algal culture, twice a day.

Spawning induction, gamete collection and *in vitro* fertilization

During the spawning season (May through July), amphioxus embryos can be obtained in large numbers by *in vitro* fertilization using gametes released in response to a thermal shock (Fuentes et al., 2007) according to the following protocol:

1. Select an adequate number of males and females with full gonads shortly before the end of the light period. Animals can be sexed using a stereomicroscope: eggs are clearly visible as small spheres inside the ovary, while testes are homogeneously filled with sperm.
2. Put the selected animals into a clean 5 l tank containing 2-3 cm of fresh seawater and no sand.
3. Place the tank into a water bath set at 23°C with the same light/dark regime used in the animal facility. Leave overnight without food and aeration.
4. The following day, shortly before the start of the dark period, transfer each animal into an individual plastic cup with 15 ml of artificial seawater and keep them at 19°C in the dark.
5. Check for spawning every 30 min using a red-light flashlight to avoid startling the animals. Adults typically spawn 1-4 h after the beginning of the dark period.
6. Collect eggs by gently pouring them into a 6 cm plastic Petri dish. Keep at 19°C until fertilization.
7. Collect sperm by pouring into a 15 ml centrifuge tube and promptly move to 4°C. Sperm remains active for about 12 h, with a marked decrease in fertilization efficiency after about 2 h.
8. Fertilize eggs by adding a few drops of sperm to the Petri dish. Gently swirl the dish to homogeneously distribute the sperm, hence ensuring synchronous fertilization.
9. Verify fertilization after 2-3 min: fertilized eggs are characterized by a clearly visible fertilization envelope.
10. Immediately transfer the fertilized eggs into a new 15 cm plastic Petri dish filled with artificial seawater to prevent embryos from sticking together.
11. Let develop until the desired stage. Note that cultures need to be kept at a constant temperature to ensure development according to predefined staging systems. The culture temperature most widely used for *B. lanceolatum* is 19°C, which was also used here.
12. After spawning, return the adults to the animal facility. Separate animals that did not spawn from those that did. While the former can be shocked again during the ongoing spawning season, the latter can be kept in the animal facility: around a third of the animals that spawned out will redevelop gonads ahead of the next spawning season (Carvalho et al., 2017).

Fixation of amphioxus embryos

Embryos are fixed with 4% (wt/v) paraformaldehyde in MOPS-EGTA buffer (0.1 M MOPS, 1 mM EGTA, 2 mM $MgSO_4$, 0.5 M NaCl, pH 7.5, in DEPC-treated water) and stored in RNase-free 70% ethanol. The following protocol must be performed under a fume hood.

1. Fill a 1.5 ml screw-cap microcentrifuge tube with 1 ml of ice-cold fixative, label it appropriately and place it on ice.
2. Take a dish containing treated embryos, open it, turn the lid upside down and place a basket inside.
3. To concentrate the embryos in a small volume, transfer them from the dish to the basket using a micropipette with a 1,000 µl tip. Make sure that the basket does not overflow. Repeat until all the

embryos have been moved from the dish into the basket. If needed, pipette the embryos up and down inside the basket to remove the fertilization envelope.

4. Using tweezers, move the basket into a well of a 4-well plate containing 600 µl of artificial seawater.
5. Using a micropipette with a 200 µl tip, transfer the embryos from the basket into the tube placed on ice and containing the fixative. Carefully add the embryos drop by drop to the tube. Do not transfer more than 600 µl to one tube.
6. Invert the tube several times and place on ice until the embryos have settled at the bottom of the tube.
7. Remove the solution and replace with fresh ice-cold fixative. Invert the tube several times. Fix at +4°C overnight in an upright position to let the embryos settle.
8. Remove the fixative and replace with ice-cold storage solution. Invert the tube several times.
9. Place the tube on ice and wait until the embryos have settled. Remove the solution and replace with fresh ice-cold storage solution. Invert the tube several times. Leave at +4°C overnight.
10. Remove the solution and replace with fresh 70% ethanol. Samples can be conserved for years at -20°C.

Sequence identification and phylogenetic analyses

BLAST searches of the *B. lanceolatum* genome using the Ensembl Metazoa browser (metazoa.ensembl.org/Branchiostoma_lanceolatum/Info/Index) and of the *B. lanceolatum* transcriptome using the MARIMBA database (marimba.obs-vlfr.fr/blast) were performed to identify *B. lanceolatum* orthologs of the vertebrate glial markers *scospondin* (*sspo*), *glutamine synthase* (*GS*), *excitatory amino acid transporters* (*EAATs*), *GFAP/vimentin* and *olig*. The corresponding sequences of *B. floridae* and *B. belcheri* were obtained, respectively, from JGI (genome.jgi.doe.gov/Brafl1/Brafl1.home.html) and LanceletDB (http://genome.bucm.edu.cn/lancelet/).

Alignments of amino acid sequences were performed using ClustalW in the MEGALIGN program from Lasergene (DNASTAR) and alignments were subsequently improved manually. Phylogenetic trees were calculated with the maximum likelihood (ML) and neighbor-joining (NJ) methods using MEGA X (Kumar et al., 2018). The appropriate evolutionary models for phylogenetic inference were identified using Model Selection as implemented in MEGA X (Kumar et al., 2018). The sequences used for the phylogenetic analyses are listed in Table S1.

Gene cloning

B. lanceolatum genes were amplified from cDNA prepared from adults, embryos and larvae. Total RNA was extracted using TRI Reagent (Sigma-Aldrich, 93289) following the manufacturer's instructions. First-strand cDNA was synthesized from 0.5-1 µg total RNA using the SuperScript first-strand synthesis system (Invitrogen, 18080051) and Oligo(dT) primers. RT-PCR reactions were performed with specific primers

listed in Table 4. The PCR products were cloned into the pCRII-TOPO vector (Invitrogen, K4600J10) and sequenced with T7 and Sp6 primers.

Table 4. Probes used in this study and relative primers

Gene	Forward primer	Reverse primer
EAAT2	5'-GCCGCCAGCCCGAAGGAGTC-3'	5'-CAGCATGCCGCCGTAGAACCAGAG-3'
EAATa	5'-AGGTCGAACATCGTCTTACCCTGAGAGCGA-3'	5'-GTCTCCATAGCCTGGTTCTCGTGGCCGT-3'
EAATb	5'-CCCGGCCTACACCCCTCCCAACAT-3'	5'-GCCCCACAGCCGTCAGAACAATCA-3'
GS	5'-ATGTACGTGTGGATCGACGGCAGTGGCGAA-3'	5'-CTCCCCCAGAACAACTGTACGCACAATCGC-3'
hu-elav	(Zieger et al., 2018)	
IF B1	5'-ATGACCCGCGCCCACGAGAAACA-3'	5'-GCTGCTGCTGCTGCTGCTGGAC-3'
IF B2	5'-AGGAGCGCAACACCAAACTGAC-3'	5'-CTCGCCGGTGATGGACTGTAGA-3'
IF N2	5'-GGCGGGGGAGGCACCAACAAC-3'	5'-TCGATCTGCACCACCGCCTTCTG-3'
oliga	5'-GACGGCCAAGTGGGTCCTGA-3'	5'-AACGGCCACGGGCTGAAG-3'
oligb	5'-CGGTGAGGCGGGCAGAAGC -3'	5'-AAAAGACGCGGCATGGAACAAACA-3'
oligc	5'-GACGGCCAAGTGGGTCCTGA-3'	5'-GGGCTGCGGTCGTGATGGTGCTC-3'
scospondin	5'-ACCCAGTATCGTTATCGCACCTGCAGCGAC-3'	5'-ATGTCCAGGTGCTCCATTCCCCATCCGTAG-3'
synapsin	5'-CGGTTTGAG TGCCCTAACGG GCCAGG ATTA-3'	5'-TTGTTTCCCGCTGCCGCTAGGGCTCTC-3'
VAChT	(Candiani, Lacalli, et al., 2008)	
VGlut	(Candiani et al., 2012)	

Whole mount *in situ* hybridization

Whole mount *in situ* hybridization (ISH) allows the detection of mRNAs in entire embryos with cellular resolution. This technique is widely used to determine the spatiotemporal expression patterns of developmental genes. Standard protocols are based on the hybridization of the target sequence with a complementary riboprobe labeled either with digoxigenin or fluorescein. These antigens are subsequently recognized by specific antibodies that are conjugated with a reporter activity. The following protocol is adapted from Bozzo et al. (2020).

Stock solutions

- 0.1 M triethanolamine (TEA): dilute TEA to 0.1 M in DEPC-treated water. Adjust to pH 8 with 1 N HCl. Do not treat TEA with DEPC and do not autoclave. Can be stored at +4°C for several months
- 1M Tris-HCl, pH 8.2 or pH 9.6: dissolve RNase-free TRIZMA base in DEPC-treated water and adjust to either pH 8.2 or pH 9.6 with 1 N HCl. Do not treat with DEPC. Filter. Can be stored at 4°C for several months
- 10% BSA: dissolve to 10% (wt/v) in PBS. Can be stored in aliquots at -20°C for several months

- 10% glycine: dissolve RNase-free glycine to 10% (wt/v) in DEPC-treated water. Can be stored in aliquots at -20°C for several months
- 10% Tween-20: dilute to 10% (v/v) with distilled water. DEPC-treat and autoclave. Can be stored at room temperature for several months
- 10x PBS (phosphate buffer saline): 26 mM sodium phosphate monobasic, 174 mM sodium phosphate dibasic, 9% (wt/v) NaCl, pH 7.4. DEPC-treat and autoclave. Can be stored at room temperature for several months
- 20x saline sodium citrate (SSC): dissolve NaCl to 3M and sodium citrate to 300 mM. Adjust to pH 7 with 1 N HCl, DEPC-treat and autoclave. Can be stored at room temperature for several months
- DEPC-treated water: prepare as described in section 5.3
- Hoechst stock: dissolve to 10 mg/ml in distilled water. Can be stored in the dark at +4°C for several months
- Proteinase K stock: dissolve to 10 mg/ml in DEPC-treated water. Can be stored in aliquots at -20°C for several months
- RNase A stock: dissolve to 10 mg/ml in TE buffer. Boil for 10 min then quickly cool on ice. Can be stored in aliquots at -20°C for several months
- RNase T1 stock: dilute RNase T1 to 10,000 U/ml in 0.1 M sodium acetate, pH 5.5. Boil for 10 min then quickly cool on ice. Can be stored in aliquots at -20°C for several months
- Sheep serum: inactivate by heating to 55°C for 30 min. Cool on ice and prepare 1 ml aliquots that can be stored at -20°C for several months

Working solutions

- 0.25% or 0.5% acetic anhydride in TEA. Prepare fresh. Do not store
- 1x PBS: Prepare diluting 10x PBS stock with DEPC-treated water. Can be stored at room temperature for several months
- 2 mg/ml glycine: dilute 10% glycine 1:50 with PBSTw
- 80% glycerol: dilute glycerol with PBS/sodium azide. Can be stored at room temperature for several months
- Alkaline phosphatase (AP) buffer with $MgCl_2$: 100 mM NaCl, 50 mM $MgCl_2$, 100 mM Tris-HCl pH 9.6, 0.1% Tween-20, 1 mM levamisole in DEPC-treated water. Prepare fresh and filter
- Antibody solution: anti-DIG AP-conjugated antibody 1:3,000, 2 mg/ml BSA, 6.5% heat-inactivated sheep serum, 1x PBS, 0.1% TritonX-100. Can be stored in 1 ml aliquots at -20°C for several months
- AP buffer without $MgCl_2$: 100 mM NaCl, 100 mM Tris-HCl pH 9.6, 0.1% Tween-20, 1 mM levamisole in DEPC-treated water. Prepare fresh and filter
- Blocking solution: 2 mg/ml BSA, 10% heat-inactivated sheep serum in PBSTw. Prepare fresh

- Hybridization buffer (HB): 50 % (v/v) formamide, 100 µg/ml heparin, 5x SSC, 0.1 % (v/v) Tween-20, 5 mM EDTA, 1 mg/ml torula yeast RNA, 1x Denhardt's solution in DEPC-treated water. Warm solution to 60°C before adding torula yeast RNA. Can be stored in aliquots at -20°C for several months
- PBS/sodium azide: 20 mM sodium phosphate buffer, pH 7.4, 0.9 % (wt/v) NaCl, 0.1% (wt/v) sodium azide. Can be stored at room temperature for several months
- PBSTw: 20 mM sodium phosphate buffer, pH 7.4, 0.9 % (wt/v) NaCl, 0.1 % (v/v) Tween-20 in DEPC-treated water. Prepare fresh from 10x PBS and 10% Tween-20 stocks and filter
- Proteinase K working solution: 7.5 µg/ml in PBSTw prepared fresh from the stock. We recommend a two-step dilution as follows. First, dilute 1 µl proteinase K stock in 99 µl of PBSTw and mix vigorously. Second, add 75 µl of this solution to 925 µl of PBSTw and mix vigorously
- RNase mix: 20 µg/ml preboiled RNase A, 10 U/ml preboiled RNase T1 in WS3
- Staining solution: 2.5 µl/ml NBT, 3.5 µl/ml BCIP in AP buffer with $MgCl_2$. Mix vigorously and keep in the dark.
- Wash solution 1 (WS1): 50 % (v/v) formamide, 5x SSC, 1% SDS in DEPC-treated water. Mix formamide, SSC and water and heat to 60°C before adding the SDS. Can be stored in aliquots at -20°C for several months
- Wash solution 2 (WS2): 50% formamide, 2x SSC, 1% SDS in DEPC-treated water. Mix formamide, SSC and water and heat to 60°C before adding the SDS. Can be stored in aliquots at -20°C for several months
- Wash solution 3 (WS3): 2x SSC, 0.1% Tween-20 in DEPC-treated water. Filter. Can be stored in aliquots at -20°C for several months
- Wash solution 4 (WS4): 0.2x SSC, 0.1% Tween-20 in DEPC-treated water. Filter. Can be stored in aliquots at -20°C for several months
- Wash solution 5 (WS5): 2 mg/ml BSA in PBSTw. Prepare fresh

Protocol for whole mount *in situ* hybridization

Before starting, clean bench, pipettes and tweezers with RNaseZAP. Always use gloves to manipulate solutions, reagents and equipment. Use only RNase-free filtered tips. If not otherwise stated, all steps of the protocol are performed in 500 µl of solution, at room temperature and rotating the embryos horizontally at 35-40 rpm. For changing solutions, use tweezers to move baskets between two wells.

1. For each experimental condition, select 10-15 embryos and transfer them to a basket placed inside a well of a 24-well plate.
2. Move the basket into a new well containing PBSTw and rotate for 5 min to rehydrate the embryos. Repeat twice with fresh PBSTw.

3. Digest with freshly diluted proteinase K.
4. Add 10 µl of 10% glycine to each basket to stop the digestion and incubate for 1 min. Quickly transfer into 2 mg/ml glycine and incubate for 5 min.
5. Wash with 0.1 M TEA for 1 min, followed by a second wash of 5 min.
6. Transfer into freshly prepared 0.25% acetic anhydride. Incubate for 5 min. Do not rotate.
7. Transfer into freshly prepared 0.5% acetic anhydride. Incubate for 5 min. Do not rotate.
8. Wash with PBSTw for 1 min, followed by a second wash of 5 min.
9. Transfer to HB, pre-warmed to 60°C. Incubate for 1 min.
10. Transfer into fresh pre-warmed HB. Seal the lid of the plate with paper tape then place the plate into a disposable zipper bag. Seal the bag and rock in a hybridization oven at 60°C for at least 2 h.
11. Dilute the probe to 1 ng/µl in pre-warmed HB. Denature at 70°C for 5 min.
12. Remove the plate from the hybridization oven, add the probe solution to a new well and transfer basket into probe solution.
13. Re-seal the plate with paper tape, place the plate into a zipper bag and rock in the hybridization oven at 60°C overnight.
14. Pre-warm WS1 and WS2 to 60°C. Thaw WS3 and WS4. Work quickly in steps 15-18 to keep embryos at hybridization temperature.
15. Unseal the plate and remove the probe solution, which can be stored at -20°C for reuse.
16. Wash twice with pre-warmed WS1 at 60°C for 5 min.
17. Wash twice with pre-warmed WS1 at 60°C for 15 min.
18. Wash with pre-warmed WS2 at 60°C for 5 min, then move the plate to room temperature and rotate for 10 min.
19. Wash with WS2 for 15 min.
20. Wash with WS3 for 1 min, followed by a second wash of 5 min.
21. Incubate with RNase mix at 37°C for 20 min.
22. Wash twice with WS3 for 20 min.
23. Wash with WS4 for 20 min.
24. Wash with freshly prepared WS5 for 5 min.
25. Transfer into freshly prepared blocking solution and incubate for at least 2 h.
26. Transfer into freshly thawed antibody solution and incubate at 4°C overnight.
27. Remove antibody solution and store at -20°C. Can be re-used once, if supplemented with fresh antibody solution.
28. Wash four times with fresh PBSTw for 20 min.
29. Transfer into freshly prepared AP buffer without $MgCl_2$ for a quick wash, then transfer into fresh solution and rotate for 10 min.

30. Transfer into freshly prepared AP buffer with $MgCl_2$ and rotate for 10 min. Repeat twice with fresh buffer.
31. Take embryos out of the basket and transfer them into a 4-well plate. Pipet embryos up and down in a 200 µl tip to prevent them from sticking to the bottom of the well. Remove fibers and debris that might have accumulated in the well.
32. Change for 300 µl of staining solution. Incubate at room temperature in the dark or at 37°C with gentle rotation.
33. Monitor the progress of the staining reaction by observing the embryos with a stereomicroscope on a white background every 15-30 min. Staining time can vary significantly between probes, from 15 min to several days.
34. Every 3 h, if the staining reaction requires more time, wash briefly with AP buffer with $MgCl_2$ and change for freshly prepared staining solution. The staining reaction needs to be stopped before the appearance of conspicuous background staining. A correctly stained embryo is thus transparent or slightly pinkish, and stained cells are dark blue or purple. To optimize the signal-to-noise ratio, do not incubate in staining solution overnight. Instead, wash briefly with AP buffer with $MgCl_2$ and leave at +4°C in fresh AP buffer with $MgCl_2$. The following day pick up the protocol at step 32.
35. When the signal is fully developed, stop the staining reaction by washing briefly with AP buffer without $MgCl_2$.
36. Change for fresh AP buffer without $MgCl_2$ and wash for 10 min.
37. Wash with PBSTw for 10 min.
38. To counterstain nuclei, incubate with freshly diluted 1:5,000 Hoechst stock in PBSTw in the dark for 15 min.
39. Wash twice with PBSTw for 10 min.
40. Wash with PBS/sodium azide for 10 min.
41. Change solution for 80% glycerol. Stained embryos can be stored at +4°C for several months.

Double whole mount *in situ* hybridization

Double ISH can be performed using two probes, differentially labelled with digoxigenin (DIG) or with fluorescein (FLUO) and then detecting DIG and FLUO sequentially with specific AP-conjugated antibodies and different chromogenic substrates (NBT/BCIP and Fast Red). The protocol for double ISH is very similar to that for single ISH presented above, except that both DIG- and FLUO-labelled probes are added in steps 11-12. In addition. Then, after the signal of the first probes has been developed with NBT/BCP (step 35), the protocol continues as follows:

36. Wash three times with fresh PBSTw for 5 min.
37. Transfer into freshly prepared 0.1 M glycine pH 2.2 and rotate for 10 minutes.

38. Transfer into freshly prepared blocking solution and incubate for at least 1 h.
39. Transfer into fresh antibody solution and incubate at 4°C overnight. If the first probe was DIG-labelled, use an anti-FLUO antibody and *vice versa*.
40. Remove antibody solution and store at -20°C. Can be re-used once, if supplemented with fresh antibody solution.
41. Wash four times with fresh PBSTw for 20 min.
42. Transfer to freshly prepared AP buffer with $MgCl_2$ and incubate for 10 min. Repeat twice with fresh buffer.
43. Prepare Fast Red solution by dissolving a tablet (Sigma-Aldrich, F4523) according to the manufacturer's instructions.
44. Change for freshly prepared Fast Red solution staining solution. Incubate at room temperature in the dark with gentle rotation.
45. Monitor the progress of the staining reaction by observing the embryos with a stereomicroscope on a white background every 15-30 min. Staining time can vary significantly between probes, from 15 min to several days.
46. Every 3 h, if the staining reaction requires more time, wash briefly with 100 mM Tris-HCl pH 8.2 + 0.2% Tween-20 and change for freshly prepared Fast Red staining solution. The staining reaction needs to be stopped before the appearance of conspicuous background staining. A correctly stained embryo is yellowish, and stained cells are red. To optimize the signal-to-noise ratio, do not incubate in staining solution overnight. Instead, wash briefly with 100 mM Tris-HCl pH 8.2 + 0.2% Tween-20 and leave at +4°C in fresh buffer. The following day pick up the protocol at step 44.
47. When the signal is fully developed, stop the staining reaction by washing briefly with AP buffer without $MgCl_2$.
48. Wash with PBSTw for 10 min.
49. To counterstain nuclei, incubate with freshly diluted 1:5,000 Hoechst stock in PBSTw in the dark for 15 min.
50. Wash twice with PBSTw for 10 min.
51. Wash with PBS/sodium azide for 10 min.
52. Change solution to 80% glycerol. Stained embryos can be stored at +4°C in the dark.

Sectioning and imaging

Whole mount embryos were mounted glass slides in 80% glycerol using three layers of Scotch tape as spacers between the slide and the coverslip. Specimens were imaged using an Olympus IX70 inverted microscope equipped with a Color View II camera. Adobe Photoshop CS4 was used for minor adjustments and to perform focus-stacking of whole mount samples.

Photographed whole-mount embryos and larvae were retrieved from the slides, counterstained with Ponceau S, dehydrated in an ethanol series, embedded in Spurr resin and sectioned at 3 µm using a Leica RM2145 microtome equipped with glass knives. Sections were imaged using a Leitz Laborlux S upright microscope equipped with a Moticam 3+ camera. Since Fast Red is extracted by ethanol series, pictures of double ISH were only acquired for whole mount embryos, in brightfield and confocal.

Confocal microscopy for chromogenic *in situ* hybridization

Chromogenic ISH can be visualized in brightfield but, to increase the cellular resolution of the staining, also with a confocal microscope. While Fast Red and Hoechst are intended for use in fluorescence microscopy and are thus bright fluorochromes, the acquisition of NBT/BCIP fluorescence is more challenging. Two approaches are possible. Since NBT/BCIP forms crystals that reflect light, it can be visualized by setting a narrow acquisition window that includes the excitation wavelength (Jékely & Arendt, 2007). Although the signal-to-noise ratio is generally good, this method should be used with caution, as some anatomical structures (such as the amphioxus pigment spots) are also reflective and thus indistinguishable from the NBT/BCIP-derived signal. Moreover, some fluorochromes can also be reflective, limiting the use of this approach when analyzing different stainings in a single embryo. For these reasons, it's advisable to acquire NBT/BCIP fluorescence in the far-red spectrum (Trinh et al., 2007). However, since the emission spectrum of NBT/BCIP peaks at 850 nm, which is beyond the maximum wavelength measurable by most commercial confocal microscopes, the signal tends to be weak and needs to be acquired several times, averaging the obtained values.

Confocal images were acquired with a Leica TCS SP8 microscope using the following parameters: Hoechst (excitation 405 nm, emission 420-480 nm), Fast Red (excitation 552 nm, emission 565-590 nm), NBT/BCIP (excitation 638 nm, emission 700-800 nm) (Matteo Bozzo et al., 2020). Raw data were analyzed with Fiji (Schindelin et al., 2012). Single images were assembled into figures using Adobe Photoshop CS4.

Transmission electron microscopy

Transmission electron microscopy (TEM) of *B. lanceolatum* embryos was performed in collaboration with Dr. Federico Caicci and Prof. Lucia Manni at the Department of Biology of the University of Padova (Italy). Old TEM sections of a *B. floridae* pre-metamorphic larva were provided and re-examined in collaboration with Prof. Thurston Lacalli (University of Victoria, Canada).

B. lanceolatum T1 stage embryos fixed with 2.5% glutaraldehyde in 0.1 M sodium cacodylate buffer pH 7.4 over-night at 4°C and postfixed with 1% osmium tetroxide in 0.1 M sodium cacodylate buffer for 1 hour at 4°. After three washes in buffer, samples were dehydrated in a graded ethanol series and embedded in an epoxy resin (Sigma-Aldrich). Sections were obtained with an Ultrotome V (LKB) ultramicrotome. Semithin sections (1 µm) stained with toluidine blue were verified under a light microscope before

producing ultrathin sections (60-70 nm) counterstained with uranyl acetate and lead citrate. Ultrathin sections were subsequently analyzed with a Tecnai G^2 (FEI) transmission electron microscope operating at 100 kV. Images were captured with a Veleta (Olympus Soft Imaging System) digital camera. Additional TEM data, on *B. floridae*, are from a previously prepared serial section series through the anterior nerve cord of a 12-day larva, extending from the frontal eye to the end of somite pair 2, methods as described by Lacalli et al. (1994).

Bibliography

Albuixech-Crespo, B., Lo, L., Moreno-bravo, J. A., Maeso, I., Sa, L., Somorjai, I., Pascual-anaya, J., Puelles, E., & Bovolenta, P. (2017). Molecular regionalization of the developing amphioxus neural tube challenges major partitions of the vertebrate brain. *PloS Biolgy*, *15*(4). https://doi.org/10.1371/journal.pbio.2001573

Alexandre, P., Reugels, A. M., Barker, D., Blanc, E., & Clarke, J. D. W. (2010). Neurons derive from the more apical daughter in asymmetric divisions in the zebrafish neural tube. *Nature Neuroscience*, *13*(6), 673–679. https://doi.org/10.1038/nn.2547

Anlauf, E., & Derouiche, A. (2013). Glutamine Synthetase as an Astrocytic Marker: Its Cell Type and Vesicle Localization. *Frontiers in Endocrinology*, *4*, 144. https://doi.org/10.3389/fendo.2013.00144

Annona, G., Holland, N. D., & D'Aniello, S. (2015). Evolution of the notochord. In *EvoDevo* (Vol. 6, Issue 1). https://doi.org/10.1186/s13227-015-0025-3

Araque, A., Parpura, V., Sanzgiri, R. P., & Haydon, P. G. (1999). Tripartite synapses: Glia, the unacknowledged partner. *Trends in Neurosciences*, *22*(5), 208–215. https://doi.org/10.1016/S0166-2236(98)01349-6

Beaster-Jones, L., Kaltenbach, S. L., Koop, D., Yuan, S., Chastain, R., & Holland, L. Z. (2008). Expression of somite segmentation genes in amphioxus: A clock without a wavefront? *Development Genes and Evolution*, *218*(11–12), 599–611. https://doi.org/10.1007/s00427-008-0257-5

Becker, C. G., & Becker, T. (2015). Neuronal regeneration from ependymo-radial glial cells: cook, little pot, cook! *Developmental Cell*, *32*(4), 516–527. https://doi.org/10.1016/j.devcel.2015.01.001

Beckers, P., Helm, C., & Bartolomaeus, T. (2019). The anatomy and development of the nervous system in Magelonidae (Annelida) - Insights into the evolution of the annelid brain. *BMC Evolutionary Biology*, *19*(1), 1–21. https://doi.org/10.1186/s12862-019-1498-9

Beckers, P., Helm, C., Purschke, G., Worsaae, K., Hutchings, P., & Bartolomaeus, T. (2019). The central nervous system of Oweniidae (Annelida) and its implications for the structure of the ancestral annelid brain. *Frontiers in Zoology*, *16*(1), 6. https://doi.org/10.1186/s12983-019-0305-1

Bertrand, S., & Escriva, H. (2011). Evolutionary crossroads in developmental biology: amphioxus. *Development*, *138*(22), 4819–4830. https://doi.org/10.1242/dev.066720

Bertrand, S., Le Petillon, Y., Somorjai, I. M. L., & Escriva, H. (2017). Developmental cell-cell communication pathways in the cephalochordate amphioxus: actors and functions. *The International Journal of Developmental Biology*, *61*(10-11–12), 697–722. https://doi.org/10.1387/ijdb.170202sb

Bone, Q. (1959). The Central Nervous System in Larval Acraniates. *Journal of Cell Science*, *s3-100*(52), 509–527.

Bone, Q. (1960). The central nervous system in amphioxus. *Journal of Comparative Neurology*, *115*(1), 27–64. https://doi.org/10.1002/cne.901150105

Bourlat, S. J., Juliusdottir, T., Lowe, C. J., Freeman, R., Aronowicz, J., Kirschner, M., Lander, E. S., Thorndyke, M., Nakano, H., Kohn, A. B., Heyland, A., Moroz, L. L., Copley, R. R., & Telford, M. J. (2006). Deuterostome phylogeny reveals monophyletic chordates and the new phylum Xenoturbellida. *Nature*, *444*(7115), 85–88. https://doi.org/10.1038/nature05241

Bozzo, M, Candiani, S., & Schubert, M. (2020). Whole mount in situ hybridization and immunohistochemistry for studying retinoic acid signaling in developing amphioxus. In *Methods in Enzymology*. https://doi.org/10.1016/bs.mie.2020.03.007

Bozzo, Matteo, Candiani, S., & Schubert, M. (2020). Whole mount in situ hybridization and immunohistochemistry for studying retinoic acid signaling in developing amphioxus. In *Methods in Enzymology*. Academic Press Inc. https://doi.org/10.1016/bs.mie.2020.03.007

Bozzo, M., Macrì, S., Calzia, D., Sgarra, R., Manfioletti, G., Ramoino, P., Lacalli, T., Vignali, R., Pestarino, M., & Candiani, S. (2017). The HMGA gene family in chordates: evolutionary perspectives from amphioxus. *Development Genes and Evolution*, *227*(3), 201–211. https://doi.org/10.1007/s00427-017-0581-8

Bozzo M., Lacalli T.C., Obino V., Caicci F., Marcenaro E., Bachetti T., Manni L., Pestarino M., Schubert M., Candiani S. (2021). Amphioxus neuroglia: Molecular characterization and evidence for early compartmentalization of the developing nerve cord. *Glia*. Epub ahead of print. https://doi: 10.1002/glia.23982.

Bramanti, V., Tomassoni, D., Avitabile, M., Amenta, F., & Avola, R. (2010). Biomarkers of glial cell proliferation and differentiation in culture. *Frontiers in Bioscience - Scholar*, *2 S*(2), 558–570. https://doi.org/10.2741/s85

Bullock, T. H., & Horridge Adrian G. (1965). *Structure and function in the nervous systems of invertebrates*. W.H. Freeman.

Burighel, P., & Cloney, R. A. (1997). Urochordata: Ascidiacea. In F. W. Harrison & E. Ruppert (Eds.), *Microscopic Anatomy of Invertebrates, Volume 15: Hemichordata, Chaetognatha, and the Invertebrate Chordates* (pp. 221–347). Wiley-Liss Inc.

Butler, A. B., & Hodos, W. (2005). Comparative Vertebrate Neuroanatomy: Evolution and Adaptation. In *Comparative Vertebrate Neuroanatomy: Evolution and Adaptation: Second Edition* (2nd ed.). WIley. https://doi.org/10.1002/0471733849

Cai, J., Qi, Y., Hu, X., Tan, M., Liu, Z., Zhang, J., Li, Q., Sander, M., & Qiu, M. (2005). Generation of oligodendrocyte precursor cells from mouse dorsal spinal cord independent of Nkx6 regulation and Shh signaling. *Neuron*, *45*(1), 41–53. https://doi.org/10.1016/j.neuron.2004.12.028

Cameron, C. B. (2005). A phylogeny of the hemichordates based on morphological characters. In *Canadian Journal of Zoology* (Vol. 83, Issue 1, pp. 196–215). NRC Research Press Ottawa, Canada . https://doi.org/10.1139/z04-190

Candiani, S., Holland, N. D., Oliveri, D., Parodi, M., & Pestarino, M. (2008). Expression of the amphioxus Pit-1 gene (AmphiPOU1F1/Pit-1) exclusively in the developing preoral organ, a putative homolog of the vertebrate adenohypophysis. *Brain Research Bulletin*, *75*(2–4), 324–330. https://doi.org/10.1016/j.brainresbull.2007.10.023

Candiani, S., Lacalli, T. C., Parodi, M., Oliveri, D., & Pestarino, M. (2008). The cholinergic gene locus in amphioxus: Molecular characterization and developmental expression patterns. *Developmental Dynamics*, *237*(5), 1399–1411. https://doi.org/10.1002/dvdy.21541

Candiani, S., Moronti, L., Pennati, R., De Bernardi, F., Benfenati, F., & Pestarino, M. (2010). The synapsin gene family in basal chordates: evolutionary perspectives in metazoans. *BMC Evolutionary Biology*, *10*(1), 32. https://doi.org/10.1186/1471-2148-10-32

Candiani, S., Moronti, L., Ramoino, P., Schubert, M., & Pestarino, M. (2012). A neurochemical map of the developing amphioxus nervous system. *BMC Neuroscience*, *13*(1), 59. https://doi.org/10.1186/1471-2202-13-59

Cannon, Johanna T., Kocot, K. M., Waits, D. S., Weese, D. A., Swalla, B. J., Santos, S. R., & Halanych, K. M. (2014). Phylogenomic resolution of the hemichordate and echinoderm clade. *Current Biology*, *24*(23), 2827–2832. https://doi.org/10.1016/j.cub.2014.10.016

Cannon, Johanna T, Rychel, A. L., Eccleston, H., Halanych, K. M., & Swalla, B. J. (2009). Molecular phylogeny of hemichordata, with updated status of deep-sea enteropneusts. *Molecular Phylogenetics and Evolution*, *52*(1), 17–24. https://doi.org/10.1016/j.ympev.2009.03.027

Cannon, Johanna Taylor, Vellutini, B. C., Smith, J., Ronquist, F., Jondelius, U., & Hejnol, A. (2016). Xenacoelomorpha is the sister group to Nephrozoa. *Nature*, *530*(7588), 89–93. https://doi.org/10.1038/nature16520

Cantaut-Belarif, Y., Sternberg, J. R., Thouvenin, O., Wyart, C., & Bardet, P. L. (2018). The Reissner Fiber in the Cerebrospinal Fluid Controls Morphogenesis of the Body Axis. *Current Biology*, *28*(15), 2479-2486.e4. https://doi.org/10.1016/j.cub.2018.05.079

Carvalho, J. E., Lahaye, F., & Schubert, M. (2017). Keeping amphioxus in the laboratory: an update on available husbandry methods. *The International Journal of Developmental Biology*, *61*(10-11–12), 773–783. https://doi.org/10.1387/ijdb.170192ms

Carvalho, J. E., Lahaye, F., Yong, L. W., Croce, J. C., Université, S., & Biologie, L. De. (2020). An updated staging system for cephalochordate development: one table suits them all. *BioRxiv*, 2020.05.26.112193. https://doi.org/10.1101/2020.05.26.112193

Castro, A., Becerra, M., Manso, M. J., & Anadón, R. (2015). Neuronal organization of the brain in the adult amphioxus (Branchiostoma lanceolatum): A study with acetylated tubulin immunohistochemistry. *Journal of Comparative Neurology*, *523*(15), 2211–2232. https://doi.org/10.1002/cne.23785

Cerfontaine, P. (1906). Recherches sur le développement de l'Amphioxus. In *Recherches sur le développement de l'Amphioxus.* Imprimerie H. Vaillant-Carmanne. https://doi.org/10.5962/bhl.title.140340

Chaudhry, F. A., Lehre, K. P., Lookeren Campagne, M. van, Ottersen, O. P., Danbolt, N. C., & Storm-Mathisen, J. (1995). Glutamate transporters in glial plasma membranes: Highly differentiated localizations revealed by quantitative ultrastructural immunocytochemistry. *Neuron*, *15*(3), 711–720. https://doi.org/10.1016/0896-6273(95)90158-2

Chen, J. Y. (2008). Early crest animals and the insight they provide into the evolutionary origin of craniates. *Genesis*, *46*(11), 623–639. https://doi.org/10.1002/dvg.20445

Coggeshall, R. E., & Fawcett, D. W. (1964). The fine structure of the central nervous system of the leech, Hirudo medicinalis. *Journal of Neurophysiology*, *27*, 229–289. https://doi.org/10.1152/jn.1964.27.2.229

Coles, J. A. (2009). Glial cells: Invertebrate. In *Encyclopedia of Neuroscience* (pp. 749–759). Elsevier Ltd. https://doi.org/10.1016/B978-008045046-9.01011-1

Cong, P. Y., Hou, X. G., Aldridge, R. J., Purnell, M. A., & Li, Y. Z. (2015). New data on the palaeobiology of the enigmatic yunnanozoans from the Chengjiang Biota, Lower Cambrian, China. *Palaeontology*, *58*(1), 45–70. https://doi.org/10.1111/pala.12117

Costa, O. G. (1834). *Cenni zoologici ossia descrizione sommaria delle specie nuove di animali discoperti in diverse contrade del regno nell' anno 1834 : con illustrazioni sopra talune altre meno ovvie*. Tipografia di Azzolino E Comp.

Deitmer, J. W., Rose, C. R., Munsch, T., Schmidt, J., Nett, W., Schneider, H.-P., & Lohr, C. (1999). Leech giant glial cell: functional role in a simple nervous system. *Glia*, *28*(3), 175–182. https://doi.org/10.1002/(SICI)1098-1136(199912)28:3<175::AID-GLIA1>3.0.CO;2-7

Delsuc, F., Brinkmann, H., Chourrout, D., & Philippe, H. (2006). Tunicates and not cephalochordates are the closest living relatives of vertebrates. *Nature*, *439*, 965–968. https://doi.org/10.1038/nature04336

Delsuc, F., Philippe, H., Tsagkogeorga, G., Simion, P., Tilak, M. K., Turon, X., López-Legentil, S., Piette, J., Lemaire, P., & Douzery, E. J. P. (2018). A phylogenomic framework and timescale for comparative studies of tunicates. *BMC Biology*, *16*(1), 39. https://doi.org/10.1186/s12915-018-0499-2

Dohrn, A. (1875). *Der ursprung der wirbelthiere und das princip des functionswechsels: genealogische skizzen*. Wilhelm Engelmann.

Driever, W. (2018). Developmental Biology: Reissner's Fiber and Straightening of the Body Axis. In *Current Biology* (Vol. 28, Issue 15, pp. R833–R835). Cell Press. https://doi.org/10.1016/j.cub.2018.05.080

Dupont, S., Thorndyke, W., Thorndyke, M. C., & Burke, R. D. (2009). Neural development of the brittlestar Amphiura filiformis. *Development Genes and Evolution*, *219*(3), 159–166. https://doi.org/10.1007/s00427-009-0277-9

Edwards, T. N., & Meinertzhagen, I. A. (2010). The functional organisation of glia in the adult brain of Drosophila and other insects. In *Progress in Neurobiology* (Vol. 90, Issue 4, pp. 471–497). Pergamon. https://doi.org/10.1016/j.pneurobio.2010.01.001

Fan, C., Zhang, S., Liu, Z., Li, L., Luan, J., & Saren, G. (2007). Identification and expression of a novel class of glutathione-S-transferase from amphioxus Branchiostoma belcheri with implications to the origin of vertebrate liver. *International Journal of Biochemistry and Cell Biology*, *39*(2), 450–461. https://doi.org/10.1016/j.biocel.2006.09.013

Fogarty, M., Richardson, W. D., & Kessaris, N. (2005). A subset of oligodendrocytes generated from radial glia in the dorsal spinal cord. *Development*, *132*(8), 1951–1959. https://doi.org/10.1242/dev.01777

Formery, L., Orange, F., Formery, A., Yaguchi, S., Lowe, C. J., Schubert, M., & Croce, J. C. (2020). Neural anatomy of echinoid early juveniles and comparison of nervous system organization in echinoderms. *Journal of Comparative Neurology*, 1–22. https://doi.org/10.1002/cne.25012

Freeman, M. R., Delrow, J., Kim, J., Johnson, E., & Doe, C. Q. (2003a). Unwrapping glial biology: Gcm target genes regulating glial development, diversification, and function. *Neuron*, *38*(4), 567–580. https://doi.org/10.1016/S0896-6273(03)00289-7

Freeman, M. R., Delrow, J., Kim, J., Johnson, E., & Doe, C. Q. (2003b). Unwrapping glial biology: Gcm target genes regulating glial development, diversification, and function. *Neuron*, *38*(4), 567–580. https://doi.org/10.1016/S0896-6273(03)00289-7

Fuentes, M., Benito, E., Bertrand, S., Paris, M., Mignardot, A., Godoy, L., Jimenez-Delgado, S., Oliveri, D., Candiani, S., Hirsinger, E., D'Aniello, S., Pascual-Anaya, J., Maeso, I., Pestarino, M., Vernier, P., Nicolas, J. F., Schubert, M., Laudet, V., Geneviere, A. M., … Escriva, H. (2007). Insights into spawning behavior and development of the European amphioxus (Branchiostoma lanceolatum). *Journal of Experimental Zoology Part B: Molecular and Developmental Evolution*, *308*(4), 484–493. https://doi.org/10.1002/jez.b.21179

Fuentes, M., Schubert, M., Dalfo, D., Candiani, S., Benito, E., Gardenyes, J., Godoy, L., Moret, F., Illas, M., Patten, I., Permanyer, J., Oliveri, D., Boeuf, G., Falcon, J., Pestarino, M., Fernandez, J. G., Albalat, R., Laudet, V., Vernier, P., & Escriva, H. (2004). Preliminary observations on the spawning conditions of the European amphioxus (Branchiostoma lanceolatum) in captivity. *Journal of Experimental Zoology Part B: Molecular and Developmental Evolution*. https://doi.org/10.1002/jez.b.20025

Gans, C., & Northcutt, R. G. (1983). Neural crest and the origin of vertebrates: a new head. *Science*, *220*(4594), 268–273. https://doi.org/10.1126/science.220.4594.268

Giaume, C., Koulakoff, A., Roux, L., Holcman, D., & Rouach, N. (2010). Astroglial networks: A step further in neuroglial and gliovascular interactions. In *Nature Reviews Neuroscience* (Vol. 11, Issue 2, pp. 87–99). Nature Publishing Group. https://doi.org/10.1038/nrn2757

Gillis, A. J., Fritzenwanker, J. H., & Lowe, C. J. (2012). A stem-deuterostome origin of the vertebrate pharyngeal transcriptional network. *Proceedings of the Royal Society B: Biological Sciences*, *279*(1727), 237–246. https://doi.org/10.1098/rspb.2011.0599

Ginhoux, F., Lim, S., Hoeffel, G., Low, D., & Huber, T. (2013). Origin and differentiation of microglia. In *Frontiers in Cellular Neuroscience* (Vol. 7, Issue 45). Frontiers. https://doi.org/10.3389/fncel.2013.00045

Gobron, S., Creveaux, I., Meiniel, R., Didier, R., Dastugue, B., & Meiniel, A. (1999). SCO-spondin is evolutionarily conserved in the central nervous system of the chordate phylum. *Neuroscience*, *88*(2), 655–664. https://doi.org/10.1016/S0306-4522(98)00252-8

Gobron, S., Monnerie, H., Meiniel, R., Creveaux, I., Lehmann, W., Lamalle, D., Dastugue, B., & Meiniel, A. (1996). SCO-spondin: A new member of the thrombospondin family secreted by the subcommissural organ is a candidate in the modulation of neuronal aggregation. *Journal of Cell Science*, *109*(5), 1053–1061.

Götz, M. (2013). Radial glial cells. In H. Kettenmann & B. R. Ransom (Eds.), *Neuroglia* (3rd ed., pp. 50–61). Oxford University Press. https://doi.org/10.1093/med/9780199794591.001.0001

Haeckel, E. (1868). *Natürliche Schöpfungsgeschichte*. Verlag von Georg Reimer.

Halanych, K. M. (1995). The Phylogenetic Position of the Pterobranch Hemichordates Based on 18S rDNA Sequence Data. *Molecular Phylogenetics and Evolution*, *4*(1), 72–76. https://doi.org/10.1006/mpev.1995.1007

Hartenstein, V. (2019). Development of the nervous system of invertebrates. In *The Oxford Handbook of Invertebrate Neurobiology* (pp. 70–122). Oxford University Press. https://doi.org/10.1093/oxfordhb/9780190456757.013.3

Hartline, D. K. (2011). The evolutionary origins of glia. *Glia*, *59*(9), 1215–1236. https://doi.org/10.1002/glia.21149

Hatschek, B. (1893). The Amphioxus and its development. In J. Tuckey (Ed.), *The Amphioxus and its development / by Dr. B. Hatschek. Translated and edited by James Tuckey.* Swan Sonnenschein & CO. https://doi.org/10.5962/bhl.title.3749

Hatten, M. E., & Mason, C. A. (1990). Mechanisms of glial-guided neuronal migration in vitro and in vivo. *Experientia*, *46*(9), 907–916. https://doi.org/10.1007/BF01939383

Hejnol, A., & Rentzsch, F. (2015). Neural nets. In *Current Biology* (Vol. 25, Issue 18, pp. R782–R786). Cell Press. https://doi.org/10.1016/j.cub.2015.08.001

Helm, C., Karl, A., Beckers, P., Kaul-Strehlow, S., Ulbricht, E., Kourtesis, I., Kuhrt, H., Hausen, H., Bartolomaeus, T., Reichenbach, A., & Bleidorn, C. (2017). Early evolution of radial glial cells in Bilateria. *Proceedings of the Royal Society B: Biological Sciences*, *284*(1859), 20170743. https://doi.org/10.1098/rspb.2017.0743

Herculano-Houzel, S., & Lent, R. (2005). Isotropic fractionator: A simple, rapid method for the quantification of total cell and neuron numbers in the brain. *Journal of Neuroscience*, *25*(10), 2518–2521. https://doi.org/10.1523/JNEUROSCI.4526-04.2005

Hickman, C. P., Keen, S. L., Eisenhour, D. J., Larson, A., & L'Anson, H. (2017). *Integrated principles of Zoology, 17th edition*. McGraw-Hill Education.

Hirakow, R., & Kajita, N. (1990). An electron microscopic study of the development of amphioxus, Branchiostoma belcheri tsingtauense: Cleavage. *Journal of Morphology*, *203*(3), 331–344. https://doi.org/10.1002/jmor.1052030308

Hirakow, R., & Kajita, N. (1991). Electron microscopic study of the development of amphioxus, Branchiostoma belcheri tsingtauense: The gastrula. *Journal of Morphology*. https://doi.org/10.1002/jmor.1052070106

Hirakow, R., & Kajita, N. (1994). Electron microscopic study of the development of amphioxus, Branchiostoma belcheri tsingtauense: the neurula and larva. *Kaibogaku Zasshi. Journal of Anatomy*, *69*(1), 1–13. http://www.ncbi.nlm.nih.gov/pubmed/8178614

Hirokawa, T., Komatsu, M., & Nakajima, Y. (2008). Development of the nervous system in the brittle star Amphipholis kochii. *Development Genes and Evolution*, *218*(1), 15–21. https://doi.org/10.1007/s00427-007-0196-6

Hirsinger, E., Carvalho, J. E., Chevalier, C., Lutfalla, G., Nicolas, J.-F., Peyriéras, N., & Schubert, M. (2015). Expression of Fluorescent Proteins in Branchiostoma lanceolatum by mRNA Injection into Unfertilized Oocytes. *Journal of Visualized Experiments*. https://doi.org/10.3791/52042

Holland, L Z, Albalat, R., Azumi, K., Benito-Gutierrez, E., Blow, M. J., Bronner-Fraser, M., Brunet, F., Butts, T., Candiani, S., Dishaw, L. J., Ferrier, D. E. K., Garcia-Fernandez, J., Gibson-Brown, J. J., Gissi, C., Godzik, A., Hallbook, F., Hirose, D., Hosomichi, K., Ikuta, T., … Holland, P. W. H. (2008). The amphioxus genome illuminates vertebrate origins and cephalochordate biology. *Genome Research*, *18*(7), 1100–1111. https://doi.org/10.1101/gr.073676.107

Holland, Linda Z. (2015). Cephalochordata. In *Evolutionary Developmental Biology of Invertebrates 6: Deuterostomia* (pp. 91–134). Springer Vienna. https://doi.org/10.1007/978-3-7091-1856-6_3

Holland, Linda Z. (2016). Tunicates. In *Current Biology* (Vol. 26, Issue 4, pp. R146–R152). Cell Press. https://doi.org/10.1016/j.cub.2015.12.024

Holland, Linda Z., & Onai, T. (2012). Early development of cephalochordates (amphioxus). *Wiley Interdisciplinary Reviews: Developmental Biology*, *1*(2), 167–183. https://doi.org/10.1002/wdev.11

Holland, N. D., Holland, L. Z., & Heimberg, A. (2015). Hybrids between the Florida amphioxus (Branchiostoma floridae) and the Bahamas lancelet (Asymmetron lucayanum): Developmental morphology and chromosome counts. *Biological Bulletin*, *228*(1), 13–24. https://doi.org/10.1086/BBLv228n1p13

Holland, N. D., & Somorjai, I. M. L. (2020). The sensory peripheral nervous system in the tail of a cephalochordate studied by serial blockface scanning electron microscopy. *Journal of Comparative Neurology*, *528*(15), 2569–2582. https://doi.org/10.1002/cne.24913

Holmberg, K., & Olsson, R. (1984). The origin of Reissner's fibre in an Appendicularian, Oikopleura dioica. *Videnskabelige Meddelelser Fra Dansk Naturhistorisk Forening i Kobenhavn*, *145*, 43–52.

Hopwood, N. (2015). The cult of amphioxus in German Darwinism; or, Our gelatinous ancestors in Naples' blue and

balmy bay. *History and Philosophy of the Life Sciences*, *36*(3), 371–393. https://doi.org/10.1007/s40656-014-0034-x

Horie, T., Shinki, R., Ogura, Y., Kusakabe, T. G., Satoh, N., & Sasakura, Y. (2011). Ependymal cells of chordate larvae are stem-like cells that form the adult nervous system. *Nature*, *469*(7331), 525–529. https://doi.org/10.1038/nature09631

Huang, S., Chen, Z., Yan, X., Yu, T., Huang, G., Yan, Q., Pontarotti, P. A. ntoin., Zhao, H., Li, J., Yang, P., Wang, R., Li, R., Tao, X., Deng, T., Wang, Y., Li, G., Zhang, Q., Zhou, S., You, L., … Xu, A. (2014). Decelerated genome evolution in modern vertebrates revealed by analysis of multiple lancelet genomes. *Nature Communications*, *5*, 5896. https://doi.org/10.1038/ncomms6896

Igawa, T., Nozawa, M., Suzuki, D. G., Reimer, J. D., Morov, A. R., Wang, Y., Henmi, Y., & Yasui, K. (2017). Evolutionary history of the extant amphioxus lineage with shallow-branching diversification. *Scientific Reports*, *7*(1). https://doi.org/10.1038/s41598-017-00786-5

Imai, J. H., & Meinertzhagen, I. A. (2007). Neurons of the ascidian larval nervous system in Ciona intestinalis: I. Central nervous system. *Journal of Comparative Neurology*, *501*(3), 316–334. https://doi.org/10.1002/cne.21246

IUCN. (2020). *The IUCN red list of threatened species. Version 2020-3: Table 1a*. https://www.iucnredlist.org

Jefferies, R. P. S. (1991). Two types of bilateral symmetry in the Metazoa: chordate and bilaterian. In G. R. Bock & J. Marsh (Eds.), *Novartis Foundation Symposium* (pp. 94–127). Ciba Foundation. https://dockscl.com/two-types-of-bilateral-symmetry-in-the-metazoa-chordate-and-bilaterian_5ef34c7e097c47c94c8b4579.html

Jékely, G., & Arendt, D. (2007). Cellular resolution expression profiling using confocal detection of NBT/BCIP precipitate by reflection microscopy. *BioTechniques*, *42*(6), 751–755. https://doi.org/10.2144/000112462

Jurisch-Yaksi, N., Yaksi, E., & Kizil, C. (2020). Radial glia in the zebrafish brain: Functional, structural, and physiological comparison with the mammalian glia. In *GLIA*. John Wiley and Sons Inc. https://doi.org/10.1002/glia.23849

Kálmán, M., & Gould, R. M. (2001). GFAP-immunopositive structures in spiny dogfish, Squalus acanthias, and little skate, Raia erinacea, brains: Differences have evolutionary implications. *Anatomy and Embryology*, *203*(6), 59–80. https://doi.org/10.1007/s004290100180

Kaltenbach, S. L., Yu, J. K., & Holland, N. D. (2009). The origin and migration of the earliest-developing sensory neurons in the peripheral nervous system of amphioxus. *Evolution and Development*, *11*(2), 142–151. https://doi.org/10.1111/j.1525-142X.2009.00315.x

Kapli, P., Natsidis, P., Leite, D., Fursman, M., Jeffrie, N., Rahman, I., Philippe, H., Copley, R., & Telford, M. (2020). Lack of support for Deuterostomia prompts reinterpretation of the first Bilateria. *BioRxiv*, 2020.07.01.182915. https://doi.org/10.1101/2020.07.01.182915

Karabinos, A. (2013). The cephalochordate Branchiostoma genome contains 26 intermediate filament (IF) genes: Implications for evolution of chordate IF proteins. *European Journal of Cell Biology*, *92*(8–9), 295–302. https://doi.org/10.1016/j.ejcb.2013.10.004

Katz, M., Corson, F., Keil, W., Singhal, A., Bae, A., Lu, Y., Liang, Y., & Shaham, S. (2019). Glutamate spillover in C. elegans triggers repetitive behavior through presynaptic activation of MGL-2/mGluR5. *Nature Communications*, *10*(1). https://doi.org/10.1038/s41467-019-09581-4

Katz, M. J. (1983). Comparative anatomy of the tunicate tadpole, Ciona intestinalis. *The Biological Bulletin*, *164*(1), 1–27. https://doi.org/10.2307/1541186

Kaul, S., & Stach, T. (2010). Ontogeny of the collar cord: Neurulation in the hemichordate Saccoglossus kowalevskii. *Journal of Morphology*, *271*(10), 1240–1259. https://doi.org/10.1002/jmor.10868

Kettenmann, H., & Verkhratsky, A. (2008). Neuroglia: the 150 years after. *Trends in Neurosciences*, *31*(12), 653–659. https://doi.org/10.1016/j.tins.2008.09.003

Kim, H., Shin, J., Kim, S., Poling, J., Park, H. C., & Appel, B. (2008). Notch-regulated oligodendrocyte specification from radial glia in the spinal cord of zebrafish embryos. *Developmental Dynamics*, *237*(8), 2081–2089. https://doi.org/10.1002/dvdy.21620

Kocot, K. M., Tassia, M. G., Halanych, K. M., & Swalla, B. J. (2018). Phylogenomics offers resolution of major tunicate relationships. *Molecular Phylogenetics and Evolution*, *121*, 166–173.

https://doi.org/10.1016/j.ympev.2018.01.005

Kowalevski, A. (1865). *Istoria razvitia lantsetnica (Amphioxus lanceolatus или Branchiostoma lumbricam)*. St. Petersburg.

Kowalevski, A. (1866). Entwicklungsgeschichte der einfachen Ascidien. *Mémoires de l'Académie Impériale Des Sciences de St. Pétersbourg, 7e Série*, *10*(15), 1–19.

Kowalevski, A. (1867). Die Entwickelungsgeschichte des Amphioxus lanceolatus. *Mémoires de l'Académie Impériale Des Sciences de St. Pétersbourg, 7e Série*, *11*(4), 11–17.

Kozmikova, I., & Kozmik, Z. (2020). Wnt/β-catenin signaling is an evolutionarily conserved determinant of chordate dorsal organizer. *ELife*, *9*. https://doi.org/10.7554/eLife.56817

Kriegstein, A., & Alvarez-Buylla, A. (2009). The glial nature of embryonic and adult neural stem cells. *Annual Review of Neuroscience*, *32*, 149–184. https://doi.org/10.1146/annurev.neuro.051508.135600

Kroehne, V., Freudenreich, D., Hans, S., Kaslin, J., & Brand, M. (2011). Regeneration of the adult zebrafish brain from neurogenic radial glia-type progenitors. *Development*, *138*(22), 4831–4841. https://doi.org/10.1242/dev.072587

Kuffler, S. W., & Potter, D. D. (1964). Glia in the leech central nervous system: Physiological properties and neuron-glia relationship. *Journal of Neurophysiology*, *27*, 290–320. https://doi.org/10.1152/jn.1964.27.2.290

Lacalli, T. (2012). The Middle Cambrian fossil Pikaia and the evolution of chordate swimming. *EvoDevo*, *3*(1), 12. https://doi.org/10.1186/2041-9139-3-12

Lacalli, T. C. (1996). Frontal eye circuitry, rostral sensory pathways and brain organization in amphioxus larvae: Evidence from 3D reconstructions. *Philosophical Transactions of the Royal Society B: Biological Sciences*, *351*(1337), 243–263. https://doi.org/10.1098/rstb.1996.0022

Lacalli, T. C. (2000). Cell morphology in amphioxus nerve cord may reflect the time course of cell differentiation. *International Journal of Developmental Biology*, *44*(8), 903–906. https://doi.org/10.1387/ijdb.11206331

Lacalli, T. C. (2002). The dorsal compartment locomotory control system in amphioxus larvae. *Journal of Morphology*, *252*(3), 227–237. https://doi.org/10.1002/jmor.1101

Lacalli, T. C. (2004). Sensory systems in amphioxus: A window on the ancestral chordate condition. *Brain, Behavior and Evolution*. https://doi.org/10.1159/000079744

Lacalli, T. C., Holland, N. D., & West, J. E. (1994). Landmarks in the anterior central nervous system of amphioxus larvae. *Philosophical Transactions of the Royal Society B: Biological Sciences*, *344*(1308), 165–185. https://doi.org/10.1098/rstb.1994.0059

Lacalli, T. C., & Kelly, S. J. (2000). The infundibular balance organ in amphioxus larvae and related aspects of cerebral vesicle organization. *Acta Zoologica*, *81*(1), 37–47. https://doi.org/10.1046/j.1463-6395.2000.00036.x

Lacalli, T. C., & Kelly, S. J. (2002). Floor plate, glia and other support cells in the anterior nerve cord of amphioxus larvae. *Acta Zoologica*, *83*(2), 87–98. https://doi.org/10.1046/j.1463-6395.2002.00101.x

Lacalli, T. C., & Kelly, S. J. (2003). Sensory pathways in amphioxus larvae II. Dorsal tracts and translumenal cells. *Acta Zoologica*, *84*(1), 1–13. https://doi.org/10.1046/j.1463-6395.2003.00065.x

Lacalli, T., & Candiani, S. (2017). Locomotory control in amphioxus larvae: New insights from neurotransmitter data. In *EvoDevo* (Vol. 8, Issue 1). BioMed Central Ltd. https://doi.org/10.1186/s13227-017-0067-9

Langeland, J. A., Holland, L. Z., Chastain, R. A., & Holland, N. D. (2006). An amphioxus LIM-homeobox gene, AmphiLim1/5, expressed early in the invaginating organizer region and later in differentiating cells of the kidney and central nervous system. *International Journal of Biological Sciences*, *2*(3), 110–116.

Lemaire, P. (2011). Evolutionary crossroads in developmental biology: The tunicates. *Development*, *138*(11), 2143–2152. https://doi.org/10.1242/dev.048975

Leys, S. P., Mackie, G. O., & Meech, R. W. (1999). Impulse conduction in a sponge. *Journal of Experimental Biology*, *202*(9), 1139–1150.

Lowe, C. J., Clarke, D. N., Medeiros, D. M., Rokhsar, D. S., & Gerhart, J. (2015). The deuterostome context of chordate origins. In *Nature* (Vol. 520, Issue 7548, pp. 456–465). Nature Research. https://doi.org/10.1038/nature14434

Mackie, G. O., & Burighel, P. (2005). The nervous system in adult tunicates: current research directions. *Canadian Journal of Zoology*, *83*(1), 151–183. https://doi.org/10.1139/z04-177

Malatesta, P., Hartfuss, E., & Götz, M. (2000). Isolation of radial glial cells by fluorescent-activated cell sorting reveals a neural lineage. *Development*, *127*(24), 5253–5263.

Marlétaz, F., Firbas, P. N., Maeso, I., Tena, J. J., Bogdanovic, O., Perry, M., Wyatt, C. D. R., de la Calle-Mustienes, E., Bertrand, S., Burguera, D., Acemel, R. D., van Heeringen, S. J., Naranjo, S., Herrera-Ubeda, C., Skvortsova, K., Jimenez-Gancedo, S., Aldea, D., Marquez, Y., Buono, L., … Irimia, M. (2018). Amphioxus functional genomics and the origins of vertebrate gene regulation. *Nature*, *564*(7734), 64–70. https://doi.org/10.1038/s41586-018-0734-6

Mashanov, V. S., Zueva, O. R., & Garcia-Arraras, J. E. (2010). Organization of glial cells in the adult sea cucumber central nervous system. *Glia*, *58*(13), 1581–1593. https://doi.org/10.1002/glia.21031

Mashanov, V. S., Zueva, O. R., & García-Arrarás, J. E. (2013). Radial glial cells play a key role in echinoderm neural regeneration. *BMC Biology*, *11*, 49. https://doi.org/10.1186/1741-7007-11-49

Mashanov, V. S., Zueva, O. R., Heinzeller, T., Aschauer, B., Naumann, W. W., Grondona, J. M., Cifuentes, M., & Garcia-Arraras, J. E. (2009). The central nervous system of sea cucumbers (Echinodermata: Holothuroidea) shows positive immunostaining for a chordate glial secretion. *Frontiers in Zoology*, *6*(1), 11. https://doi.org/10.1186/1742-9994-6-11

Mashanov, V. S., Zueva, O. R., Heinzeller, T., & Dolmatov, I. Y. (2006). Ultrastructure of the circumoral nerve ring and the radial nerve cords in holothurians (Echinodermata). *Zoomorphology*, *125*(1), 27–38. https://doi.org/10.1007/s00435-005-0010-9

Mashanov, V., Zueva, O., Rubilar, T., Epherra, L., & García-Arrarás, J. E. (2016). Echinodermata. In A. Schmidt-Rhaesa, S. Harzsch, & G. Purschke (Eds.), *Structure and Evolution of Invertebrate Nervous Systems* (pp. 665–688). Oxford University Press. https://doi.org/10.1093/acprof:oso/9780199682201.001.0001

Mayer, G., & Harzsch, S. (2007). Immunolocalization of serotonin in Onychophora argues against segmental ganglia being an ancestral feature of arthropods. *BMC Evolutionary Biology*, *7*(1), 118. https://doi.org/10.1186/1471-2148-7-118

Meiniel, O., Meiniel, R., Lalloué, F., Didier, R., Jauberteau, M. O., Meiniel, A., & Petit, D. (2008). The lengthening of a giant protein: When, how, and why? *Journal of Molecular Evolution*, *66*(1), 1–10. https://doi.org/10.1007/s00239-007-9055-3

Metschnikoff, V. E. (1881). Uber die systematische Stellung von Balanoglossus. *Zool Anzeiger*, *4*, 153–157. https://ci.nii.ac.jp/naid/10010667396

Morris, S. C., & Caron, J. B. (2012). Pikaia gracilens Walcott, a stem-group chordate from the Middle Cambrian of British Columbia. *Biological Reviews*, *87*(2), 480–512. https://doi.org/10.1111/j.1469-185X.2012.00220.x

Müller, T., Anlag, K., Wildner, H., Britsch, S., Treier, M., & Birchmeier, C. (2005). The bHLH factor Olig3 coordinates the specification of dorsal neurons in the spinal cord. *Genes and Development*, *19*(6), 733–743. https://doi.org/10.1101/gad.326105

Nicol, D., & Meinertzhagen, I. A. (1991). Cell counts and maps in the larval central nervous system of the ascidian ciona intestinalis (L.). *Journal of Comparative Neurology*, *309*(4), 415–429. https://doi.org/10.1002/cne.903090402

Nielsen, C. (2012). The authorship of higher chordate taxa. *Zoologica Scripta*, *41*(4), 435–436. https://doi.org/10.1111/j.1463-6409.2012.00536.x

Nieuwenhuys, Rudolf. (1998). Structure and Organization of Centres. In R Nieuwenhuys, H. J. ten Donkelaar, & C. Nicholson (Eds.), *The Central Nervous System of Vertebrates* (pp. 25–112). Springer. https://doi.org/10.1007/978-3-642-18262-4_2

Nieuwenhuys, Rudolf. (2000). Comparative aspects of volume transmission, with sidelight on other forms of intercellular communication. *Progress in Brain Research*, *125*, 49–126. https://doi.org/10.1016/S0079-6123(00)25006-1

Nomaksteinsky, M., Röttinger, E., Dufour, H. D., Chettouh, Z., Lowe, C. J., Martindale, M. Q., & Brunet, J. F. (2009). Centralization of the deuterostome nervous system predates chordates. *Current Biology*, *19*(15), 1264–1269. https://doi.org/10.1016/j.cub.2009.05.063

Obermüller-Wilén, H. (1979). A neurosecretory system in the brain of the lancelet, Branchiostoma lanceolatum. *Acta Zoologica*, *60*(3), 187–196. https://doi.org/10.1111/j.1463-6395.1979.tb00611.x

Obermüller-Wilén, H., & Olsson, R. (1974). The Reissner's Fiber Termination in Some Lower Chordates. *Acta Zoologica*, *55*(2), 71–79. https://doi.org/10.1111/j.1463-6395.1974.tb00181.x

Ogasawara, M. (2000). Overlapping expression of amphioxus homologs of the thyroid transcription factor-1 gene and thyroid peroxidase gene in the endostyle: Insight into evolution of the thyroid gland. *Development Genes and Evolution*, *210*(5), 231–242. https://doi.org/10.1007/s004270050309

Olsson, R. (1955). Structure and development of Reissner's fibre in the caudal end of Amphioxus and some lower vertebrates. In *Acta Zoologica* (Vol. 36, Issue 2, pp. 167–198). https://doi.org/10.1111/j.1463-6395.1955.tb00379.x

Olsson, R. (1956). The development of Reissner's fibre in the brain of the salmon. *Acta Zoologica*, *37*(3), 235–250. https://doi.org/10.1111/j.1463-6395.1956.tb00046.x

Olsson, R. (1972). Reissner's Fiber in Ascidian Tadpole Larvae. *Acta Zoologica*, *53*(1), 17–21. https://doi.org/10.1111/j.1463-6395.1972.tb00568.x

Olsson, R., Yulis, R., & Rodríguez, E. M. (1994). The infundibular organ of the lancelet (Branchiostoma lanceolatum, Acrania): an immunocytochemical study. *Cell and Tissue Research*, *277*(1), 107–114. https://doi.org/10.1007/BF00303086

Omoto, J. J., Yogi, P., & Hartenstein, V. (2015). Origin and development of neuropil glia of the Drosophila larval and adult brain: Two distinct glial populations derived from separate progenitors. *Developmental Biology*, *404*(2), 2–20. https://doi.org/10.1016/j.ydbio.2015.03.004

Orentas, D. M., Hayes, J. E., Dyer, K. L., & Miller, R. H. (1999). Sonic hedgehog signaling is required during the appearance of spinal cord oligodendrocyte precursors. *Development*, *126*(11), 2419–2429.

Ortega, A., & Olivares-Bañuelos, T. N. (2020). Neurons and Glia Cells in Marine Invertebrates: An Update. In *Frontiers in Neuroscience* (Vol. 14, p. 121). Frontiers Media S.A. https://doi.org/10.3389/fnins.2020.00121

Orts-Del'Immagine, A., Cantaut-Belarif, Y., Thouvenin, O., Roussel, J., Baskaran, A., Langui, D., Koëth, F., Bivas, P., Lejeune, F. X., Bardet, P. L., & Wyart, C. (2020). Sensory Neurons Contacting the Cerebrospinal Fluid Require the Reissner Fiber to Detect Spinal Curvature In Vivo. *Current Biology*, *30*(5), 827-839.e4. https://doi.org/10.1016/j.cub.2019.12.071

Pallas, P. S. (1774). *Spicilegia zoologica quibus novae imprrimis et obscurae animalium species iconibus, descriptionibus atque commentariis illustrantur*. Berolini.

Pascual-Anaya, J., & D'Aniello, S. (2006). Free amino acids in the nervous system of the amphioxus Branchiostoma lanceolatum. A comparative study. *International Journal of Biological Sciences*, *2*(2), 87–92. https://doi.org/10.7150/ijbs.2.87

Pentreath, V. W., Radojcic, T., Seal, L. H., & Winstanley, E. K. (1985). The glial cells and glia-neuron relations in the buccal ganglia of Planorbis corneus (L): cytological, qualitative and quantitative changes during growth and ageing. *Philosophical Transactions of the Royal Society of London. B, Biological Sciences*, *307*(1133), 399–456. https://doi.org/10.1098/rstb.1985.0002

Perea, G., Navarrete, M., & Araque, A. (2009). Tripartite synapses: astrocytes process and control synaptic information. In *Trends in Neurosciences* (Vol. 32, Issue 8, pp. 421–431). Elsevier Current Trends. https://doi.org/10.1016/j.tins.2009.05.001

Peterson, K. J., & Eernisse, D. J. (2001). Animal phylogeny and the ancestry of bilaterians: Inferences from morphology and 18S rDNA gene sequences. *Evolution and Development*, *3*(3), 170–205. https://doi.org/10.1046/j.1525-142X.2001.003003170.x

Philippe, H., Brinkmann, H., Copley, R. R., Moroz, L. L., Nakano, H., Poustka, A. J., Wallberg, A., Peterson, K. J., & Telford, M. J. (2011). Acoelomorph flatworms are deuterostomes related to Xenoturbella. *Nature*, *470*(7333), 255–260. https://doi.org/10.1038/nature09676

Poss, S. G., & Boschung, H. T. (1996). Lancelets (cephalochordata: branchiostomatidae): How many species are valid? *Israel Journal of Zoology*, *42*(SUPPL.). https://doi.org/10.1080/00212210.1996.10688872

Prosser, C. L., Nagai, T., & Nystrom, R. A. (1962). Oscular contractions in sponges. *Comparative Biochemistry And Physiology*, *6*(1), 69–74. https://doi.org/10.1016/0010-406x(62)90044-0

Putnam, N. H., Butts, T., Ferrier, D. E. K., Furlong, R. F., Hellsten, U., Kawashima, T., Robinson-Rechavi, M., Shoguchi, E., Terry, A., Yu, -Kai, Benito-Gutiérrez, L., Dubchak, I., Garcia-Fernàndez, J., Gibson-Brown, J. J., Grigoriev, I. V, Horton, A. C., De Jong, P. J., Jurka, J., Kapitonov, V. V, … Rokhsar, D. S. (2008). The amphioxus genome and the evolution of the chordate karyotype. *Nature*, *453*, 1064–1071. https://doi.org/10.1038/nature06967

Ransom, B. R., Butt, A. M., & Black, J. A. (1991). Ultrastructural identification of HRP-injected oligodendrocytes in the intact rat optic nerve. *Glia*, *4*(1), 37–45. https://doi.org/10.1002/glia.440040105

Rehkämper, G., Welsch, U., & Dilly, P. N. (1987). Fine structure of the ganglion of Cephalodiscus gracilis (Pterobranchia, Hemichordata). *Journal of Comparative Neurology*, *259*(2), 308–315. https://doi.org/10.1002/cne.902590210

Reichenbach, A., & Wolburg, H. (2013). Astrocytes and ependymal glia. In H. Kettenmann & B. R. Ransom (Eds.), *Neuroglia* (3rd ed., pp. 35–49). Oxford University Press. https://doi.org/10.1093/med/9780199794591.003.0004

Ren, Q., Zhong, Y., Xin, H., Leung, B., Xing, C., Wang, H., Hu, G., Wang, Y., Shimeld, S. M., & Li, G. (2020). Step-wise evolution of neural patterning by Hedgehog signalling in chordates. *Nature Ecology and Evolution*, 1–9. https://doi.org/10.1038/s41559-020-1248-9

Richter, S., Loesel, R., Purschke, G., Schmidt-Rhaesa, A., Scholtz, G., Stach, T., Vogt, L., Wanninger, A., Brenneis, G., Döring, C., Faller, S., Fritsch, M., Grobe, P., Heuer, C. M., Kaul, S., Møller, O. S., Müller, C. H. G., Rieger, V., Rothe, B. H., … Harzsch, S. (2010). Invertebrate neurophylogeny: Suggested terms and definitions for a neuroanatomical glossary. *Frontiers in Zoology*, *7*(1), 1–49. https://doi.org/10.1186/1742-9994-7-29

Rival, T., Soustelle, L., Strambi, C., Besson, M. T., Iché, M., & Birman, S. (2004). Decreasing glutamate buffering capacity triggers oxidative stress and neuropil degeneration in the Drosophila brain. *Current Biology*, *14*(7), 599–605. https://doi.org/10.1016/j.cub.2004.03.039

Roberts-Galbraith, R. H., Brubacher, J. L., & Newmark, P. A. (2016). A functional genomics screen in planarians reveals regulators of whole-brain regeneration. *ELife*, *5*(September2016). https://doi.org/10.7554/eLife.17002

Rose, C. D., Pompili, D., Henke, K., Van Gennip, J. L. M., Meyer-Miner, A., Rana, R., Gobron, S., Harris, M. P., Nitz, M., & Ciruna, B. (2020). SCO-Spondin Defects and Neuroinflammation Are Conserved Mechanisms Driving Spinal Deformity across Genetic Models of Idiopathic Scoliosis. *Current Biology*, *0*(0). https://doi.org/10.1016/j.cub.2020.04.020

Ross, K. G., Currie, K. W., Pearson, B. J., & Zayas, R. M. (2017). Nervous system development and regeneration in freshwater planarians. In *Wiley Interdisciplinary Reviews: Developmental Biology* (Vol. 6, Issue 3, p. e266). John Wiley and Sons Inc. https://doi.org/10.1002/wdev.266

Röttinger, E., & Lowe, C. J. (2012). Evolutionary crossroads in developmental biology: Hemichordates. *Development*, *139*(14), 2463–2475. https://doi.org/10.1242/dev.066712

Rouse, G. W., Wilson, N. G., Carvajal, J. I., & Vrijenhoek, R. C. (2016). New deep-sea species of Xenoturbella and the position of Xenacoelomorpha. *Nature*, *530*(7588), 94–97. https://doi.org/10.1038/nature16545

Ruppert, E. E. (1997). Cephalochordata (Acrania). In F. Harrison & E. Ruppert (Eds.), *Microscopic Anatomy of Invertebrates, Volume 15: Hemichordata, Chaetognatha, and the Invertebrate Chordates* (pp. 349–504). Wiley-Liss Inc.

Satoh, G., Wang, Y., Zhang, P., & Satoh, N. (2001). Early development of amphioxus nervous system with special reference to segmental cell organization and putative sensory cell precursors: A study based on the expression of pan-neuronal marker geneHu/elav. *Journal of Experimental Zoology*, *291*(4), 354–364. https://doi.org/10.1002/jez.1134

Satoh, N., Rokhsar, D., & Nishikawa, T. (2014). Chordate evolution and the three-phylum system. *Proceedings of the Royal Society B: Biological Sciences*, *281*(1794), 20141729. https://doi.org/10.1098/rspb.2014.1729

Schindelin, J., Arganda-Carreras, I., Frise, E., Kaynig, V., Longair, M., Pietzsch, T., Preibisch, S., Rueden, C., Saalfeld, S., Schmid, B., Tinevez, J. Y., White, D. J., Hartenstein, V., Eliceiri, K., Tomancak, P., & Cardona, A. (2012). Fiji: An open-source platform for biological-image analysis. In *Nature Methods* (Vol. 9, Issue 7, pp. 676–682). https://doi.org/10.1038/nmeth.2019

Schubert, M., Holland, L. Z., Stokes, M. D., & Holland, N. D. (2001). Three amphioxus Wnt genes (AmphiWnt3, AmphiWnt5, and AmphiWnt6) associated with the tail bud: The evolution of somitogenesis in chordates. *Developmental Biology*, *240*(1), 262–273. https://doi.org/10.1006/dbio.2001.0460

Singhvi, A., & Shaham, S. (2019). Glia-neuron interactions in Caenorhabditis elegans. In *Annual Review of Neuroscience* (Vol. 42, pp. 149–168). Annual Reviews Inc. https://doi.org/10.1146/annurev-neuro-070918-050314

Stach, T., Gruhl, A., & Kaul-Strehlow, S. (2012). The central and peripheral nervous system of Cephalodiscus gracilis (Pterobranchia, Deuterostomia). *Zoomorphology*, *131*(1), 11–24. https://doi.org/10.1007/s00435-011-0144-x

Stadelmann, C., Timmler, S., Barrantes-Freer, A., & Simons, M. (2019). Myelin in the central nervous system: Structure, function, and pathology. *Physiological Reviews*, *99*(3), 1381–1431. https://doi.org/10.1152/physrev.00031.2018

Su, L., Shi, C., Huang, X., Wang, Y., & Li, G. (2020). Application of CRISPR/cas9 nuclease in amphioxus genome editing. *Genes*, *11*(11), 1–9. https://doi.org/10.3390/genes11111311

Tatsumi, K., Isonishi, A., Yamasaki, M., Kawabe, Y., Morita-Takemura, S., Nakahara, K., Terada, Y., Shinjo, T., Okuda, H., Tanaka, T., & Wanaka, A. (2018). Olig2-Lineage astrocytes: A distinct subtype of astrocytes that differs from GFAP astrocytes. *Frontiers in Neuroanatomy*, *12*(8), 8. https://doi.org/10.3389/fnana.2018.00008

Telford, M. J., Bourlat, S. J., Economou, A., Papillon, D., & Rota-Stabelli, O. (2008). The evolution of the Ecdysozoa. *Philosophical Transactions of the Royal Society B: Biological Sciences*, *363*(1496), 1529–1537. https://doi.org/10.1098/rstb.2007.2243

Telford, M. J., Budd, G. E., & Philippe, H. (2015). Phylogenomic insights into animal evolution. In *Current Biology* (Vol. 25, Issue 19, pp. R876–R887). Cell Press. https://doi.org/10.1016/j.cub.2015.07.060

Theodosiou, M., Colin, A., Schulz, J., Laudet, V., Peyrieras, N., Nicolas, J.-F., Schubert, M., & Hirsinger, E. (2011). Amphioxus spawning behavior in an artificial seawater facility. *Journal of Experimental Zoology Part B: Molecular and Developmental Evolution*, *316B*(4), 263–275. https://doi.org/10.1002/jez.b.21397

Trinh, L. A., McCutchen, M. D., Bonner-Fraser, M., Fraser, S. E., Bumm, L. A., & McCauley, D. W. (2007). Fluorescent in situ hybridization employing the conventional NBT/BCIP chromogenic stain. *BioTechniques*, *42*(6), 756–759. https://doi.org/10.2144/000112476

Troutwine, B. R., Gontarz, P., Konjikusic, M. J., Minowa, R., Monstad-Rios, A., Sepich, D. S., Kwon, R. Y., Solnica-Krezel, L., & Gray, R. S. (2020). The Reissner Fiber Is Highly Dynamic In Vivo and Controls Morphogenesis of the Spine. *Current Biology*, *0*(0). https://doi.org/10.1016/j.cub.2020.04.015

Verasztó, C., Jasek, S., Gühmann, M., Shahidi, R., Ueda, N., David Beard, J., Mendes, S., Heinz, K., Alberto Bezares-Calderón, L., Williams, E., & Jékely, G. (2020). Whole-animal connectome and cell-type complement of the three-segmented Platynereis dumerilii larva. *BioRxiv*. https://doi.org/10.1101/2020.08.21.260984

Verkhratsky, A., & Butt, A. (2018). The history of the decline and fall of the glial numbers legend. *Neuroglia*, *1*(1), 188–192. https://doi.org/10.3390/neuroglia1010013

Verkhratsky, A., & Butt, A. M. (2013). Neuroglia: Definition, Classification, Evolution, Numbers, Development. In A. Verkhratsky & A. M. Butt (Eds.), *Glial Physiology an Pathophysiology* (pp. 73–104). John Wiley & Sons. https://doi.org/10.1002/9781118402061.ch3

Verkhratsky, A., Ho, M. S., & Parpura, V. (2019). Evolution of neuroglia. In A. Verkhratsky, M. S. Ho, R. Zorec, & V. Parpura (Eds.), *Advances in Experimental Medicine and Biology* (Vol. 1175, pp. 15–44). Springer New York LLC. https://doi.org/10.1007/978-981-13-9913-8_2

Verkhratsky, A., Ho, M. S., Zorec, R., & Parpura, V. (2019). The concept of neuroglia. In A. Verkhratsky, M. S. Ho, R. Zorec, & V. Parpura (Eds.), *Advances in Experimental Medicine and Biology* (Vol. 1175, pp. 1–13). Springer New York LLC. https://doi.org/10.1007/978-981-13-9913-8_1

Verkhratsky, A., & Nedergaard, M. (2018). Physiology of astroglia. *Physiological Reviews*, *98*(1). https://doi.org/10.1152/physrev.00042.2016

Viehweg, J., Naumann, W. W., & Olsson, R. (1998). Secretory Radial Glia in the Ectoneural System of the Sea Star Asterias rubens (Echinodermata). *Acta Zoologica*, *79*(2), 119–131. https://doi.org/10.1111/j.1463-6395.1998.tb01151.x

Vopalensky, P., Pergner, J., Liegertova, M., Benito-Gutierrez, E., Arendt, D., & Kozmik, Z. (2012). Molecular analysis of the amphioxus frontal eye unravels the evolutionary origin of the retina and pigment cells of the vertebrate eye. *Proceedings of the National Academy of Sciences of the United States of America*, *109*(38), 15383–15388. https://doi.org/10.1073/pnas.1207580109

Wang, I. E., Lapan, S. W., Scimone, M. L., Clandinin, T. R., & Reddien, P. W. (2016). Hedgehog signaling regulates gene expression in planarian glia. *ELife*, *5*(September2016). https://doi.org/10.7554/eLife.16996

White, J. G., Southgate, E., Thomson, J. N., & Brenner, S. (1986). The structure of the nervous system of the nematode Caenorhabditis elegans. *Philosophical Transactions of the Royal Society of London. B, Biological Sciences*, *314*(1165), 1–340. https://doi.org/10.1098/rstb.1986.0056

Wicht, H., & Lacalli, T. C. (2005). The nervous system of amphioxus: Structure, development, and evolutionary significance. In *Canadian Journal of Zoology* (Vol. 83, Issue 1, pp. 122–150). https://doi.org/10.1139/z04-163

Wickstead, J. H. (1967). Branchiostoma lanceolatum larvae: Some experiments on the effect of thiouracil on metamorphosis. *Journal of the Marine Biological Association of the United Kingdom*, *47*(1), 49–59. https://doi.org/10.1017/S0025315400033555

Winchell, C. J., Sullivan, J., Cameron, C. B., Swalla, B. J., & Mallatt, J. (2002). Evaluating hypotheses of deuterostome phylogeny and chordate evolution with new LSU and SSU ribosomal DNA data. *Molecular Biology and Evolution*, *19*(5), 762–776. https://doi.org/10.1093/oxfordjournals.molbev.a004134

Wolburg, H., Wolburg-Buchholz, K., Mack, A. F., & Reichenbach, A. (2009). Ependymal cells. In *Encyclopedia of Neuroscience* (pp. 1133–1140). Elsevier Ltd. https://doi.org/10.1016/B978-008045046-9.01001-9

Yarrell, W. (1859). A history of British fishes. In J. Richardson (Ed.), *A history of British fishes* (3rd ed.). John Van Voorst. https://doi.org/10.5962/bhl.title.168958

Yildirim, K., Petri, J., Kottmeier, R., & Klämbt, C. (2019). Drosophila glia: Few cell types and many conserved functions. In *GLIA* (Vol. 67, Issue 1, pp. 5–26). John Wiley and Sons Inc. https://doi.org/10.1002/glia.23459

Zhang, Q.-J., Luo, Y.-J., Wu, H.-R., Chen, Y.-T., & Yu, J.-K. (2013). Expression of germline markers in three species of amphioxus supports a preformation mechanism of germ cell development in cephalochordates. *EvoDevo*, *4*(1), 17. https://doi.org/10.1186/2041-9139-4-17

Zieger, E., Garbarino, G., Robert, N. S. M., Yu, J. K., Croce, J. C., Candiani, S., & Schubert, M. (2018). Retinoic acid signaling and neurogenic niche regulation in the developing peripheral nervous system of the cephalochordate amphioxus. *Cellular and Molecular Life Sciences*, *75*(13), 2407–2429. https://doi.org/10.1007/s00018-017-2734-3

Zieger, E., Lacalli, T. C., Pestarino, M., Schubert, M., & Candiani, S. (2017). The origin of dopaminergic systems in chordate brains: insights from amphioxus. *The International Journal of Developmental Biology*, *61*(10-11–12), 749–761. https://doi.org/10.1387/ijdb.170153sc

Zueva, O., Khoury, M., Heinzeller, T., Mashanova, D., & Mashanov, V. (2018). The complex simplicity of the brittle star nervous system. *Frontiers in Zoology*, *15*(1), 1. https://doi.org/10.1186/s12983-017-0247-4

Appendix 1

Table S1. List of sequences used in the phylogenetic analysis. Accession numbers provided are relative to the NCBI database (www.ncbi.nlm.nih.gov). Accession numbers in bold are relative to the EnsemblMetazoa database (metazoa.ensembl.org/Branchiostoma_lanceolatum)

Species	Gene Name	Accession number
Acropora digitifera	sspo	XP_015770945.1
Branchiostoma belcheri	sspo	NW_017804043*
Branchiostoma lanceolatum	sspo	BL96730*
Ciona intestinalis	sspo	XP_026693982.1
Gallus gallus	sspo	NP_001006351.2
Homo sapiens	sspo	CAJ43920.1
Hydra vulgaris	sspo	XP_012557682.1
Latimeria chalumnae	sspo	XP_014342845.1
Mus musculus	sspo	CAD42654.1
Petromyzon marinus	sspo	XP_032822651.1
Rattus norvegicus	sspo	NP_001007017.1
Xenopus tropicalis	sspo	XP_012809901.2
**predicted from genome sequence*		
Anopheles gambiae	GS	Q7QBX9
Branchiostoma lanceolatum	GS	**BL14839**
Ciona intestinalis	GS	XP_002127926.3
Danio rerio	GS	A0A2R8QG82

Homo sapiens	GS	A0A2R8YDT1
Hydra vulgaris	GS	XP_002157534.2
Latimeria chalumnae	GS	H3B669
Lottia gigantea	GS	V4B3R1
Macaca mulatta	GS	F7CAM5
Mus musculus	GS	P15105
Nematostella vectensis	GS	A7S6S5
Rattus norvegicus	GS	P09606
Squalus acanthias	GS	P41320
Stylophora pistillata	GS	A0A2B4SEH2
Tribolium castaneum	GS	D6WFH1
Bos taurus	olig1	NP_001193690.1
Bos taurus	olig2	XP_024849418.1
Bos taurus	olig3	XP_610701.2
Branchiostoma lanceolatum	oliga	**BL19565**
Branchiostoma lanceolatum	oligb	**BL01014**
Branchiostoma lanceolatum	oligc	**BL19561**
Canis lupus familiaris	olig1	XP_852212.3
Canis lupus familiaris	olig2	XP_005638894.1
Canis lupus familiaris	olig3	XP_022260498.1
Danio rerio	olig2	AAH65598.1
Danio rerio	olig3	NP_001103863.1
Danio rerio	olig4	CAD32563.1
Dasypus novemcinctus	olig3	XP_004468608.1
Drosophila melanogaster	oliA	NP_523592.1
Echinops telfairi	olig1	XP_004711355.1
Echinops telfairi	olig2	XP_012862354.1
Echinops telfairi	olig3	XP_004702036.1
Gallus gallus	olig2	AAL11883.1
Gallus gallus	olig3	XP_015139914.1
Homo sapiens	olig1	NP_620450.2
Homo sapiens	olig2	NP_005797.1
Homo sapiens	olig3	NP_786923.1
Macaca mulatta	olig1	AFJ72002.1
Macaca mulatta	olig2	XP_014988488.1
Macaca mulatta	olig3	XP_001096569.1

Monodelphis domestica	olig3	XP_007484682.1
Mus musculus	olig1	NP_058664.2
Mus musculus	olig2	NP_058663.2
Mus musculus	olig3	NP_443734.2
Oryzias latipes	olig1	XP_020568943.1
Oryzias latipes	olig2	XP_020568875.2
Oryzias latipes	olig3	XP_023819514.1
Oryzias latipes	olig4	ENSORLG00000017556
Pan troglodytes	olig1	XP_530336.4
Pan troglodytes	olig2	XP_001172282.1
Pan troglodytes	olig3	XP_527513.3
Rattus norvegicus	olig1	NP_068538.2
Rattus norvegicus	olig2	NP_001094027.1
Rattus norvegicus	olig3	P_001099739.1
Saccoglossus kowalevskii	olig	ABD97276.1
Sus scrofa	olig1	XP_005670384.1
Sus scrofa	olig2	XP_003358977.2
Sus scrofa	olig3	XP_001928671.1
Takifugu rubripes	olig1	XP_029697813.1
Takifugu rubripes	olig2	XP_003961674.1
Takifugu rubripes	olig3	XP_003963829.1
Takifugu rubripes	olig4	XP_029683628.1
Xenopus tropicalis	olig1	XP_004912200.1
Xenopus tropicalis	olig2	XP_004912202.1
Xenopus tropicalis	olig3	NP_001008191.1
Branchiostoma belcheri	EAAT2	XP_019620987
Branchiostoma belcheri	EAATa	XP_019632550
Branchiostoma belcheri	EAATb	XP_019640815
Branchiostoma lanceolatum	EAAT2	**BL15847**
Branchiostoma lanceolatum	EAATa	**BL18111**
Branchiostoma lanceolatum	EAATb	**BL95474**
Callorhinchus milii	EAAT2	XP_007909680
Callorhinchus milii	EAAT3	XP_007890796
Ciona intestinalis	EAAT2	XP_002130715
Ciona intestinalis	EAAT3a	XP_002124271
Ciona intestinalis	EEAT3b	XP_002131603

Danio rerio	EAAT1a	NP_997805
Danio rerio	EAAT1b	NP_001177232
Danio rerio	EAAT2a	XP_009296496
Danio rerio	EAAT2b	NP_001177234
Danio rerio	EAAT3	NP_001002666
Danio rerio	EAAT4	ADH21447
Danio rerio	EAAT5a	NP_001124094
Danio rerio	EAAT5b	NP_001177689
Gallus gallus	EAAT1	XP_425011
Gallus gallus	EAAT2	XP_015142478
Gallus gallus	EAAT3	XP_424930
Gallus gallus	EAAT4	XP_025000084
Gallus gallus	EAAT5	XP_426662
Homo sapiens	EAAT1	AAH37310
Homo sapiens	EAAT2	NP_004162
Homo sapiens	EAAT3	NP_004161
Homo sapiens	EAAT4	NP_005062
Homo sapiens	EAAT5	NP_006662
Hydra vulgaris	EAATa	XP_002156773
Hydra vulgaris	EAATb	XP_012555419
Hydra vulgaris	EAATc	XP_002154975
Mus musculus	EAAT1	NP_683740
Mus musculus	EAAT2	AAB71737
Mus musculus	EAAT3	NP_033225
Mus musculus	EAAT4	NP_033226
Mus musculus	EAAT5	NP_666367
Nematostella vectensis	EAATa	EDO39457
Nematostella vectensis	EAATb	XP_032234310
Nematostella vectensis	EAATc	XP_032227983
Strongylocentrotus purpuratus	EAAT2a	XP_030845563
Strongylocentrotus purpuratus	EAAT2b	XP_030843709
Bos taurus	desmin	NP_001075044
Bos taurus	internexin	NP_001069426
Branchiostoa floridaae	IF K1	AAD23384
Branchiostoma floridae	IF A1	CAA11441
Branchiostoma floridae	IF A2	CAA11449

Branchiostoma floridae	IF A3	CAA11442
Branchiostoma floridae	IF B1	AJ223580
Branchiostoma floridae	IF B2	CAA11443
Branchiostoma floridae	IF C1	CAA11444
Branchiostoma floridae	IF D1	CAA11448
Branchiostoma lanceolatum	IF A1	**BL25043**
Branchiostoma lanceolatum	IF A3	**BL01279**
Branchiostoma lanceolatum	IF B1	X64522
Branchiostoma lanceolatum	IF B2	**BL12139**
Branchiostoma lanceolatum	IF C2	CAA11445
Branchiostoma lanceolatum	IF D1	CAA11446
Branchiostoma lanceolatum	IF E1	CAA09068
Branchiostoma lanceolatum	IF E2	CAA09067
Branchiostoma lanceolatum	IF Y1	CAB75944
Branchiostoma lanceolatum	IF K1	CAB75942
Branchiostoma lanceolatum	IF N2	**BL10379**
Branchiostoma lanceolatum	IF X1	CAB75943
Danio rerio	vimentin	NP_571947
Danio rerio	GFAP	NP_571448
Danio rerio	lamin	NP_694503
Gallus gallus	GFAP	XP_418091
Homo sapiens	desmin	NP_001918.3
Homo sapiens	vimentin	NP_003371
Homo sapiens	GFAP	AAB22581
Homo sapiens	NFH	P12036
Homo sapiens	NFM	P07197
Homo sapiens	internexin	NP_116116
Homo sapiens	keratin type I	AAB59562
Homo sapiens	keratin type II	AAC41769
Homo sapiens	lamin	NP_733821
Mus musculus	internexin	NP_666212
Mus musculus	keratin type I	AAA39372
Mus musculus	keratin type II	AAA37548
Mus musculus	lamin	NP_001002011
Rattus norvegicus	desmin	NP_071976
Rattus norvegicus	vimentin	NP_112402
Rattus norvegicus	GFAP	NP_058705

Rattus norvegicus	internexin	NP_058705
Rattus norvegicus	lamin	NP_001002016
Xenopus tropicalis	desmin	NP_989134
Xenopus tropicalis	vimentin	NP_001128275
Xenopus tropicalis	internexin	XP_004915909
Xenopus tropicalis	keratin type II	XP_002935784
Xenopus tropicalis	lamin	NP_001039148

Appendix 2

Publications in peer-reviewed journals

1. **Bozzo M**, Lacalli TC, Obino V, Caicci F, Marcenaro E, Bachetti T, Manni L, Pestarino M, Schubert M, Candiani S. *Amphioxus neuroglia: molecular characterization and evidence for early compartmentalization of the developing nerve cord*. Glia. 2021 Feb 24. Epub ahead of print.
2. Candiani S, Carestiato S, Mack AF, Bani D, **Bozzo M**, Obino V, Ori M, Rosamilia F, De Sarlo M, Pestarino M, Ceccherini I, Bachetti T. *Alexander disease modeling in zebrafish: an in vivo system suitable to perform drug screening*. Genes (Basel). 020 Dec 11;11(12):E1490.
3. Pesce S, Trabanelli S, Di Vito C, Greppi M, Obino V, Guolo F, Minetto P, **Bozzo M**, Calvi M, Zaghi E, Candiani S, Lemoli RM, Jandus C, Mavilio D, Marcenaro E. *Cancer Immunotherapy by blocking immune checkpoints on innate lymphocytes*. Cancers (Basel). 2020 Nov 25;12(12):E3504.
4. Zullo L, **Bozzo M**, Daya A, Di Clemente A, Mancini FP, Megighian A, Nesher N, Röttinger E, Shomrat T, Tiozzo S, Zullo A, Candiani S. *The diversity of muscles and their regenerative potential across animals*. Cells. 2020 Aug 19;9(9):E1925
5. **Bozzo M**, Candiani S, Schubert M. *Whole mount in situ hybridization and immunohistochemistry for studying retinoic acid signaling in developing amphioxus*. Methods Enzymol. 2020;637:419-452.
6. Pozzolini M, Gallus L, Ghignone S, Ferrando S, Candiani S, **Bozzo M**, Bertolino M, Costa G, Bavestrello G, Scarfì S. *Insights into the evolution of metazoan regenerative mechanisms: roles of TGF superfamily members in tissue regeneration of the marine sponge* Chondrosia reniformis. J Exp Biol. 2019 Sep 3;222(Pt 17):jeb207894.